

EVALUATING THE MECHANICAL
RESPONSE OF NOVEL SYNTHETIC
FEMURS REPRESENTING
OSTEOPOROTIC BONE

EVALUATING THE MECHANICAL
RESPONSE OF NOVEL SYNTHETIC
FEMURS REPRESENTING
OSTEOPOROTIC BONE

By COOPER GLUEK, B.Eng.Mgt.

A Thesis Submitted to the School of Graduate Studies in Partial Fulfilment of the
Requirements for the Degree Master of Applied Science

McMaster University © Copyright by Cooper Gluek, August 2018

McMaster University Master of Applied Science (2018) Hamilton, Ontario
(Mechanical Engineering)

TITLE: Evaluating the mechanical response of novel
synthetic femurs representing osteoporotic bone

AUTHOR: Cooper Gluek, B.Eng.Mgt.

SUPERVISOR: Cheryl E. Quenneville, B.Sc., M.E.Sc., Ph.D.

NUMBER OF PAGES: xvii, 178

Lay Abstract

The considerations and parameters in the design of orthopaedic implants for osteoporotic bone are relatively unknown. Orthopaedic implants can be evaluated with synthetic bones, which offer a number of advantages to natural specimens, assuming they are sufficiently representative of natural bone. No physical synthetic model yet exists that represents an osteoporotic femur.

In the present work, synthetic femurs were subjected to bending, torsion, axial compression, and screw pullout and compared to natural osteoporotic specimens. The synthetics were significantly different to natural specimens in bending, torsion, and screw pullout. A numerical model was created, evaluated, and tested in finite element software alongside modified models with reduced modulus and cortical thickness to assess stiffness. Recommendations were made to improve the accuracy of a future synthetic model.

The synthetic femurs tested were not representative of osteoporotic femurs, but may be feasible alternatives with minor modifications and could be useful in future orthopaedics design.

Abstract

Osteoporosis is a disease prevalent in older adults, characterized by increased bone porosity resulting in significant fracture risk. Orthopaedic implants are designed and validated against cadavers from the general 'healthy' population, but little is known about their response in osteoporotic bone. Orthopaedic implants can also be developed using synthetic bones, if they have been demonstrated to be representative of healthy bone, and offer a number of advantages. To date, no synthetic femur has been validated for the osteoporotic population. The purpose of this study was to assess novel synthetic femurs for representing this population.

Custom jigs were manufactured to test two sets of ten synthetic femurs and five isolated cadaveric femurs in four-point bending, torsion, axial compression, axial failure, and screw pullout, using an Instron mechanical testing machine to record load-displacement data. Statistical significance was found in bending, torsion, and screw pullout between both synthetic sets and cadavers using one-way ANOVA with post-hoc Tukey analysis. In all instances, the synthetic femurs had lower coefficients of variation than natural specimens.

Both synthetic and cadaveric femurs were CT scanned prior to testing. The data were used to measure key anatomical details and to develop a series of numerical models of the synthetic bones, using Materialize Mimics® and ABAQUS® software, evaluated using axial and bending data. The model was modified by reducing cortical thickness and modulus in an attempt to make the synthetic model better represent osteoporotic bone.

Establishing synthetic femurs as suitable replacements for osteoporotic bone allows for improved orthopaedic implant development. The digital model constructed allows the synthetic to be further analyzed, improving expected response of the synthetic bones. These synthetic bones could provide a foundation for development of effective orthopaedics for this population.

Acknowledgements

Completing this research would not be possible without the help and support of many people. First and foremost, I would like to thank Dr. Cheryl Quenneville, for her unending patience and support in this work. Throughout it all, Cheryl has guided and nurtured this work, pushing me to be a better grad student. I am incredibly fortunate to have had her as a mentor.

To the lab, I would like to thank its past and present members for their friendship and guidance; in alphabetical order: Alberto, Avery, Fatemeh, Jared, Julia, Laura, and Marisa. Your companionship in and outside the lab has made the last two years a much better place. I'd also like to thank Dr. Wohl, for not only starting me on this path, but his all his assistance thereafter, despite his ridiculous schedule.

Thank you to everyone in the machine shop; Ron, John, Mike, Mark, and Dan. Without your insights into design and machining, and asking the tough questions, my jigs would have taken more than twice as long and been less than half as good.

I want to thank my parents for their support and encouragement, throughout my education. You may not understand what this document is about, but that just makes it more endearing.

Thank you to Pacific Research Laboratories for funding this work and providing specimens to test; the basis of this project. In particular, I would like to

thank Amy Posch. Thank you to DePuy Synthes as well, for providing testing materials.

Finally, I would like to thank McMaster University for funding me and having me on its campus for far too long.

Table of Contents

Lay Abstract	iii
Abstract	iv
Acknowledgements	vi
Table of Contents	viii
List of Figures	xii
List of Tables	xiv
Shorthand	xv
Acronyms and Initialisms.....	xv
Abbreviations, Symbols, and Nomenclature.....	xv
Declaration of Academic Achievement	xvii
CHAPTER 1 - INTRODUCTION	1
1.1 Motivation	1
1.2 Anatomy of Upper Leg	4
1.3 Bone Structure and Material Properties	7
1.4 Osteoporosis	8
1.4.1 Causes and Significance	9
1.4.2 Diagnosis	11
1.4.3 Treatment.....	11
1.5 Synthetic Bones	13
1.5.1 Benefits	14
1.5.2 Drawbacks.....	15
1.6 Finite Element Analysis (FEA)	16
1.7 Review of Previous Evaluation Methods	19
1.7.1 Methods for Synthetic Bone Evaluation	19
1.7.1.1 Bending.....	19
1.7.1.2 Torsion.....	21
1.7.1.3 Axial Compression	23
1.7.1.4 Screw Pullout	25
1.8 Study Rationale and Overview	27
1.8.1 Objectives	27
1.8.2 Hypotheses	28
1.9 References	29

CHAPTER 2 – DESIGN OF TESTING APPARATUS	32
2.1 Introduction	32
2.2 Review of Previous Methods Evaluation Methods	33
2.2.1 Bending	33
2.2.2 Torsion	36
2.2.3 Axial Compression	39
2.2.4 Screw Pullout	42
2.3 Design and Assembly	45
2.3.1 Design Objectives	45
2.3.2 Multi-Purpose Components	45
2.3.3 Bending	46
2.3.4 Torsion	48
2.3.5 Axial Compression	51
2.3.6 Screw Pullout	53
2.3.7 Polycarbonate Box	55
2.4 Discussion	58
2.5 Conclusion	60
2.6 References	61
CHAPTER 3 - THE MECHANICAL PROPERTIES OF OSTEOPOROTIC SYNTHETIC AND CADAVERIC FEMURS	63
3.1 Introduction	63
3.2 Methods	66
3.2.1 Specimens	66
3.2.1.1 Cadavers	66
3.2.1.2 Synthetic Bones	67
3.2.2 Potting	70
3.2.3 Testing Protocols	72
3.2.3.1 Bending	74
3.2.3.2 Torsion	76
3.2.3.3 Axial Compression	81
3.2.3.4 Screw Pullout	83
3.2.4 Analysis Methods	87
3.3 Results	89
3.3.1 Bending	89
3.3.2 Torsion	93
3.3.3 Axial Compression	97
3.3.4 Screw Pullout	101

3.4	Discussion	103
3.4.1	General Limitations	103
3.4.2	Bending	108
3.4.3	Torsion	109
3.4.4	Axial Compression	113
3.4.5	Screw Pullout	117
3.5	Conclusion	118
3.6	References	121
CHAPTER 4 – DEVELOPMENT OF A FINITE ELEMENT MODEL TO INVESTIGATE FUTURE SYNTHETIC MODEL ITERATIONS		123
4.1	Introduction	123
4.2	Methods	124
4.2.1	Standard Model Development	124
4.2.2	Altered Cortical Thickness Model Development	126
4.2.3	Interior Contact	132
4.2.4	Meshing	132
4.2.5	Mesh Sensitivity Analysis	133
4.2.6	Model Evaluation	139
4.2.7	Material Property Selection	143
4.2.8	Axial Compression	146
4.2.9	Four-Point Bending	146
4.3	Results	149
4.3.1	Axial Compression	149
4.3.2	Bending	149
4.4	Discussion	156
4.5	References	165
CHAPTER 5: GENERAL DISCUSSION AND CONCLUSIONS		166
5.1	Summary	166
5.2	Limitations and Strengths	171
5.3	Future Directions	175
5.4	Significance	176
5.5	References	178
Appendices		179
APPENDIX A: Glossary of Medical Terms		180

APPENDIX B: Technical Drawings -----	184
APPENDIX C: DXA Scan Data -----	190
APPENDIX D: Sample Test Data -----	195
APPENDIX E: Fracture Images -----	201
APPENDIX F: Orphan Mesh to Part Conversion -----	204
APPENDIX G: Second Moment of Area Calculation on 3403 Mid-diaphysis Samples -----	205

List of Figures

Figure 1.1: Femur Anatomy	6
Figure 1.2: Expected Bone Mass as a Function of Age	10
Figure 1.3: Porosity Increase from Osteoporosis	13
Figure 1.4: Nodes and Elements	18
Figure 1.5: Four-Point Bending	20
Figure 1.6: Torsion	22
Figure 1.7: Axial Rigidity	24
Figure 1.8: Screw Pullout	26
Figure 2.1: Bending Configurations	35
Figure 2.2: Torsion Configurations	38
Figure 2.3: Axial Compression Configurations	41
Figure 2.4: Screw Pullout Jig	44
Figure 2.5: Four-Point Bending Assembly	47
Figure 2.6: Torsion Assembly	50
Figure 2.7: Axial Compression Assembly	52
Figure 2.8: Screw Pullout Assembly	54
Figure 2.9: Blast Shield Design	57
Figure 3.1: Fourth Generation Sawbone Femur Geometry	69
Figure 3.2: Potting Images	71
Figure 3.3: Testing Images	73
Figure 3.4: Bending Testing Photographs	75
Figure 3.5: Radius of Rotation Calculation	78
Figure 3.6: Torsion Testing Photos	80
Figure 3.7: Axial Compression Photos	82
Figure 3.8: Predrill Guide Jig	85
Figure 3.9: Screw Pullout Photos	86
Figure 3.10: ML and AP Flexural Rigidity Graphs	92
Figure 3.11: Torsional Rigidity Graph	95
Figure 3.12: Axial Compression Results Graphs	99
Figure 3.13: Screw Pullout Load Graph	102
Figure 3.14: Demonstration of Bone Cross-Sectional Geometry Change with Age	107
Figure 3.15: Sample Sawbones with Cancellous Bubbles	116
Figure 3.16: Femoral Head Crush After Axial Loading	116
Figure 3.17: Screw Pullout Damage	120
Figure 4.1: Rough Surfaces in 3-Matic Import	128
Figure 4.2: Cortical Gap Filling	129
Figure 4.3: Model Surface Unification	130
Figure 4.4: Trabecular Components in 3-Matic	131
Figure 4.5: Levels of Cortical Mesh Refinement	136
Figure 4.6: Mesh Sensitivity Analysis Plot	137

Figure 4.7: Final Mesh -----	138
Figure 4.8: Axial Modelling Configuration -----	141
Figure 4.9: Three-Point Bending -----	145
Figure 4.10: Bending Model Configuration -----	148
Figure 4.11: Axial Compression Fringe Plots -----	151
Figure 4.12: AP and ML Bending Fringe Plots -----	152
Figure 4.13: Axial Compression Stiffness Results -----	153
Figure 4.14: AP and ML Bending Stiffness Results -----	155
Figure B.1: Dimensional Drawing of Base Fixture -----	184
Figure B.2: Dimensional Drawing of Bending Brace L-Bracket -----	185
Figure B.3: Dimensional Drawing of Top Fixture -----	185
Figure B.4: Dimensional Drawing of Axial Cup -----	186
Figure B.5: Dimensional Drawing of Axial Secure L-Bracket -----	186
Figure B.6: Dimensional Drawing of Cotter Pin Extension -----	187
Figure B.7: Dimensional Drawing of Key -----	187
Figure B.8: Dimensional Drawing of Aluminum Plate -----	188
Figure B.9: Dimensional Drawing of Torsion Secure Plate -----	188
Figure B.10: Torsion Secure Complementary Plate -----	189
Figure D.1: AP Bending Sample Test Data -----	195
Figure D.2: ML Bending Sample Test Data -----	196
Figure D.3: Torsion Sample Test Data -----	197
Figure D.4: Axial Compression Sample Test Data -----	198
Figure D.5: Cyclic Failure Sample Test Data -----	199
Figure D.6: Screw Pullout Sample Test Data -----	200
Figure E.1: 3403 Series Fracture Images -----	201
Figure E.2: 3503 Series Fracture Images -----	202
Figure E.3: Natural Femur Fracture Images -----	203

List of Tables

Table 3.1: Cadaveric Specimen Information Table	68
Table 3.2: Torsion Measurements	79
Table 3.3: Minimum and Maximum Bending Stiffness and Flexural Rigidity Values	93
Table 3.4: Torsion Original and Retest Value Comparison Table	96
Table 3.5: Minimum and Maximum Torsional Stiffness and Torsional Rigidity Values	96
Table 3.6: Minimum and Maximum Axial Stiffness Values	100
Table 3.7: Minimum and Maximum Axial Failure Load Values	100
Table 3.8: Experimental Fracture Types	100
Table 3.9: Minimum and Maximum Pullout Load and Pullout Stress	102
Table 3.10: Linear Regression and Cadaver T-Score Comparison	107
Table 4.1: Material Properties as Described by Sawbones™	135
Table 4.2: Mesh Sensitivity Analysis Model Elements and Nodes	137
Table 4.3: Model Evaluation Table	142
Table 4.4: Experimental Second Moment of Area and Modulus Values	144
Table 4.5: Simulated Material Properties	144
Table 4.6: Axial Compression Stiffness Results and Percentage Error	153
Table 4.7: AP and ML Bending Stiffness Results	154
Table 4.8: Component Volume Analysis Across Different Models	164
Table 4.9: Total Model Volume	164

Shorthand

Acronyms and Initialisms

AP	Anteroposterior
BMD	Bone Mineral Density
CAD	Computer Aided Design
CT	Computed Tomography
DXA	Dual Energy X-Ray Absorptiometry
FE	Finite Element
FEA	Finite Element Analysis
ML	Medialateral
PRL	Pacific Research Laboratories, Inc.
SD	Standard Deviation

Abbreviations, Symbols, and Nomenclature

°	Degree
“	Inch
%	Percent
1D	One-dimensional
2D	Two-dimensional
3D	Three-dimensional
ν	Poisson's Ratio
δ	Stiffness
σ_y	Yield Strength
σ_{ult}	Ultimate Strength
θ	Angle of Rotation
cm	Centimetre

E	Young's Modulus
F	Force
g	Standard Acceleration due to Gravity
G	Shear Modulus
I	Second Moment of Area
kg	kilogram
J	Polar Moment of Area
L	Length
m	Metre
mm	Millimetre
N	Newton
r	Radius
rad	Radian
T	Torque
y	Deflection
y_{max}	Maximum Deflection

Declaration of Academic Achievement

The following is a declaration that I, Cooper Gluek, completed the research outlined in this thesis and recognizes the contributions of Dr. Cheryl Quenneville, Dr. Radovan Zdero, Sandra Charbonneau, and Chantal Saab. I contributed to the study, performed the experimental testing, data analysis, finite element model creation and analysis, and writing of the thesis. Dr. Cheryl Quenneville assisted with the study design and review of the thesis. Dr. Radovan Zdero contributed to the apparatus design. Sandra Charbonneau conducted the CT scans of the specimens. Chantal Saab conducted DXA scans of the specimens.

CHAPTER 1 - INTRODUCTION

Overview: *Bone is a complex material with properties complicated by a multitude of factors. Synthetic bones look to reduce variability and resolve several problems inherent to cadaveric material. This introductory chapter outlines the anatomy of the upper leg, bone tissue characteristics, osteoporosis, synthetic bones as surrogates for testing, the concept of finite element analysis, and previous experimental and computational work. It concludes with the study rationale, including objectives and hypotheses of this research.*

1.1 Motivation¹

The use of bone analogues have wide-spread applications in the automotive, defence, medical, orthopaedics, and forensic industries, among others, especially where use of cadaveric material would be challenging. However, many factors influence the properties and characteristics of bone, such as age, gender, nutrition, and activity level. Simplifications are also made in research, such as the exclusion of ligaments, tendons, muscles,

¹ Anatomical terms used throughout this document are listed in APPENDIX A: Glossary of Medical Terms.

and the use of rudimentary geometry. Cadavers must be used due to the moral and ethical limitations of research conducted *in vivo*. Due to restricted sample sizes and the variability of interpersonal specimens, a large standard deviation (SD) is typically present in reported values. As such, it is very difficult to create a surrogate representative of the entire population.

Synthetic bones (e.g. Sawbones™, by Pacific Research Labs, Vashon Island, WA, USA) attempt to rectify some of these issues. Models are composed of short glass fibres in an epoxy resin to replicate cortical bone, pressure injected around a dense foam to replicate cancellous bone (MatWeb 2017). As such, they are much easier to store, handle, and dispose of, with standard geometry and material properties that reduce variability. Unfortunately, Sawbones™ are not perfect substitutes. Manufacturing constraints in synthetic bones offer much lower interspecimen variability but may not replicate the exact geometry and distribution of cancellous and cortical bone as seen in the pilot holes and cast lines present. To ensure accurate mechanical response, synthetic femurs require their properties to be validated.

An alternative bone surrogate is finite element analysis (FEA), a computational method where digital models are discretized and subjected to loading. Simulation allows for highly precise, repeatable testing to be

performed, where conditions can be altered slightly and compared. Each test is ideal in terms of loading vectors and bone orientation; however, these models still require cadaveric specimens to verify their accurate response. Unfortunately, FEA can also be quite limited: boundary conditions, muscle, tendon, and ligament modelling, and crush can be very difficult to recreate and cannot be validated readily.

Disease can present another key challenge in the attempt to assess and replicate the properties of bone. Osteoporosis is one such disease. While not inherently destructive, it significantly increases bone fragility to the point where everyday activities can cause potentially devastating fractures, typically in the hip, wrist, or spine (World Health Organization 2004). Osteoporosis is becoming increasingly prevalent, with over 1.5 million Canadians suffering from the disease in 2010. Of that number, 21% have reported a related fracture at a common site of occurrence (Public Health Agency of Canada 2010). With complications associated with fracture, and an aging population, prevention of osteoporosis is considered essential in the pursuit of health, quality of life, and independence by the World Health Organization (2004). Osteoporosis does not yet have a cure. Treatment options are quite limited, with unknown optimal treatment durations and the potential for fracture occurring from “oversuppression” of bone remodelling due to accrued microcracks (Heath III 2017). Treatment

may also carry significant side effects and unknown consequences after treatment has ended (Heath III 2017). A validated synthetic or finite element model of an osteoporotic femur would alleviate demand on limited cadaveric (undamaged) resources and promote knowledge and understanding of the disease. To the best of the author's knowledge, no validated physical synthetic osteoporotic models are known to exist.

The overall purpose of this research was to assess the mechanical response of two newly developed synthetic osteoporotic femurs and to provide recommendations for ways to improve them to better match the osteoporotic population. An FEA model could assist in refining the synthetic femurs by addressing the influence of material and geometric properties such as density, modulus, and cortical thickness on mechanical response. If successful, these femurs could become a significant research aid, reducing requisite sample sizes and testing variability.

1.2 Anatomy of Upper Leg

The lower extremity (more commonly referred to as a 'leg') is the distal portion of the body extending from the hip to the foot. It includes the thigh, knee, shank, ankle, and foot. The thigh contains one long bone, the femur. The femur (Figure 1.1) joins proximally to the acetabulum of the hip at the femoral head, and distally at the knee to the tibia via the medial and lateral

condyles. The femur connects laterally to the fibula through the lateral collateral ligament and to the patella via the quadriceps tendon (American Academy of Orthopaedic Surgeons 2014).

Like other long bones, the femur has a relatively cylindrical midsection known as the diaphysis. The diaphysis contains the medullary canal and is primarily formed of cortical bone (Section 1.3). The ends of the bone, known as the epiphyses, are irregularly shaped and primarily filled with trabecular bone, surrounded by cortical bone. There are other irregularities in the geometry of the femur, including the lesser and greater trochanter, the intertrochanteric crest, and linear aspera, among others.

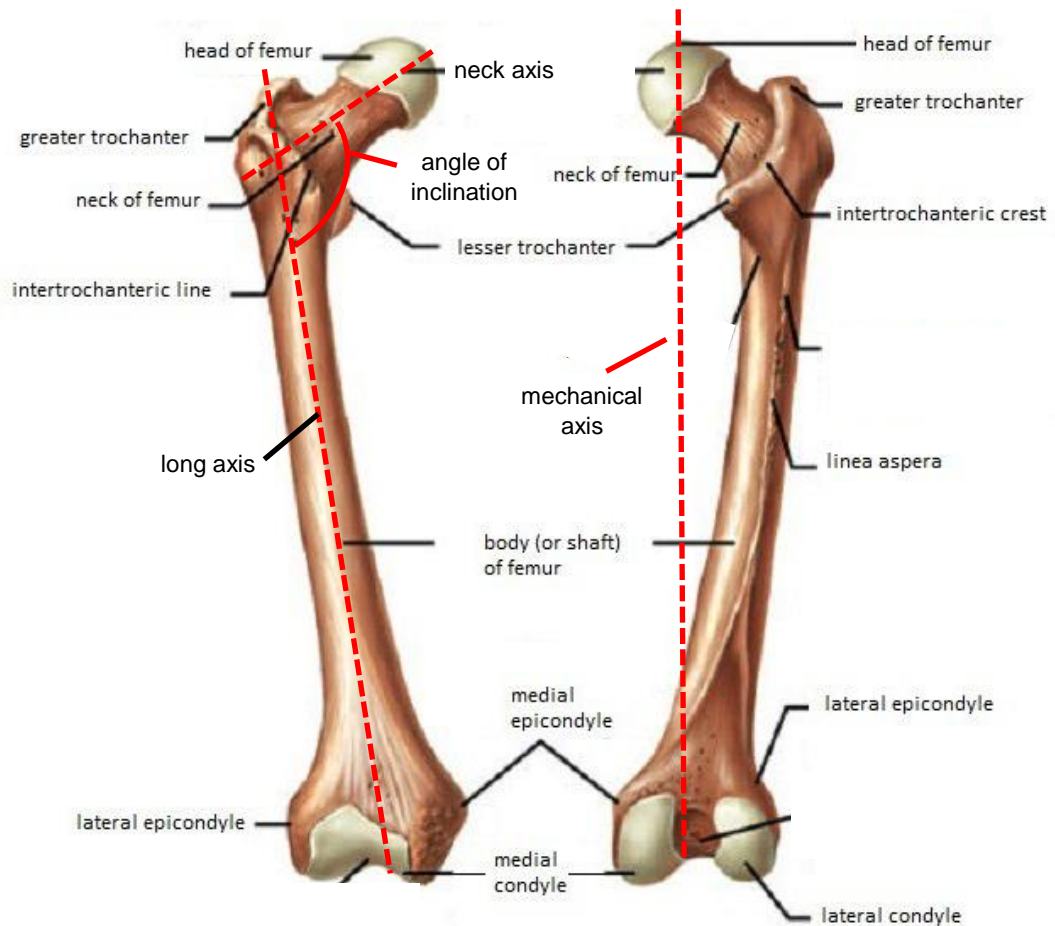


Figure 1.1: Femur Anatomy

Anterior (left) and posterior (right) views of the human femur, with anatomical landmarks and key axes identified, adapted from (Singh 2017).

1.3 Bone Structure and Material Properties

Complicated by the influence of age, height, weight, race, gender, diet, hormone levels, exercise habits, geometry, and genetics, the properties of bone are notoriously difficult to assess.

The primary difference between cancellous and cortical bone are their apparent densities. Cancellous bone is more porous and thus less dense than cortical bone, with an apparent density of 0.05-0.07 g/cm³ (Kowalski et al. 2001). It exists as interconnected rods and plates (or 'trabeculae') resulting in a range of densities and porosity values inside the cancellous tissue. Power-law relationships can explain 60-90% of variation in modulus and strength of trabecular bone when using bone density as an explanatory variable; indicative that changes in apparent density are critically linked to its mechanical behaviour (Karim et al. 2017). In the femur alone, reported modulus values of trabecular bone in bending vary from 389 to 3230 MPa (Karim et al. 2017). The anisotropic properties of bone can be attributed to the realignment of trabecular bone to accommodate loading patterns (Huiskes et al. 2000)

Cortical bone is significantly denser, with an apparent density of 1.8 g/cm³ (Kowalski et al. 2001). The biomechanical properties of cortical bone are largely determined by its porosity and the degree of mineralization of

the bone matrix (Marcus et al. 2017). The strength of cortical bone can also be roughly approximated (approximately 80% is accounted for) with a power law relationship, with matrix mineralization and porosity as explanatory variables (Karim et al. 2017). Cortical bone is found surrounding the femur, thickest along the diaphysis tapering to a thin shell along the distal and proximal ends.

1.4 Osteoporosis

Osteoporosis (osteo – relating to bone, porosis – porous) is a condition generalized as an increase in bone porosity, or skeletal degradation resulting in such fragility that fracture can occur even in everyday activities (Marcus et al. 2017). With a fracture risk of 30-40% in developed countries, osteoporosis poses a similar risk of mortality to that of coronary heart disease (World Health Organization 2004). Fractures can significantly influence independence and quality of life and carry a risk of morbidity due to associated complications. In older adults, the mortality rate of a hip fracture after 1 year is 22% (Johnell et al. 2004). The reduced bone quality associated with osteoporosis complicates surgery due to low, often “unpredictable” fixation, requiring a “thoughtful, and often unique approach to maximize the strength of repair” (Gardner and Collinge 2016). Screw cut-out, postoperative non-union, and implant migration are common

complications negatively affecting recovery, requiring additional tools such as bone cement (Kammerlander et al. 2016). With less than 30% of patients expected to regain total function (Huiskes and Van Rietbergen 2004), osteoporosis is a significant cause of people to become bedridden (World Health Organization 2004). Such a number could be reduced, with improved patient treatment times and outcomes, if a standardized osteoporotic model were available for use in the development of specialized orthopaedic devices.

1.4.1 Causes and Significance

Average life-expectancy is increasing, gaining almost 20 years for both men and women in Canada in the last century (Government of Canada 2012). However, bone mass naturally decreases with age (Figure 1.2), peaking around age 30 (Kowalski et al. 2001). Coupled with aging “baby boomers”, this results in a significant population with skeletal fragility. Both men and women of all ages can develop osteoporosis, possibly as a result from a significant decrease in exercise, such as during long periods of bed-rest. Older women suffer increased risk due to the significant decrease in estrogen levels after entering menopause (Kowalski et al. 2001; Choices 2015).

There are many factors that guide bone's ability to resist fracture, including: the amount of, shape, and microarchitecture of bone (Marcus et al. 2017). With a thinning in the trabeculae of cancellous bone, the increased porosity means larger gaps between the supporting microarchitecture of trabecular struts, significantly reducing local strength. When a strut is broken no load can be transferred, and the remnants resorb. Given bone's mechanical dependence on porosity, the decreased density caused by osteoporosis decreases Young's Modulus, as well as yield strength and ultimate strength.

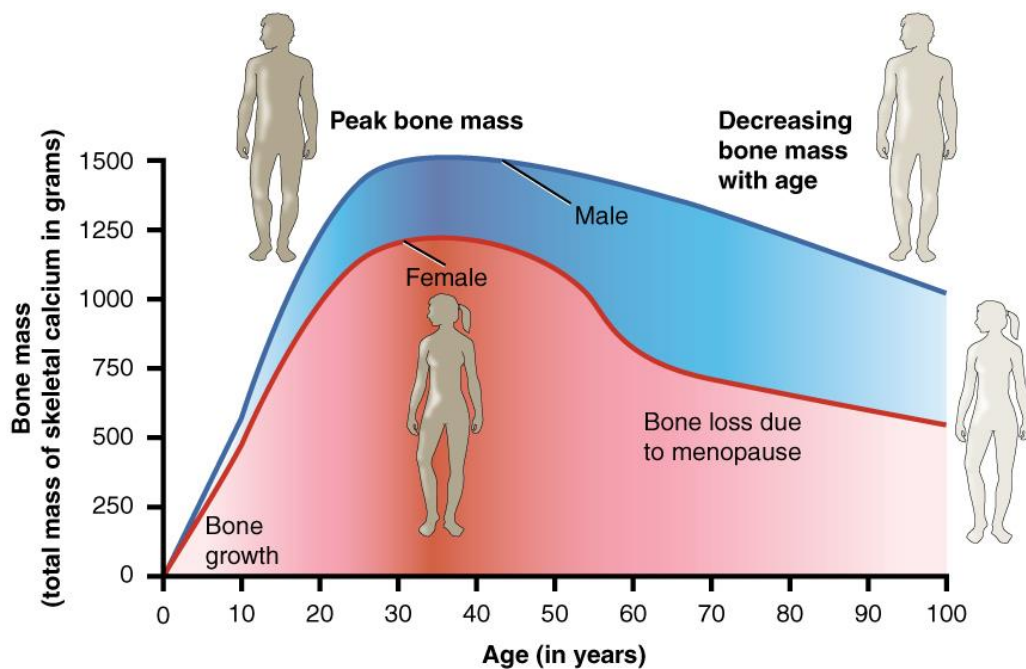


Figure 1.2: Expected Bone Mass as a Function of Age
Male and female bone mass increases from birth and peaks at approximately 30 years old (OpenStax 2017).

1.4.2 Diagnosis

Osteoporosis is officially diagnosed as a bone mineral density 2.5 standard deviations (SD) below the average value for young, healthy, adult women. This is more commonly referred to as a “T-score <-2.5 SD” (World Health Organization 2004), with absolute values varying with race and gender. A bone mineral density 1 – 2.4 SD below the average is diagnosed as osteopenic. A decrease of only 1 SD has been associated with a 2-3x increase in long-term fracture risk (Marcus et al. 2017).

The T-score is calculated via dual energy x-ray absorptiometry (DXA), also known as a bone density scan or a bone densitometry scan (National Health Services 2016). The DXA process is a quick and relatively low risk x-ray based method of assessing bone density, seen as the current gold standard. However, a typical assessment only scans the hip and lumbar spine, overlooking low density sites elsewhere. Scans are not weight-adjusted, nor do they assess bone-turnover rate, both of which are important risk factors for fracture (Marcus et al. 2017), making osteoporosis difficult to correctly diagnose and treat.

1.4.3 Treatment

Treatment for osteoporosis is currently limited. Many drugs are available but each has significant limitations in both longevity and benefits,

as well as safety issues. In general, no drug can return bone strength and reduce fracture risk to that of a young, healthy person (Heath III 2017).

With current treatment options being limited, it is important to understand the mechanical and structural properties of osteoporotic bone in support of future research. Understanding bone strength is critical to understanding fracture risk (Marcus et al. 2017).

The incidence of osteoporosis is increasing. Without effective treatment options, millions of people could suffer from reduced independence and quality of life, associated with an enormous international economic burden. The development of an effective surrogate model is imperative in preparing optimal orthopaedic implants for the increasing prevalence of osteoporosis.

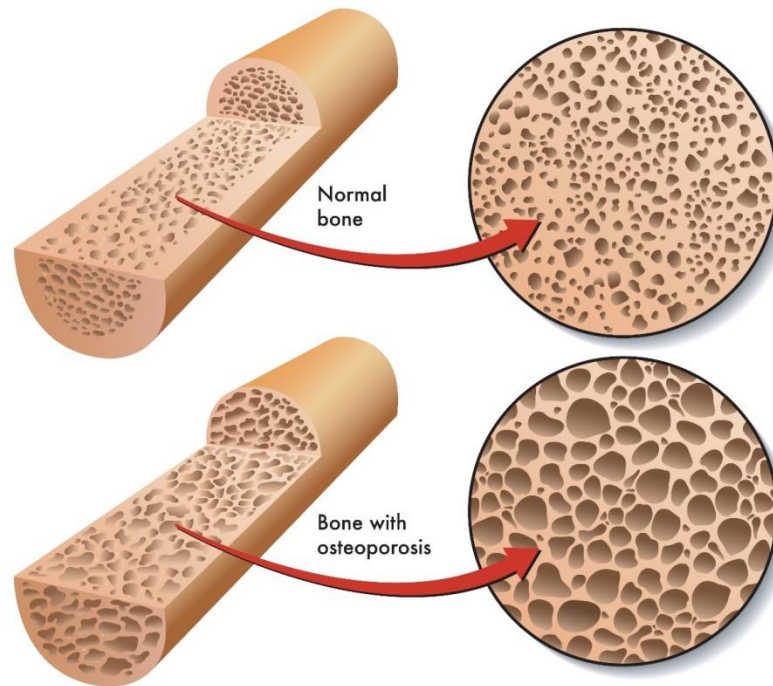


Figure 1.3: Porosity Increase from Osteoporosis

Comparison of healthy and osteoporotic diaphysis, highlighting the increased porosity induced by osteoporosis (Laurie 2016). Osteoporosis also decreases cortical bone mass, demonstrated in the reduced thickness.

1.5 Synthetic Bones

Pacific Research Laboratories (Pacific Research Laboratories Inc, Vashon, WA, USA) was founded in 1975, and is the producer of Sawbones™ with the goal of “Precise, Repeatable Testing” (Sawbones 2017). Sawbones™ have created their fourth generation of composite bones, with short glass fibers and epoxy resin to simulate natural cortical bone, which offer enhanced fracture toughness, fatigue life, tensile strength and modulus. When compared to third generation bones, while maintaining

the same geometry (MatWeb 2017). This glass/resin mixture is pressure injected around a polyurethane foam core, used to model the trabecular bone (MatWeb 2017).

The purpose of these models is for the design and evaluation of orthopaedic components in benchtop studies, for which they are gaining wide acceptance within the research community (Papini et al. 2007; Zdero et al. 2007; Schemitsch 2008).

1.5.1 Benefits

Synthetic bone models, in comparison to cadaveric tissue, are easy to procure and relatively inexpensive. There are no availability issues from lack of donors, and they do not have to be processed by a hospital or have surrounding soft tissue removed by trained personnel. Sawbones™ are not biohazardous, making them easier to store, transport, handle, and dispose of. This requires less training, storage facilities, and lab regulations; reducing laboratory costs.

One of the largest benefits to Sawbones™ is that they are manufactured, and thus inherently repeatable. When compared to cadaveric bone, Sawbones™ will have a significantly reduced interspecimen variability with a near constant geometry and set of structural properties.

1.5.2 Drawbacks

Models are limited by the available production techniques with remnants of the molding and creation process including cast lines, pilot holes, and slight differences in geometry when compared to cadaveric specimens. While a standardized geometry is effective in reducing variability, one size limits their applicability (eg. comparisons to 5th and 95th percentile women) and may produce designs optimized for only a single portion of the population.

The synthetic femurs use a hollow core to approximate the marrow cavity, which tapers from the distal to proximal end. With current manufacturing techniques, it is unrealistic to fill the distal end with trabecular foam and surface it with a cortical shell. This may make the Sawbones™ impractical for distal femur orthopaedics testing, where a large portion of the trabecular tissue used to anchor screws is now missing. Furthermore, the cancellous foam used as a surrogate to trabecular tissue is isotropic and homogeneous, which does not represent the natural adaptation for load transmission present in the natural body, corresponding to variations in modulus and density throughout the bone. Typical validation procedures have potted synthetic femur models at both ends (eg. Heiner and Brown 2001; Heiner 2008), limiting investigation to the diaphysis. Further, few adjacent tissues are available, such fascia, cartilage, ligaments, and

tendons, outside of a few spine surrogates. Exclusion of these components simplify testing but may alter response when compared to *in vivo* tests.

The overall failure response of composite synthetic tibias has been found to differ from cadaveric bone (Quenneville et al. 2010). One failure method was delamination of the epoxy resin from the polyurethane foam. As such, they have not been recommended for injury investigation in axial impact loading (Quenneville et al. 2010). Synthetic bones may also fail catastrophically and fracture into several pieces, even at low loading rates, unlike cadaveric bones.

Sawbones™ offer a number of advantages and have many demonstrated applications, given an understanding of their limitations. Further analysis and refinement could reduce these limitations and improve overall response, which would increase their applicability in testing.

1.6 Finite Element Analysis (FEA)

Another means to address the limitations of cadaveric testing is the use of FEA. FEA is a numerical computational technique used to approximate stress and strain values throughout a modelled system, ideal for irregular geometries where an exact mathematical calculation would be impossible

or impractical. In practice, FEA is “widely accepted as the most practical and reliable method of analysis for mechanical structures” (Ota et al. 1999).

In FEA, a discrete number of nodes are created and dispersed across the model; locations at which displacement is calculated and used to determine the stress and strain values inside the element. Nodes are joined to create elements, of which two main types are used: tetrahedral and hexahedral, described by their geometry (Figure 1.4). Elements may be composed of different numbers of nodes representing the geometric order and corresponding shape function, which will influence element deformation. For large deformations in linear structural analysis, quadratic elements are typically more accurate and less computationally expensive (Sharcnet 2017).

Elements are assembled to create a mesh. Meshes can be produced automatically, manually, or via voxel values, none of which are inherently superior, with each well-suited to certain applications (Viceconti et al. 1998). Automatically generated meshes typically use hexahedral or tetrahedral elements, with tetrahedral being more dependent on mesh quality (Ramos and Simões 2006), and slightly less accurate but with reduced computational intensity; likely the best method when a solid model is available (Viceconti et al. 1998). It is recommended that second-order

tetrahedral (rather than hexagonal or mapped meshing) be used for human femurs in quasi-static analysis (Papini et al. 2007), where hexahedral elements are the industry standard for dynamic simulation.

Higher mesh densities use more elements in an effort to increase accuracy, at the expense of computational power and time. To balance this, mesh densities are usually increased only in areas of interest or regions of very complex geometry, such as the femoral neck or epiphyses. Mesh density is increased (reducing element size) until the results plateau within a reasonable range. More reliable models can be created with imaging techniques such as Computed Tomography scans, which produce accurate internal and external geometry of the femur with regional density distributions which can be correlated to modulus values (Wille et al. 2012).

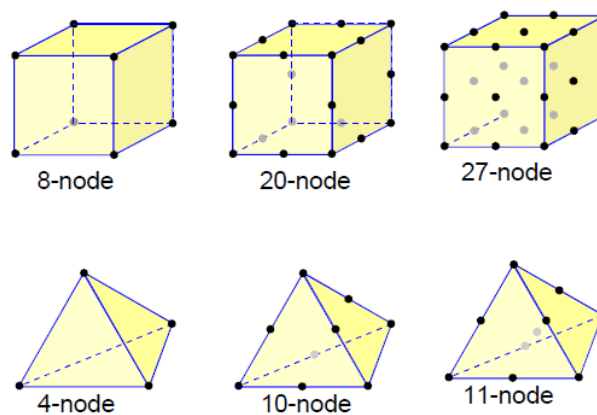


Figure 1.4: Nodes and Elements

Two types of solid elements available in FEA, hexahedral (top row) and tetrahedral (bottom row). Nodes are indicated by dots. This image also identifies elements with different numbers of nodes, adapted from (Eng-Tips 2012).

1.7 Review of Previous Evaluation Methods

1.7.1 Methods for Synthetic Bone Evaluation

1.7.1.1 Bending

One method of assessment is bending, typically used to quantify the Young's Modulus, E , of a material. This is usually done with a cross-section of uniform standard geometry, such as a rectangle or hollow cylinder, where second moment of area, I , is exactly defined and unchanging throughout the length of the sample. The geometry of bone is complex and non-uniform, so flexural rigidity, which incorporates both material and geometries properties, is often assessed instead. Flexural rigidity is calculated as modulus (E) multiplied by second moment of area (I), EI . The calculation of flexural rigidity is dependent on the boundary conditions of the beam, as well as the location(s) where force, F , is applied. A corresponding displacement value, y , is also required (Equation 1.1). Femurs are typically assessed in bending in both the medial-lateral and anterior-posterior planes as the cross-section of the diaphysis is irregularly shaped.

$$EI = \frac{Fa(4a^2 - 3L^2)}{24y_{max}} \quad \text{Equation 1.1: Flexural Rigidity}$$

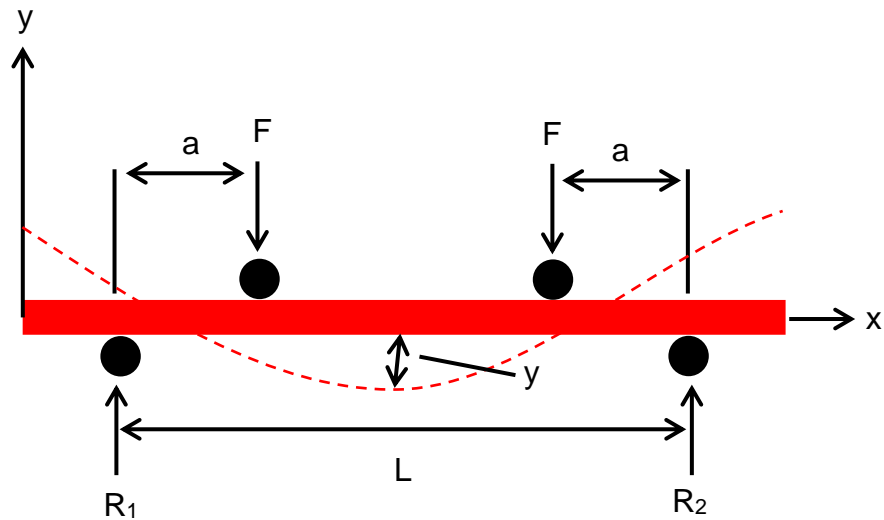


Figure 1.5: Four-Point Bending

Schematic corresponding to the calculation of flexural rigidity (Equation 1.1) of four-point bending with equally spaced loads. The exaggerated displacement, y , of the beam is indicated by the dotted red line.

1.7.1.2 Torsion

Similar to bending, the unique geometry and non-uniform cross-section of the femur make torsional rigidity a better comparison tool between specimens; the product of shear modulus, G , a material property; and polar moment of inertia, J , a geometric property. In testing, force, F , and displacement are recorded. However, the displacement is converted to an angle of rotation, θ . The difficulty in calculating torsional rigidity comes from the exact position of application of force related to the axis of rotation of the bone and consistency in measurement between anatomical locations. This will affect the radius, r , and thus, the torque, T , where torque is equal to the product of force and radius. Torsional rigidity is also subject to the length between the applied force and the static end of the specimen, L (Equation 1.2).

$$GJ = \frac{TL}{\theta} = \frac{FrL}{\theta}$$

Equation 1.2:
Torsional Rigidity

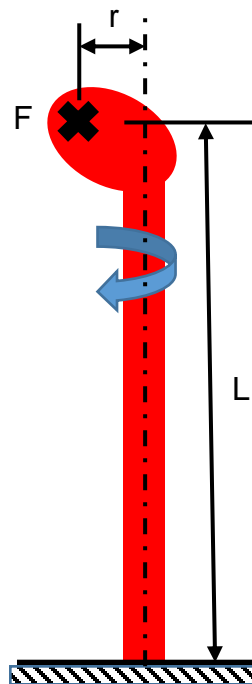


Figure 1.6: Torsion

A torque is applied to the femur with force directed into the page (denoted by the black 'X') exerted on the femoral head, creating a twist in the long axis of the femur (following the blue arrow) and displacement of the femoral head, also into the page.

1.7.1.3 Axial Compression

Axial loading is often used to simulate single-leg stance. In this instance, force is applied along the mechanical axis of the femur to the femoral head and the resultant displacement is measured. Due to the geometry of the femur, a resultant bending moment in the diaphysis and femoral neck is unavoidable. This is typically simplified by simply ignoring the bending moment and assuming a pure axial compression in the specimen (Papini et al. 2007). Unlike bending and torsion, axial stiffness (Equation 1.3) is often reported instead of axial rigidity (Equation 1.4), being the product of modulus and cross-sectional area, EA , rather than modulus and second moment of area, EI . Axial stiffness, defined as force, F , over displacement, d , is related to the rigidity by a factor L , the length of the sample.

$$\partial = \frac{F}{d}$$

Equation 1.3: Axial Stiffness

$$EA = \frac{FL}{d}$$

Equation 1.4: Axial Rigidity

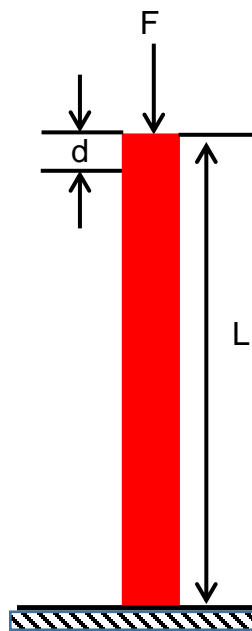


Figure 1.7: Axial Rigidity

A force is applied vertically to the femoral head with the distal end potted. Displacement, d , and force, F , are recorded as well as the total length, L .

1.7.1.4 Screw Pullout

With synthetic femurs representing an important alternative to natural specimens for orthopaedics development, it is important to assess their similarity in screw purchase and failure. Screws are commonly used in orthopaedic implants such as plates and can fail in a number of methods, such as screw pullout, screw ‘toggling’, screw bending or torsion, and screw stress risers (Zdero et al. 2009). In testing, a screw is inserted into the bone, normal to the surface, and then extracted. The maximum force is recorded as the extraction force, F , used with the contact area, A , to calculate the extraction shear stress, τ . As most screws are effectively cylindrical, the extraction force can be approximated as the surface area of a cylinder, defining height, h , as the depth of contact with the bone - typically the cortical thickness. In some tests (eg. Zdero et al. 2007; Zdero et al. 2009), the area around the screw is supported to prevent failure in bending, ensuring the failure mode is screw pullout.

$$\tau = \frac{F}{A} = \frac{F}{\pi Dh}$$

**Equation 1.5: Screw
Pullout**

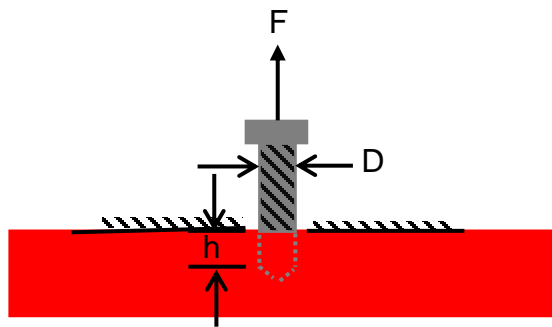


Figure 1.8: Screw Pullout

A screw is inserted into the sample and then a force, F , is exerted to remove it. The maximum force is known as the pullout load.

1.8 Study Rationale and Overview

Synthetic bones offer a number of advantages over natural specimens, such as ease of use and reduced variability. However, the accuracy of their response and associated limitations must be considered and understood before they can be used in lieu of natural specimens. Many studies have been conducted to assess the properties of bone. These analyses have been carried forward to determine the applicability of a surrogate, which has also been thoroughly tested. Osteoporosis is a disease which is becoming increasingly prevalent with increased life expectancy and an aging population, requiring a representative synthetic model for the development of orthopaedics effective in this population. An investigation into the similitude between such bones and synthetic composite femurs could provide much greater access to research opportunities involving osteoporosis, providing the ability to better understand it and accommodate it in design.

1.8.1 Objectives

The objectives of this thesis were:

1. To develop a series of testing jigs that would subject cadaveric and synthetic femurs to bending, torsion, axial compression, and screw pullout while recording force and displacement;

2. To investigate the structural properties of newly developed osteoporotic Sawbones™ and contrast them to osteoporotic cadaveric specimens; and
3. To develop a finite element model of the Sawbone and determine how to improve biofidelity.

1.8.2 Hypotheses

The hypotheses of this research were:

1. Osteoporotic Sawbones™ will have a significantly reduced mechanical variability when compared to cadaveric specimens; and
2. Sawbones™ will not be statistically different from cadaveric specimen.

1.9 References

- American Academy of Orthopaedic Surgeons. 2014. Common Knee Injuries - OrthoInfo. [accessed 2017 Jun 13]. <http://orthoinfo.aaos.org/topic.cfm?topic=a00325>.
- Choices N. 2015. DEXA (DXA) Scan - NHS Choices. DEXA Scan. [accessed 2017 Jun 13]. <http://www.nhs.uk/conditions/dexa-scan/pages/introduction.aspx>.
- Eng-Tips. 2012. Hex vs Tets / Different Stress Level - Finite Element Analysis (FEA) Engineering. Eng-Tips; Eng. Forums. [accessed 2017 Jun 30]. <http://www.eng-tips.com/viewthread.cfm?qid=320515>.
- Gardner MJ, Collinge C. 2016. Management Principles of Osteoporotic Fractures. *Injury* 47:S33–S35. doi:10.1016/S0020-1383(16)47006-3.
- Government of Canada. 2012. Life Expectancy at Birth, by Sex, by Province. Stat. Canada. doi:https://www.google.ca/webhp?ie=utf-8&oe=utf-8&gws_rd=cr&ei=46_HVtnZE8a0a8jArrAE#q=life+expentency+canada. [accessed 2017 Jun 13]. <http://www.statcan.gc.ca/tables-tableaux/sum-som/l01/cst01/health26-eng.htm>.
- Heath III H. 2017. The Past, Present, and Uncertain Future of Therapeutic Innovation in Osteoporosis. In: *Osteoporosis*. Fourth Edi. Elsevier. p. 1987–1995.
- Heiner AD. 2008. Structural Properties of Fourth-Generation Composite Femurs and Tibias. *J. Biomech.* 41:3282–3284. doi:10.1016/j.jbiomech.2008.08.013.
- Heiner AD, Brown TD. 2001. Structural Properties of a New Design of Composite Replicate Femurs and Tibias. *J. Biomech.* 34:773–781. doi:10.1016/S0021-9290(01)00015-X.
- Huiskes R, Rulmerman R, Van Lenthe GH, Janssen JD. 2000. Effects of Mechanical Forces on Maintenance and Adaptation of Form in Trabecular Bone. *Nature* 405:704–706. doi:10.1038/35015116.
- Johnell O, Kanis JA, Odén A, Sernbo I, Redlund-Johnell I, Petterson C, De Laet C, Jönsson B. 2004. Mortality After Osteoporotic Fractures. *Osteoporos. Int.* 15:38–42. doi:10.1007/s00198-003-1490-4.
- Kammerlander C, Neuerburg C, Verlaan JJ, Schmoelz W, Miclau T,

- Larsson S. 2016. The Use of Augmentation Techniques in Osteoporotic Fracture Fixation. *Injury* 47:S36–S43. doi:10.1016/S0020-1383(16)47007-5.
- Karim L, Hussein AI, Morgan EF, Bouxsein ML. 2017. The Mechanical Behavior of Bone. In: *Osteoporosis*. Fourth Edi. Elsevier. p. 431–452.
- Kowalski RJ, Ferrara LA, Benzel EC. 2001. Biomechanics of Bone Fusion. In: Mow VC, Huiskes R, editors. *Neurosurgical Focus*. Vol. 10. 3rd ed. Philadelphia, PA: Lippincott Williams & Wilkins. p. 1–7.
- Laurie. 2016. Be Aware of Bone Diseases in the Elderly. [accessed 2017 Jun 13]. <http://dyingandgrief.com/tag/osteoporosis-seniors-exercise-tips>.
- Marcus R, Dempster DW, Bouxsein ML. 2017. The Nature of Osteoporosis. In: *Osteoporosis*. Fourth Edi. Elsevier. p. 21–30.
- MatWeb. 2017. Sawbones Fourth-Generation Simulated Cancellous Bone (Rigid Polyurethane Bone). [accessed 2017 Jun 13]. <http://www.matweb.com/search/datasheettext.aspx?matguid=42cd25dc7f414bfc4432a8bcb969889>.
- OpenStax. 2017. Exercise, Nutrition, Hormones, and Bone Tissue. [accessed 2017 Jun 13]. <http://cnx.org/contents/g-vsB2Y2@4/Exercise-Nutrition-Hormones-an>.
- Ota T, Yamamoto I, Morita R. 1999. Fracture Simulation of the Femoral Bone using the Finite-Element Method: How a Fracture Initiates and Proceeds. *J. Bone Miner. Metab.* 17:108–112. doi:10.1007/s007740050072.
- Papini M, Zdero R, Schemitsch EH, Zalzal P. 2007. The Biomechanics of Human Femurs in Axial and Torsional Loading: Comparison of Finite Element Analysis, Human Cadaveric Femurs, and Synthetic Femurs. *J. Biomech. Eng.* 129:12. doi:10.1115/1.2401178.
- Public Health Agency of Canada. 2010. What is the Impact of Osteoporosis in Canada and What are Canadians Doing to Maintain Healthy Bones? Public Health Agency of Canada. [accessed 2017 Jun 13]. <https://www.canada.ca/en/public-health/services/chronic-diseases/osteoporosis/what-impact-osteoporosis-what-canadians-doing-maintain-healthy-bones.html>.
- Quenneville CE, Greeley GS, Dunning CE. 2010. Evaluation of Synthetic Composite Tibias for Fracture Testing Using Impact Loads. *Proc. Inst.*

Mech. Eng. H. 224:1195–1199. doi:10.1243/09544119JEIM736.

Ramos A, Simões JA. 2006. Tetrahedral Versus Hexahedral Finite Elements in Numerical Modelling of the Proximal Femur. *Med. Eng. Phys.* 28:916–924. doi:10.1016/j.medengphy.2005.12.006.

Schemitsch EH. 2008. The Effect of Screw Pullout Rate on Screw Purchase in Synthetic Cancellous Bone. *J. Biomech. Eng.* 131:024501. doi:10.1115/1.3005344.

Sharcnet. 2017. Choosing Between Linear and Higher Order Elements. Sharnet.ca. [accessed 2018 Aug 4]. https://www.sharcnet.ca/Software/Ansys/17.0/en-us/help/ans_mod/Hlp_G_MOD2_4.html.

Singh AP. 2017. Femur Anatomy and Attachments. *Bone Spine*. [accessed 2018 Aug 3]. <https://boneandspine.com/femur-anatomy-and-attachments/>.

Viceconti M, Bellingeri L, Cristofolini L, Toni A. 1998. A Comparative Study on Different Methods of Automatic Mesh Generation of Human Femurs. *Med. Eng. Phys.* 20:1–10. doi:S1350-4533(97)00049-0 [pii].

Wille H, Rank E, Yosibash Z. 2012. Prediction of the Mechanical Response of the Femur With Uncertain Elastic Properties. *J. Biomech.* 45:1140–1148. doi:10.1016/j.jbiomech.2012.02.006.

World Health Organization. 2004. WHO Scientific Group on the Assessment of Osteoporosis at Primary Health Care Level. In: Summary Meeting Report. Brussels, Belgium. [accessed 2017 Jun 13]. <http://www.who.int/chp/topics/Osteoporosis.pdf>.

Zdero R, Elfallah K, Olsen M, Schemitsch EH. 2009. Cortical Screw Purchase in Synthetic and Human Femurs. *J. Biomech. Eng.* 131:094503. doi:10.1115/1.3194755.

Zdero R, Rose S, Schemitsch EH, Papini M. 2007. Cortical Screw Pullout Strength and Effective Shear Stress in Synthetic Third Generation Composite Femurs. *J. Biomech. Eng.* 129:289–293. doi:10.1115/1.2540926.

CHAPTER 2 – DESIGN OF TESTING APPARATUS

Overview: *This chapter details the methods used for evaluating bones, and the development of a series of custom jigs for use in four-point bending, torsion, axial compression, and screw pullout; used to perform the experimental studies found in Chapter 3.*

2.1 Introduction

The bones of the human body have unique properties. The material is immensely complex, with microarchitecture constantly remodelling itself to repair damage and best suit loading, resulting in properties that are anisotropic, inhomogeneous, and strain-rate dependent, making it difficult to model and test. The femur, for example, undergoes axial loading and bending during standing and walking, torsion when rising from a chair, and screw stress during loading after a fracture plate has been implanted. The resultant intervariability of specimens also muddles comparisons, necessitating large sample sizes. The intricate geometry of bones also complicates standard testing methods with undesirable loading conditions in the bone, such as bending during axial compression of the femur.

Two common measurement outcomes in assessing bones are stiffness and rigidity values, which can be determined for items with complex geometries, making them more suitable for comparison across multiple sample populations. These values can be calculated with basic apparatus information and load and displacement data.

This chapter outlines the development of custom jigs designed to facilitate these measurements in a controlled, repeatable manner, based on previous evaluation methods, for sets of synthetic and natural femurs.

2.2 Review of Previous Methods Evaluation Methods

2.2.1 Bending

To quantify flexural rigidity, one must decide between cantilevered, three-point bending, and four-point bending. Cantilevered was discarded because very little research is available in this loading mode, limiting comparisons to previous work.

Three-point bending (Figure 2.1 (a)) is easier to implement as it requires the manufacture of one less loading point. However, in 3-point bending, the maximum moment is applied at only one location: the central support. Due to the femur's irregular geometry, the maximum bending moment may not occur at this location, inducing high shear stresses near the mid-region (Karim et al. 2017), which may damage specimens.

Four-point bending (Figure 2.1 (b,c)) is similar but applies a constant moment across the two interior supports. Cristofolini *et al.* (1996) and Heiner and Brown (2001) conducted four-point bending using four rollers mounted to a material testing machine, with supports equally spaced at 62 mm for a total of 186 mm. This method was adapted for femurs from previous research used to assess the performance of medullary nails (Cristofolini *et al.* 1996). Proximal clamps were applied at the distal support to keep the femurs from rotating during testing.

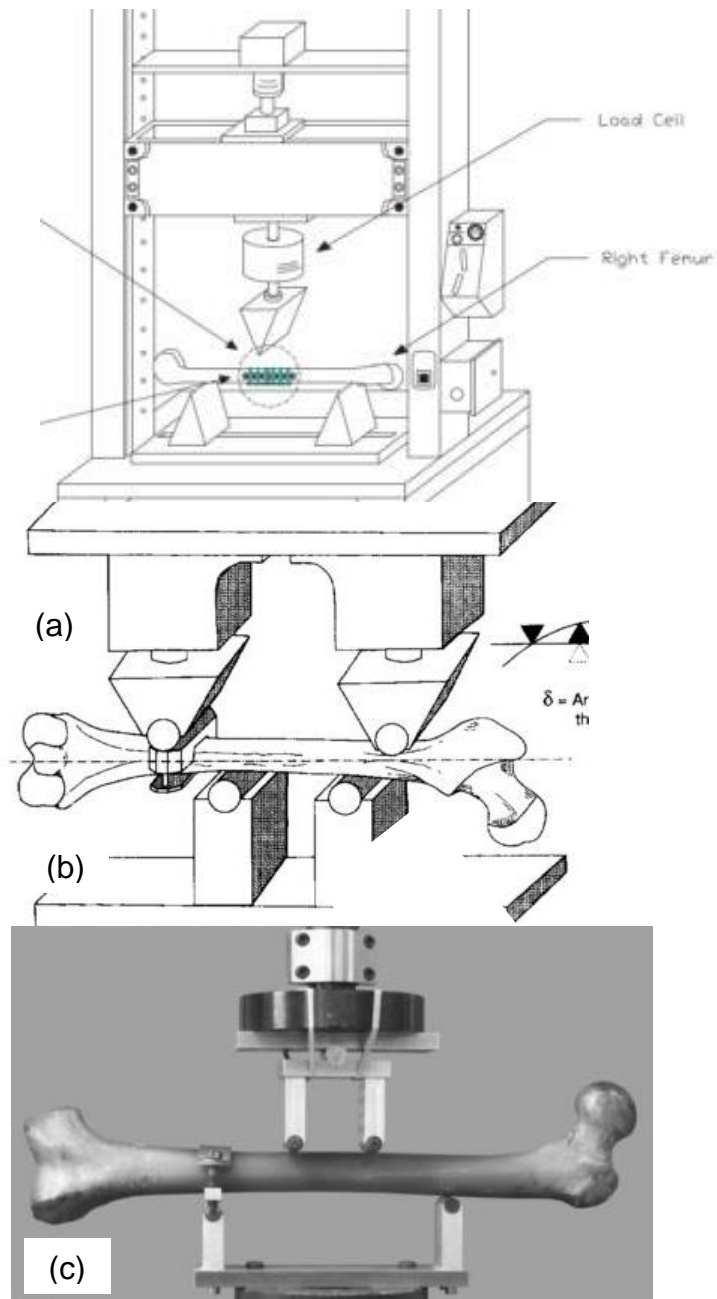


Figure 2.1: Bending Configurations

Design alternatives are outlined by Saunders (2015) (a), illustrating a femur in three-point bending. Four-point bending has been conducted by Cristofolini *et al.* (1996) (b) and Heiner (2001) (c).

2.2.2 Torsion

Researchers have applied torque to bones in previous studies using several distinct methods. The asymmetry in each femur creates local bending moments, making pure torsion nearly impossible to apply.

To test femurs in torsion, Cristofolini *et al.* (1996) clamped the proximal and distal ends in a materials testing machine, with the main axis of the femur visually aligned to the rotational axis of the Instron. Torque was applied to create an external rotation in the proximal end of the femur via a torsional load plate and an angular encoder (Figure 2.2 (a)).

Heiner and Brown (2001) potted both the proximal and distal ends of the femur, with 30.5 cm between pots (Figure 2.2 (b)). Femurs were aligned prior to distal potting with a mold attached to the testing machine, which also held the femurs vertically, along the torsional axis of the testing machine. The bones were constrained such that only axial displacement was possible, described as allowing the bones to “float”. Torque was applied creating internal rotation at the proximal end. A similar setup was suggested by Saunders (2015). The use of potting for both the proximal and distal ends reduces specimen variability, but constrains analysis to the diaphysis only, which may not be representative of torsional loading undergone *in vivo*.

The testing done in Zdero et al. (2010) measured both torsion and tension simultaneously using a materials testing machine in an attempt to assess the relationship between torque loading and tension. The femurs were not potted, relying instead on a ring with 12 protruding screws to secure the distal end (Figure 2.2 (c)). Torque and tension were applied with a hemispherical concave cup through which screws secured the femoral head. Femurs were potted with the centre of the femoral head directly over the lateral third of the medial femoral condyle and tested in both external and internal rotation. An advantage of this method is how it keeps the distal and proximal ends unrestricted, simplifying adjustments during and for any subsequent testing. This is limited, however, by the minor movements between the specimen and the screws, producing data scatter as the screws slide and vibrate.

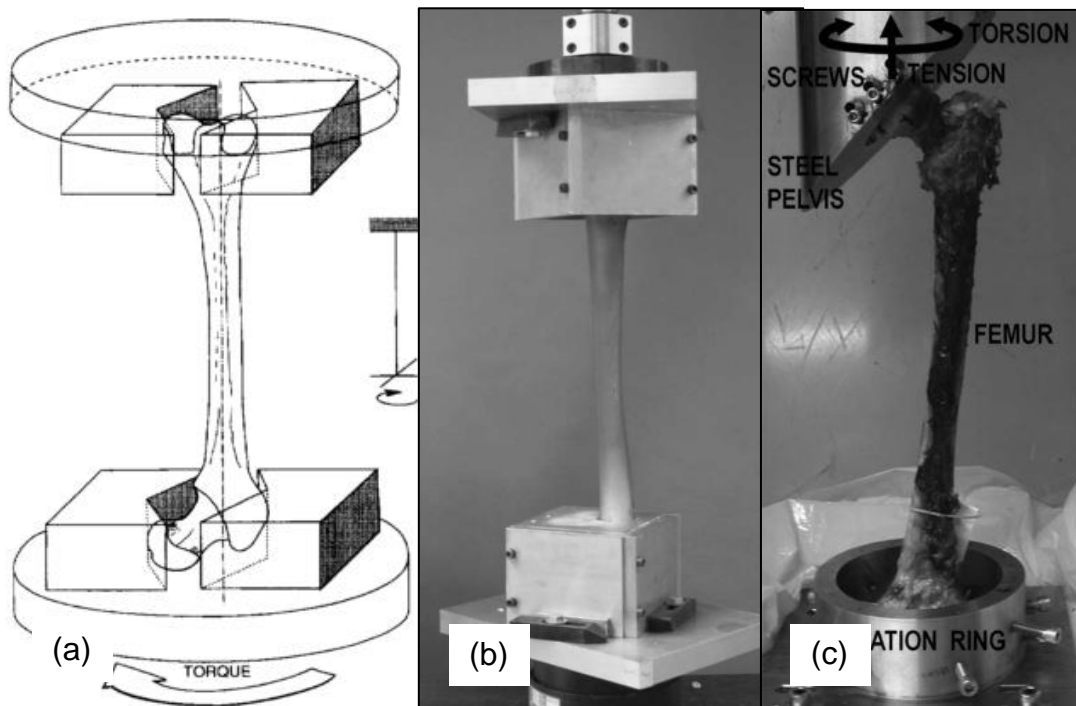


Figure 2.2: Torsion Configurations

Several methods are possible for assessing torsion response. Previous tests have clamped (a, Cristofolini et al. 1996) or potted (b, Heiner and Brown 2001) both ends of the specimen, which limits analysis to the diaphysis. Another alternative has been securing the femoral head to a metal cup representing the acetabulum via screws (c, Zdero et al. 2010).

2.2.3 Axial Compression

To test femurs in compression, previous studies have potted specimens in single-leg stance at 11° in adduction (Cristofolini et al. 1996; Heiner and Brown 2001); however, this can range “between 7 degrees and 25 degrees” (Shah et al. 2012). To improve repeatability, the femur can be oriented with a mold (Heiner and Brown 2001) or a jig before dental cement is poured.

Axial loading have been conducted using several fixation mechanisms, including potting (e.g. Cristofolini and Viceconti (2000)), platen (e.g. Heiner and Brown (1996)), and cup (e.g. Papini et al. (2007)). Axial loading along the mechanical axis also induces a bending moment that is typically ignored, likely why stiffness is reported, not rigidity. Potting the entire femoral head (Figure 2.3 (a)) protects the femoral head but limits the loading and analysis to the diaphysis, which was considered unacceptable for the present research. Platens (Figure 2.3 (b)) are simple to manufacture and produce the same load transmission regardless of specimen shape or size, and can be used on different types of bones. The flat surface, requires care in application: if the load is not distributed uniformly across the specimen surface, error can occur in the load readout due to the induced moment, as well as premature specimen failure from the concentrated load induced (Saunders 2015). Heiner and Brown (2001) also tested synthetic and

cadaveric femurs under axial loading. The femurs were loaded using a platen that conformed to the femoral head. A cup on the femoral head (Figure 2.3 (c)) provide a rough approximation of the acetabulum, without the cushioning and load distribution of cartilage present *in vivo*. The cup also limits the translation of the femoral head to the mechanical axis.

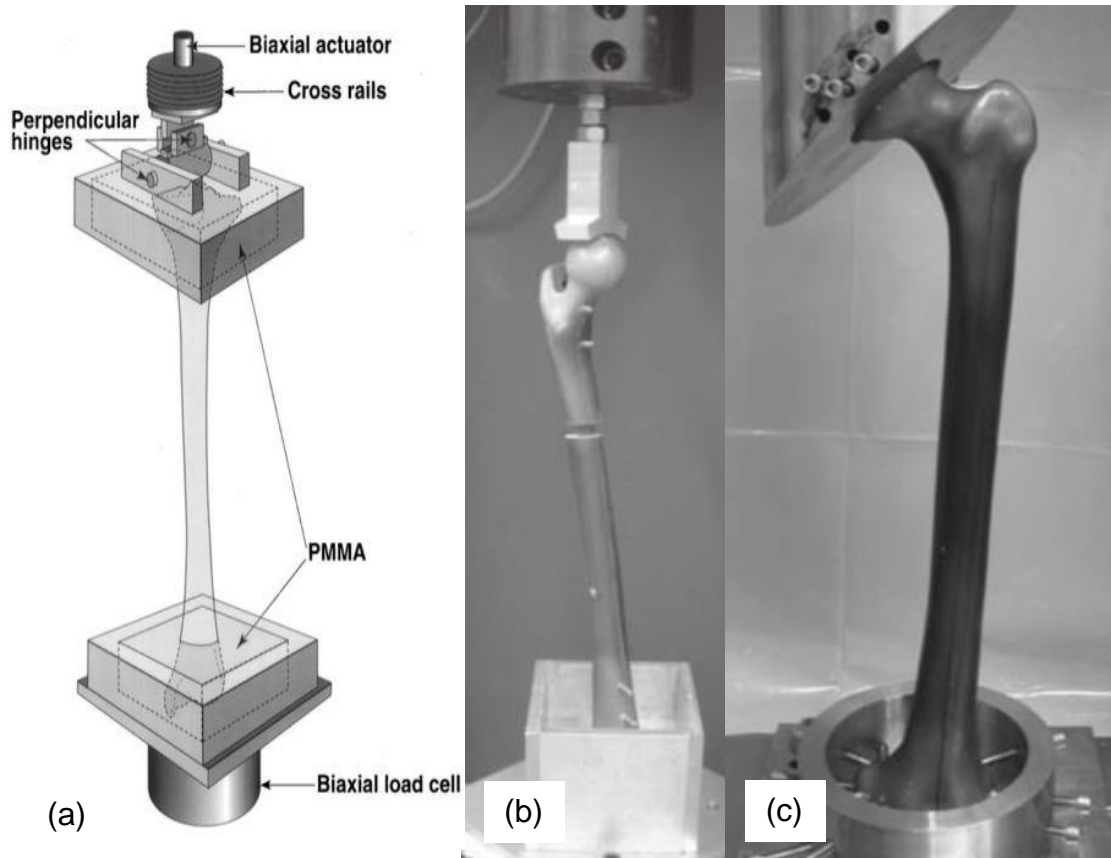


Figure 2.3: Axial Compression Configurations

Axial compression can be conducted with both ends potted (a, Cristofolini and Viceconti 2000), using a platen (b, Saunders 2015), or with a cup (c, Papini *et al.* 2007).

2.2.4 Screw Pullout

To conduct screw pullout tests, Zdero et al. (2007, 2009) utilized a jig that restrained the anterior surface of the bone on either side of the screw (Figure 2.4 (a)). The screw was inserted normal to the anterior surface of the femur and extracted with a materials testing machine. The horizontal plate through which the screw was extracted was used to prevent failure by bending in the femur.

Another design to facilitate screw pullout was put forth by Saunders (2015) (Figure 2.4 (b)). This design assessed a 'Bone Block', which was clamped laterally with threaded rods in a vice grip.

The flat configuration used by Zdero provides a large distribution of force over the anterior surface of the diaphysis. However, it is unclear what changes were made to accommodate screw-pullout at the proximal and distal ends of the femur, where contact areas would be significantly reduced due to the irregular geometry. More concentrated forces could cause localized crush in the contact areas, which would absorb some of the energy and artificially increase maximum screw pullout load.

While the Saunders method is relatively simple and fits a range of specimen sizes, it would not be practical without high-friction contact on each end. This would require relatively even, parallel specimen surfaces,

and induce transverse loading through the specimen, which would cause the specimen to deform, altering pullout results.

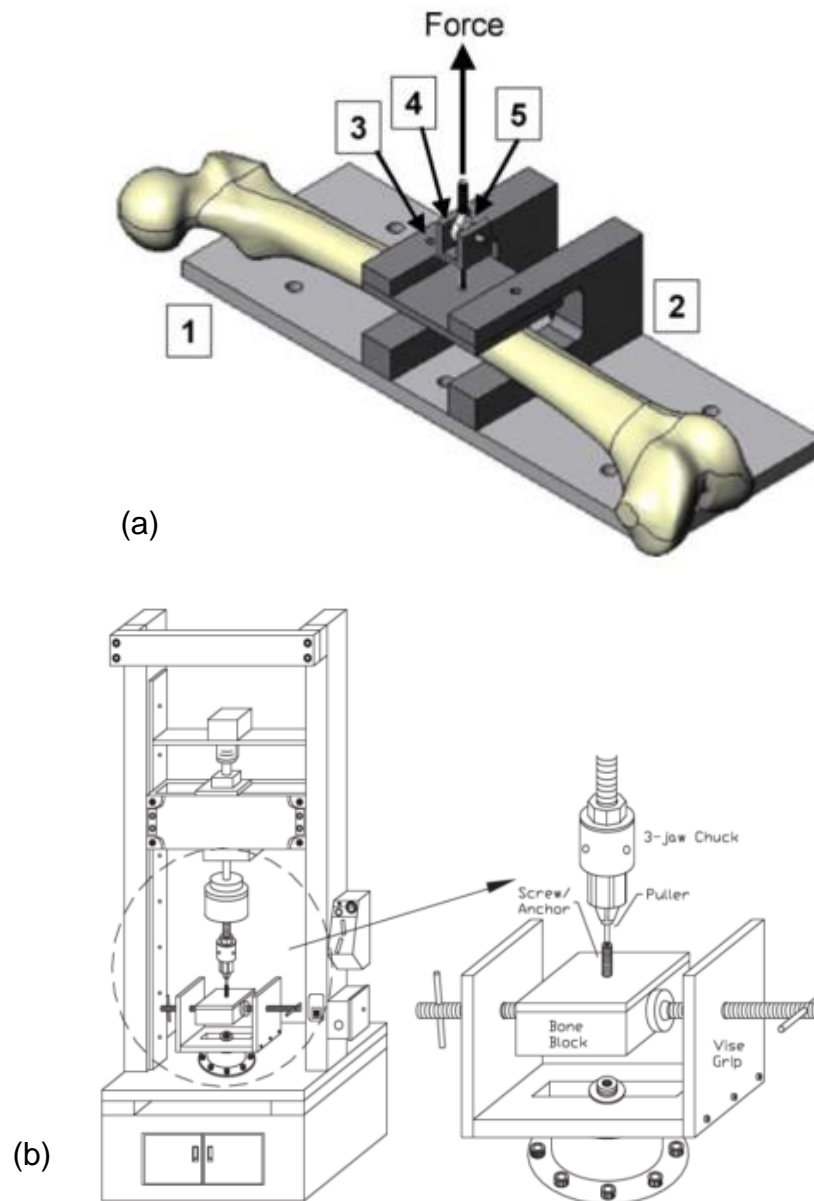


Figure 2.4: Screw Pullout Jig

A screw pullout jig from Zdero et al. (2007, 2009) (a) which includes a U-channel screw extraction grip (4) and a universal swivel pin (5). Screw pullout can also be conducted with an isolated bone block, allowing it to be clamped on either end (b, Saunders 2015).

2.3 Design and Assembly

2.3.1 Design Objectives

The objectives of the design and manufacture of the testing jigs were:

- 1) To create a flexible system that could accommodate a range of bone sizes and geometries in testing:
 - a. Four-point bending, with 62 mm between load points;
 - b. Torsion, with the lesser trochanter supported;
 - c. Axial compression, in single-leg stance; and
 - d. Screw pullout, with support around the screw-bone interface.
- 2) The system should be low in cost and easy to manufacture and clean.
- 3) The system must fit within the constraints of the Instron 5967 base.
- 4) To design a containment method and means of protection from projectile fragments during axial compression failure.

2.3.2 Multi-Purpose Components²

A modular system was designed, using a long, grooved base with keys and screws to mount L-brackets that could control load application during various modes. A smaller, complementary system was manufactured to

² Component drawings used for all testing configurations are listed in APPENDIX B: Technical Drawings.

adhere to the crossbeam of the materials testing machine, as needed. All components were made of aluminum, chosen for its rust resistance, light weight, and ease in machining. Unless indicated, all screws were 0.25" in diameter, as this was considered suitable for all future load requirements and the easiest to procure in all lengths.

2.3.3 Bending

Four L-brackets were used as loading points (Figure 2.5). The vertical feature of the L-bracket was ground to a 45° angle and rounded at the tip. Each tip was spaced 62 mm apart, as in previous research (e.g. Cristofolini et al. 1996; Heiner and Brown 2001; Heiner 2008), using lines etched in the base and confirmed with calipers. Supports were wide enough to allow for any bone diameter, while the distances between supports could be adjusted in the case of very short specimen length or for future studies of other bones.

An important inclusion in four-point bending was the implementation of rotation in the top platform to accommodate for the irregular geometry of the diaphysis. This rotation guaranteed equally distributed force across the two upper loading points, a key requirement in four-point bending to produce a constant moment across the diaphysis.

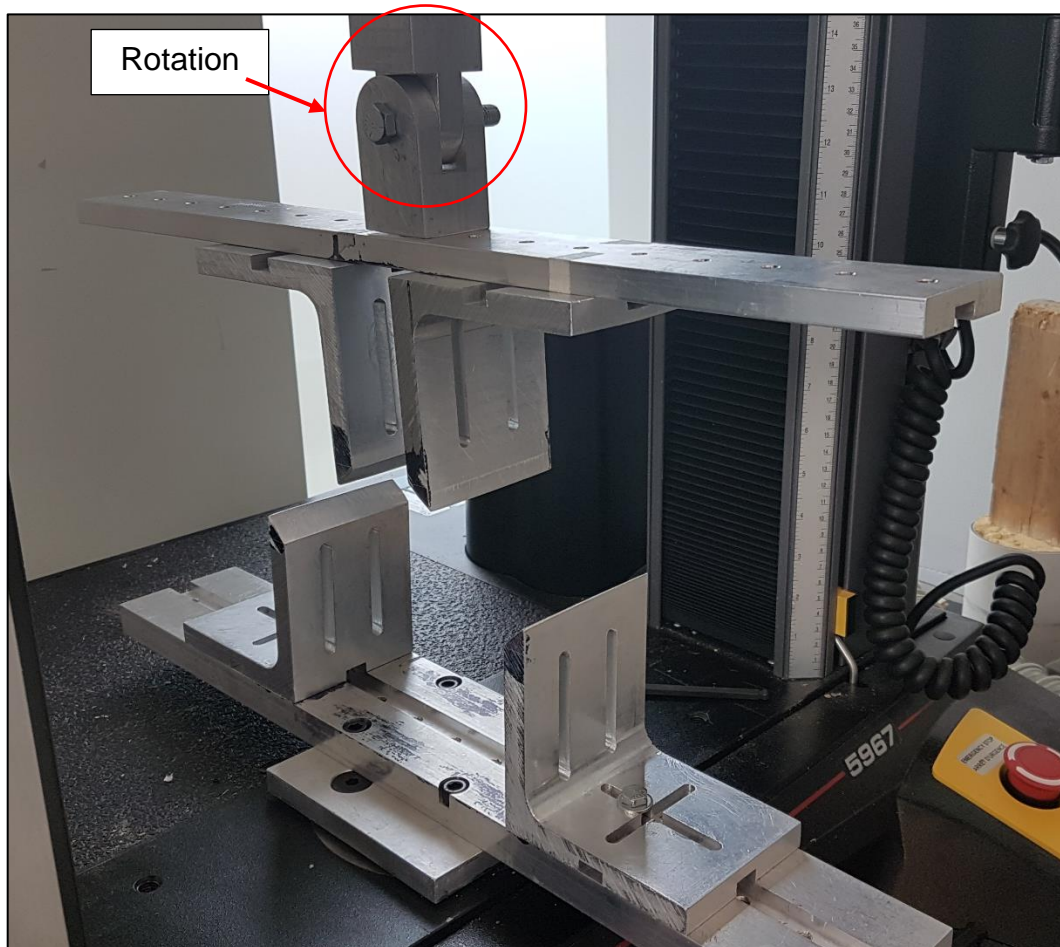


Figure 2.5: Four-Point Bending Assembly

The four-point bending test assembled with 62 mm distance between supports and allowed rotation in the top platform to equally distribute force over the irregular geometry of the femur.

2.3.4 Torsion

The Instron 5967 is only capable of vertical movement, making the methods implemented by Cristofolini *et al.* (1996), Heiner (2001), and Zdero *et al.* (2010) impossible. The method adopted required potting of the distal end, which would complicate bending testing due to the additional load, also likely requiring more intensive specimen restraint. In addition, the axial compression that preceded torsion testing made potting the proximal end of the femur (seen in Heiner and Brown (2001)) impractical; when access to the proximal end was necessary for axial compression testing. However, prior to testing, the distal femoral condyles were potted in square aluminum tube with the pot clamped with aluminum plates and threaded rods.

The L-brackets used in bending testing were designed to accommodate an aluminum plate to support the lesser trochanter during torsion testing (Figure 2.6). Two channels were milled along the vertical side, along with a corresponding slot of 2" length, perpendicular to the bending channel. These slots in the vertical feature would be used to secure an aluminum block at the required height to support the femur's lesser trochanter as loading was applied to the femoral head, creating rotation.

To apply loading, a 2.5" diameter aluminum cylinder was designed to attach to the crossbeam platform. A custom dental cement cast was made

for the anterior side of each femoral head, which distributed the load over the largest possible area of femoral head. Maintaining the integrity of the femoral head was imperative for axial loading and fracture analysis in the subsequent tests; if the femoral head was damaged in torsion, these tests would be compromised. The top platform was designed to be rotated to best align the aluminum cylinder to the cement cast, creating internal rotation at the proximal end as the crossbeam descended.

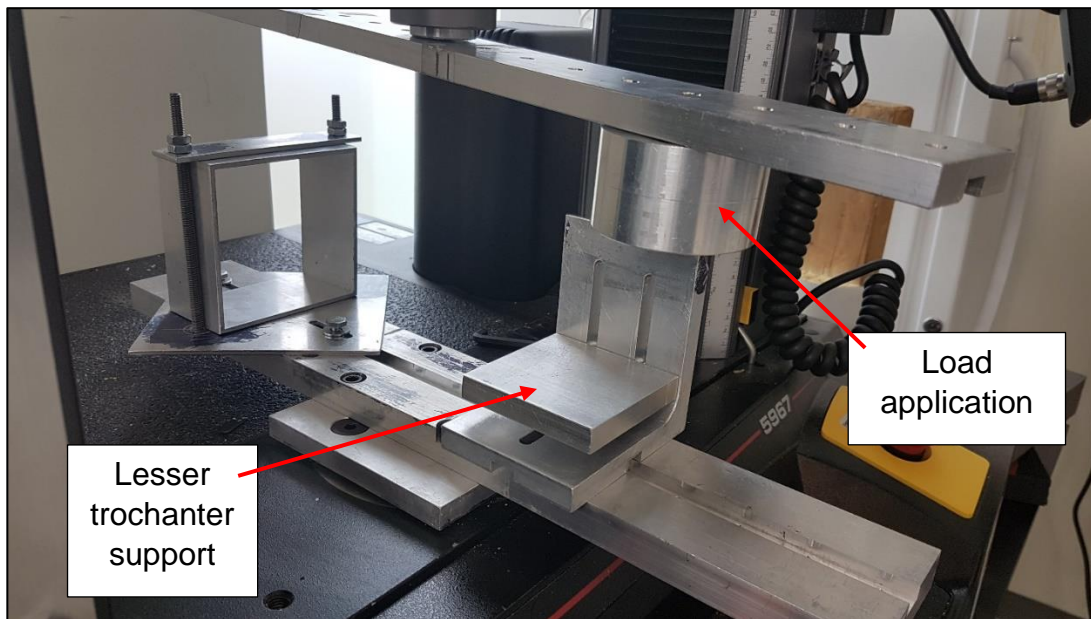


Figure 2.6: Torsion Assembly

Femurs were potted distally in square aluminum prior to torsion testing. The torsion assembly secured the aluminum tubing with an aluminum plate. Torsion could be applied by supporting the lesser trochanter (variable in height to accommodate bones of different sizes) and applying a load to the femoral head.

2.3.5 Axial Compression

A custom cup was created for axial compression, using similar geometry to a human acetabulum, a design very similar to that seen in previous research by Papini *et al.* (2007) (Figure 2.7). The cup was crafted from a 2.75" diameter aluminum cylinder cut at a 45° angle and then processed with a CNC mill. Two courses of CNC machining were required, first to remove the bulk of the material and then to refine the interior surface. After milling, the cup was thoroughly brushed and filed by hand to achieve a uniform surface finish. The cup was mounted directly to the Instron load cell without the crossbeam platform used for the other loading modes.

Jigs were designed assuming the specified order of testing (bending, torsion, then axial compression) and associated potting requirements. Potting was used to secure the specimen to the base of the materials testing machine using L-brackets and threaded rods to ensure the specimen would not move during offset axial compression. Each L-bracket had a wide rectangular hole in its base to allow for translational and rotational movement with which to properly align each specimen to the cup before being secured to the base platform.

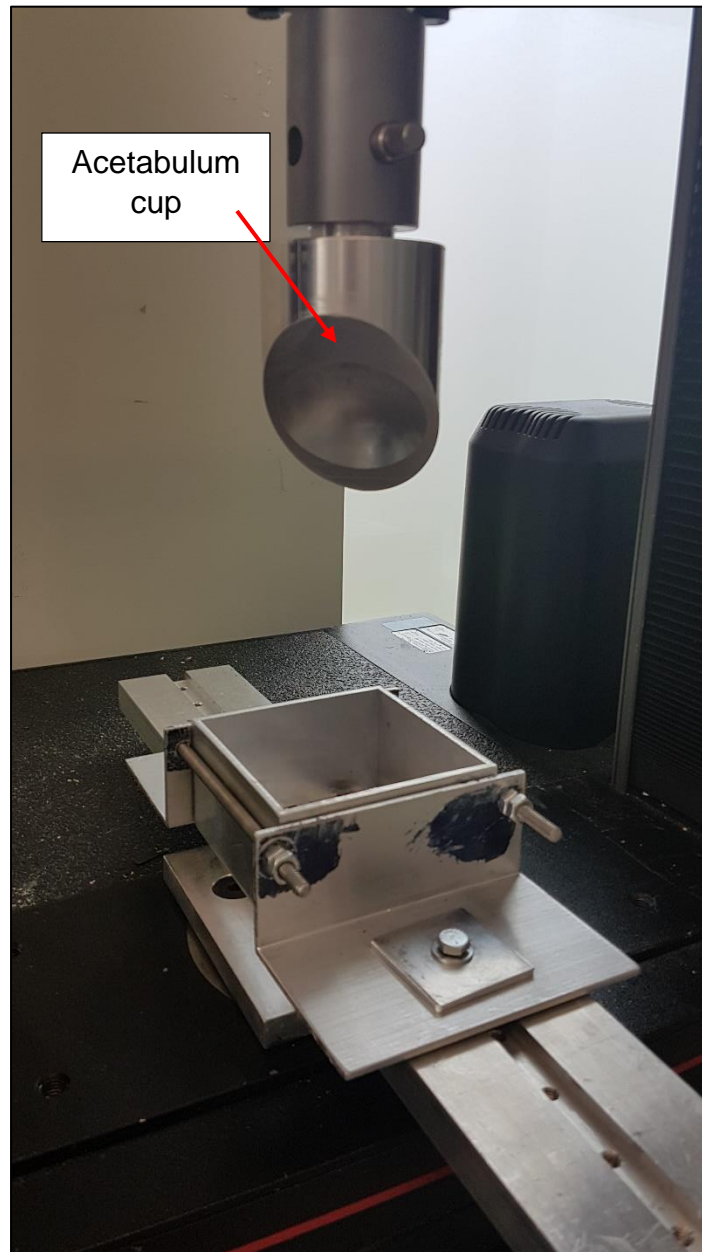


Figure 2.7: Axial Compression Assembly

L-brackets were used to secure the potting. Loading was applied to the femoral head with an aluminum jig representing an acetabulum.

2.3.6 Screw Pullout

The screw pullout assembly used the aluminum plate and L-bracket configuration seen in torsion, with the plate at the top of the bracket; paired to create a similar test setup to those of Zdero *et al.* (2007, 2009). Screws were provided DePuy Synthes (Synthes, Monument, Colorado, USA), described as self-tapping cortex screws 4.5 mm in diameter and 38 mm in length.

The pullout jig was designed with freedom of rotation via an eye bolt and U-block to prevent forces from developing inside the jig due to any misalignment between the screw and the load cell (Figure 2.8). Two plates with small cuts bracketed the cortical screw. The jig was designed with the plan that the epiphyses would be trimmed. The mid-diaphysis was chosen as the screw pullout location, similar to literature (*e.g.* Zdero *et al.* 2007; Zdero *et al.* 2009), while also isolating screw pullout to cortical tissue and providing a relatively uniform surface in contact with the aluminum plates. Fixtures were designed to support the diaphysis of the femur, with two plates to surround the 4.5 mm screw that provided reinforcement for the femur between the aluminum blocks to ensure failure occurred by screw pullout and not via bending.

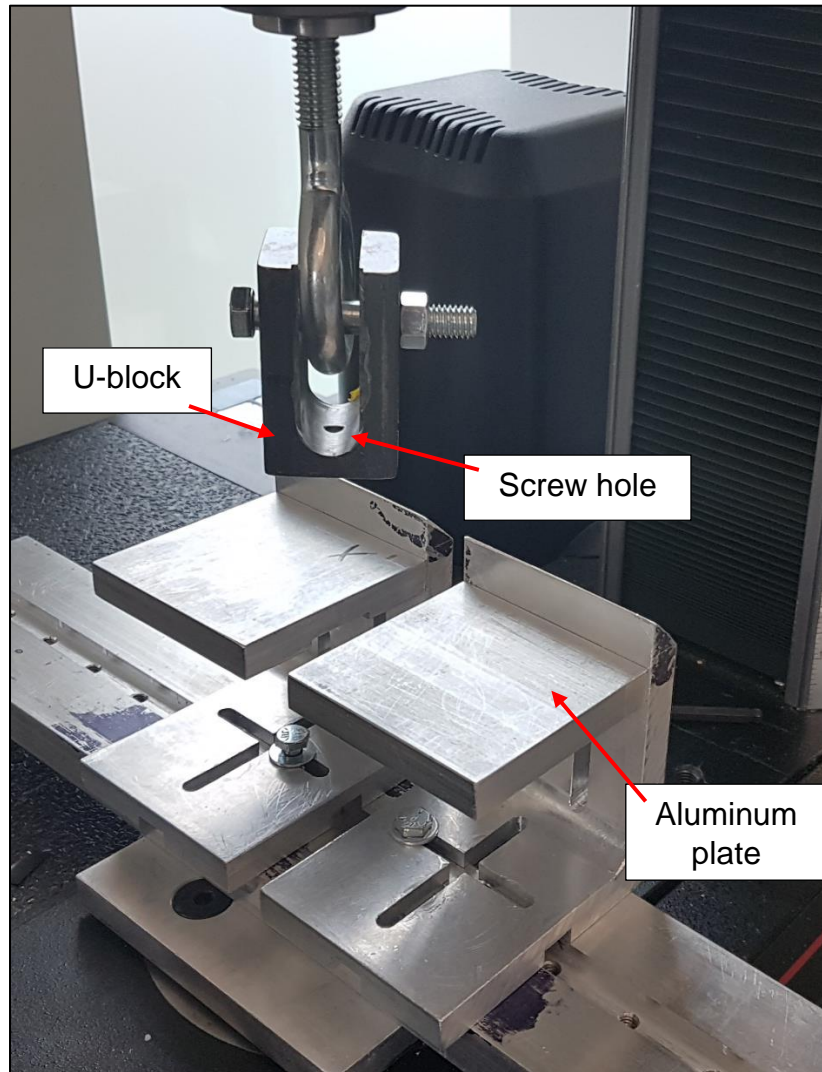


Figure 2.8: Screw Pullout Assembly

An eye bolt attached to a U-block that extracted the screw with the specimen restrained by two aluminum plates.

2.3.7 Polycarbonate Box

‘Safety is the overriding priority’ (manufacturing proverb). As synthetic femurs were expected to fracture with a brittle response, this posed safety concerns. A second safety consideration during the destructive testing was the potential for biological aerosols to be released during cadaveric tests. A system was needed that would act both as a shield from fragments and as a method of containment for aerosols, which could then be filtered via the lab’s HVAC system.

There were several design objectives:

- Effective against fragment projectiles;
- Could be joined by a hose to the HVAC system installed in the lab;
- Made of materials that can be decontaminated easily, such as plastic;
- Easily assembled and disassembled;
- Oversized footprint, making it useful in other experimental testing, while still being contained within the Instron;
- Must secure to the Instron; and
- At least 18” in vertical movement, with a minimum height of 18”.

The final design was a box made of polycarbonate with wooden boards on the top and bottom, plated with polycarbonate (Figure 2.9). The top (mobile) box was supported by the crossbeam of the Instron. Two holes were cut to accommodate the cotter pin extending from the load cell and to act as an exhaust vent. Polycarbonate was chosen for its clarity, ease of cleaning, and high impact resistance. Three pieces of 1/8" polycarbonate were attached along the sides and rear, extending 18" vertically, based on the thickness used in previous blast shielding available in the lab. The bottom board had a square hole cut to accommodate the pre-existing aluminum plate that attached to the Instron. The 0.25" thick polycarbonate was attached to the sides and rear, each 18" tall; 0.25" being the minimum available thickness able to stand vertically with minimal support. The bottom polycarbonate surrounded the top polycarbonate boards at 0.25" gaps, providing airflow and blast protection, even when fully extended. Finally, a 0.25" thick polycarbonate 'door' was attached to the Instron frame with t-nuts and an aluminum hinge, which could swing shut and be secured with two hasps, thus providing protection but ease of access for setup and specimen positioning.

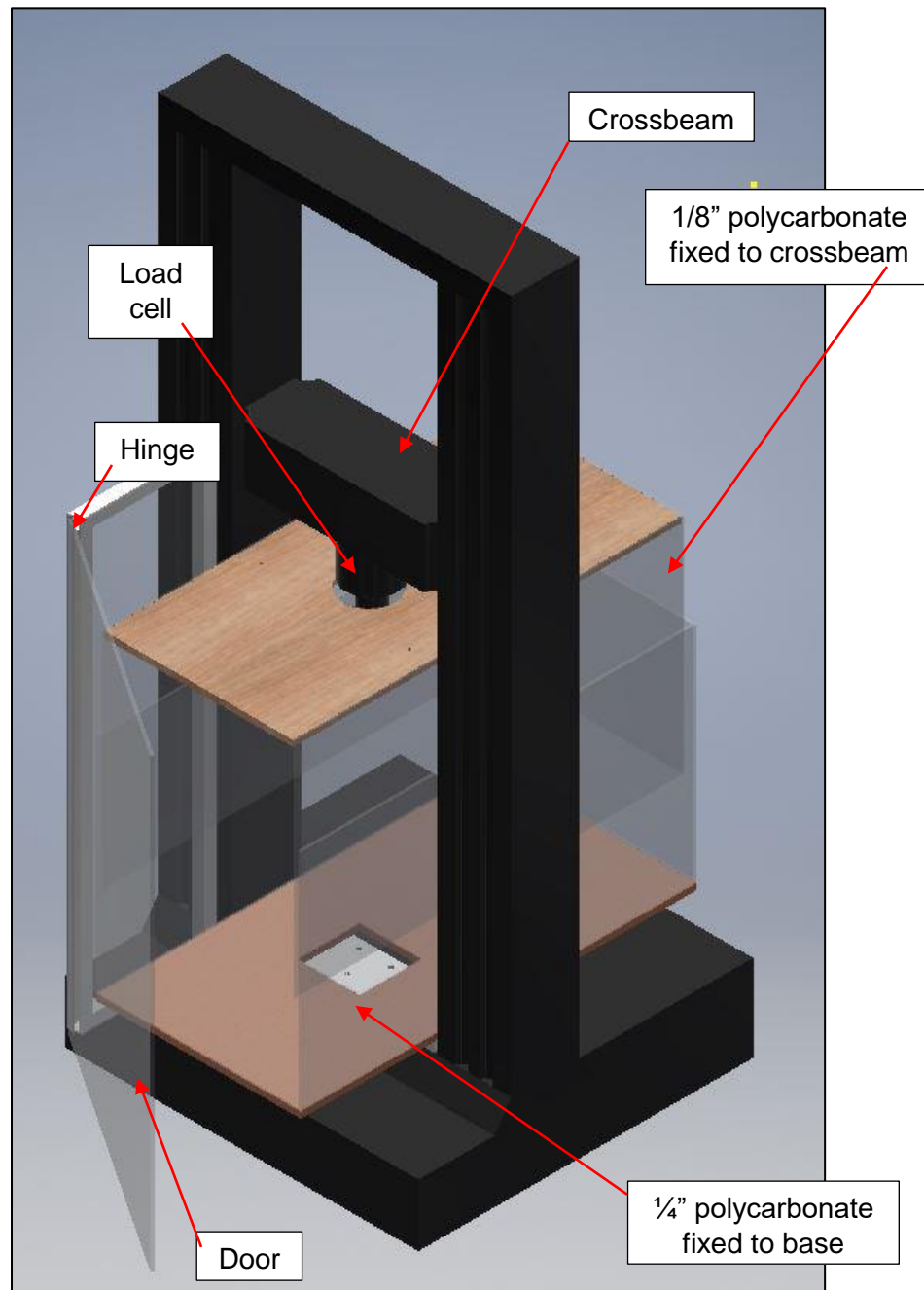


Figure 2.9: Blast Shield Design

AutoCAD Inventor mock-up of the completed blast shield assembled within the Instron.

2.4 Discussion

This work developed a suite of jigs suitable for a broad range of testing methods on a variety of femur sizes and geometries. Each configuration fits within the enclosure of the Instron base and uses standard, common fasteners to join components. In some configurations, such as bending and screw pullout, the fine adjustment of components was not required as the configuration was independent of size and shape. However, torsion testing and axial compression were influenced by the size and geometry of the femur, requiring the ability to shift the apparatus to properly align with the specimen, while still being properly restrained. It is in this way that repeatable testing and result consistency can be achieved, even with test specimens as variable as human bones.

The bending configuration was recreated with the same specifications as those recorded in previous research, using the same number of and distance between supports. This should provide a solid basis of comparison with literature, allowing for further insight into the characteristics of the samples to be assessed.

Previously used torsion configurations could not be achieved due to the limitations of the available equipment. A new method was developed that could accommodate a variety of human femurs without potting both

ends of the femur. This was advantageous in that it allowed investigation into the overall bone torsional response, from femoral head through the neck to the diaphysis, but did not allow isolated torsional loading to be applied. However, it should be recognized that previous authors (e.g. Cristofolini and Viceconti 2000; Heiner 2008) have found precise alignment of a bone along its long axis for true torsional testing to be extremely challenging, and as such a modified torsional test may allow a more consistent investigation of a more natural loading mode to the femur.

Similarly, the methods used in axial compression in the literature were modified. To better align testing with previous research, a cup loosely representing the acetabulum was created using a CNC machine, albeit with a larger diameter than necessary and no cartilage to distribute the load, thus likely resulting in a point load configuration and an expected greater level of friction than *in vivo*.

Although several screw pullout methods are available, the method utilized by Zdero et al. (2007, 2009) was selected due its ease of execution. The same method of screw extraction was utilized, including the planned trimming of some sections of bone. The manufacture of other support plates is relatively low cost; more plates could be produced with different geometries that would allow other screw sizes to be tested.

Blast shielding was also produced, which maximizes the available work area limited by the footprint of the testing machine base. The shielding offers 18” of vertical movement, allowing objects up to 36” long to be tested without compromising safety. It can be attached to the lab’s HVAC system to protect against biological aerosol generation during cadaveric fracture. The polycarbonate surfaces are easy to clean, with the system able to be removed with low effort.

2.5 Conclusion

This chapter has outlined the development of a system that can facilitate multiple tests over a wide range of specimen sizes and geometries using a minimal number of parts. The system can also be used in conjunction with blast shielding for a variety of future studies of other natural and synthetic samples.

2.6 References

- Cristofolini L, Viceconti M. 2000. Mechanical Validation of Whole Bone Composite Tibia Model. *Pergamon* 2:525–535. doi:10.1227/01.NEU.0000297048.04906.5B0.
- Cristofolini L, Vicecontia M, Cappello A, Toni A. 1996. Mechanical Validation of Whole Bone Composite Femur Models. *J. Biomech.* 29:525–535.
- Heiner AD. 2008. Structural Properties of Fourth-Generation Composite Femurs and Tibias. *J. Biomech.* 41:3282–3284. doi:10.1016/j.jbiomech.2008.08.013.
- Heiner AD, Brown TD. 2001. Structural Properties of a New Design of Composite Replicate Femurs and Tibias. *J. Biomech.* 34:773–781. doi:10.1016/S0021-9290(01)00015-X.
- Karim L, Hussein AI, Morgan EF, Boussein ML. 2017. The Mechanical Behavior of Bone. In: *Osteoporosis*. Fourth Edi. Elsevier. p. 431–452.
- Papini M, Zdero R, Schemitsch EH, Zalzal P. 2007. The Biomechanics of Human Femurs in Axial and Torsional Loading: Comparison of Finite Element Analysis, Human Cadaveric Femurs, and Synthetic Femurs. *J. Biomech. Eng.* 129:12. doi:10.1115/1.2401178.
- Saunders MM. 2015. *Mechanical Testing for the Biomechanical Engineer: A Practical Guide*. Enderle JD, editor. Morgan & Claypool Publishers.
- Shah S, Bougherara H, Schemitsch EH, Zdero R. 2012. Biomechanical Stress Maps of an Artificial Femur Obtained using a New Infrared Thermography Technique Validated by Strain Gages. *Med. Eng. Phys.* 34:1496–1502. doi:10.1016/j.medengphy.2012.02.012.
- Zdero R, Elfallah K, Olsen M, Schemitsch EH. 2009. Cortical Screw Purchase in Synthetic and Human Femurs. *J. Biomech. Eng.* 131:094503. doi:10.1115/1.3194755.
- Zdero R, McConnell AJ, Peskun C, Syed KA, Schemitsch EH. 2010. Biomechanical Measurements of Torsion-Tension Coupling in Human Cadaveric Femurs. *J. Biomech. Eng.* 133:014501. doi:10.1115/1.4002937.
- Zdero R, Rose S, Schemitsch EH, Papini M. 2007. Cortical Screw Pullout Strength and Effective Shear Stress in Synthetic Third Generation Composite Femurs. *J. Biomech. Eng.* 129:289–293.

doi:10.1115/1.2540926.

CHAPTER 3 - THE MECHANICAL PROPERTIES OF OSTEOPOROTIC SYNTHETIC AND CADAVERIC FEMURS

Overview: *This chapter details the testing conducted using the jigs constructed in Chapter 2 to determine the mechanical and structural properties of synthetic bones and their ability to serve as a surrogate for natural bones in future testing. Bones were evaluated under bending, torsion, axial compression to failure, and screw pullout. A discussion of the future orthopaedic applications of the synthetic femurs concludes the chapter.*

3.1 Introduction

Knowledge of bone properties and response to loading has utility in the design and analysis of many products and safety implementations. Orthopaedic devices are frequently evaluated using cadavers, but conclusions can be limited as a result of high specimen variability due to influences of gender, age, medical history, diet, and exercise level, among others. Sample sizes are also typically quite small in testing, limited by cost and availability. Such restrictions have prompted the development of alternatives such as synthetic models (Sawbones, Pacific Research

Laboratories, Vashon, WA, USA), designed for repeatable testing and high availability at a lower cost than cadavers. Previous testing has proven Sawbones to be a reasonable replacement for cadavers, especially for comparative analyses, given their much lower variability (Cristofolini et al. 1996; Cristofolini and Viceconti 2000; Heiner and Brown 2001; Heiner 2008).

The societal burdens of osteoporosis are expected to increase by more than three-fold by 2054, tied to an aging population (World Health Organization 2004). Osteoporosis is a degenerative disease, reducing the stiffness, elastic energy absorption, and yield stress of bone (Dickenson et al. 1981), and is typically seen in an older population.

One of the consequences of osteoporosis is a significantly increased susceptibility to fracture. Prevention of such fractures has been correlated to a higher standard of living, maintenance of health, and independence (World Health Organization 2004). The femur is one of the primary points of analysis for diagnosing osteoporosis. However, diagnosis can be difficult and current methods cannot always accurately predict the likelihood of fracture.

Another concern for aging populations is osteoarthritis, which also often requires hip replacements. In fact, almost 56 000 Canadians received

total or partial hip replacements in 2016-2017, increasing from 42 000 in 2010-2011 (Canadian Institute for Health Information 2018). The implants used for hip replacement are designed and evaluated based on normal, 'healthy' bone, which may be unsuitable for osteoporotic bone. For example, some hip replacements are dimpled to improve integration and healing with trabecular bone, but the extreme porosity from osteoporosis may require different dimple sizing or make this characteristic entirely irrelevant. To evaluate orthopaedic devices for an aging osteoporotic population, an appropriate surrogate that properly replicates the mechanical response of natural osteoporotic bone needs to be developed as a means to progress effective treatment option and ultimately increase independence and quality of life for its sufferers. Unfortunately, to the author's knowledge, the mechanical properties of osteoporotic bone are not readily available in the literature.

Pacific Research Labs is the primary producer of synthetic models, with their fourth-generation femur validated as representative of the general population; used in the design of orthopaedics. Two new models have been created in a small batch based on alterations to attempt to represent an osteoporotic population, which now must be evaluated.

The purpose of this study was to quantify and compare the mechanical properties of synthetic and human osteoporotic femurs using four methods of testing: bending, torsion, axial compression to failure, and screw pullout.

3.2 Methods

3.2.1 Specimens

3.2.1.1 Cadavers

Five fresh-frozen isolated cadaveric femurs were obtained (female, mean age 84.4 ± 8.8 years, no history of femoral trauma or surgery) from Science Care Inc. (Science Care, Phoenix, AZ, USA), alongside initial t-score assessments. All specimens were then Dual-Energy X-Ray Absorptiometry (DXA) imaged at McMaster Children's Hospital (Hamilton, Ontario) to confirm t-scores (Table 3.1), presented in APPENDIX C: DXA Scan Data.

Prior to testing, femurs were thawed at room temperature for approximately 12 hours (e.g. Papini et al. 2007; Zdero et al. 2009) and were hydrated during testing (e.g. Bayraktar et al., 2004; Li & Aspden, 1997) by wrapping each specimen in saline-soaked paper towels.

3.2.1.2 Synthetic Bones

Standard fourth generation Sawbones (model number: 3403) were created using a cortical bone analog composed of a mixture of short glass fibers and epoxy resin and a cancellous bone represented by a solid rigid polyurethane foam. Each standard fourth generation Sawbone was representative of the external geometry of the left femur of a 50th percentile male (Figure 3.1). To fabricate the bones, the short glass fiber and epoxy resin was pressure injected around the foam core (MatWeb 2017). There were several unique morphological features in the synthetic specimens as a result of the casting process, such as a less distinguished linea aspera, as well as pilot holes and cast lines. The Sawbones also contained a hollow, curved centre channel representing the intramedullary canal, with an opening at the distal end with an approximate diameter of 13 mm through the foam and glass-resin.

Two series of 10 synthetic femurs (totalling 20 femurs, Pacific Research Labs, Vashon, WA, USA) were tested, visually differentiated by the colour of their cortical bone – brown and blue. The 3403 composite femurs (brown) had a wall thickness reduced by approximately 2-5 mm in the diaphysis while the 3503 (blue) composite femurs had both reduced

cortical stiffness and similar wall reductions. Synthetic bones were tested in dry conditions and stored at room temperature.

Table 3.1: Cadaveric Specimen Information Table

Five whole female human femurs were received and DXA scanned by Science Care Inc. and confirmed at the McMaster Children's Hospital to ensure they were suitably osteoporotic. Specimen 171987 was included despite falling short of the -2.5 t-score threshold as the neck t-score was -3.0, indicating a high level of osteoporosis in the neck.

Specimen Number	Gender	Age	Side	Total T-Score (Science Care, McMaster)	Neck T-Score (Science Care, McMaster)
161569	F	76	L	-3.6, -3.2	-4.3, -4.0
161607	F	80	L	-2.6, -2.1	-2.8, -2.4
171519	F	76	L	-3.0, -2.1	-4.6, -3.7
171987	F	99	R	-2.4, -2.6	-3.0, -3.2
172202	F	85	L	-2.7, -2.1	-1.7, -3.2

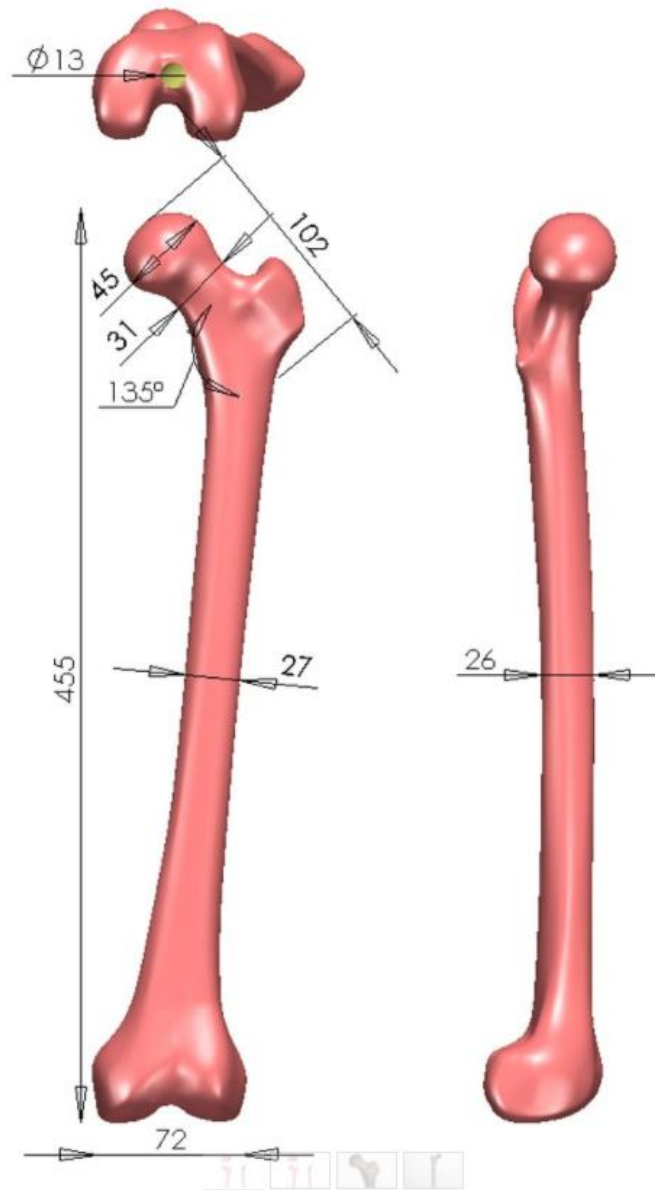


Figure 3.1: Fourth Generation Sawbone Femur Geometry

The anatomy of the femur is irregular and complex. Several critical dimensions (in millimetres) are listed, representative of the standard fourth generation synthetic femurs which (to our knowledge) share external dimensions with the samples used in this study (Sawbones 2017).

3.2.2 Potting

Femurs were aligned using a previously-developed custom testing jig (Figure 3.2(a)). The jig used four threaded rods to provide support to the bone and allow fine adjustment in all planes. Laser levels were used to align the long axis of the shaft against the threaded rods while ensuring that the coronal plane of the specimen was vertical. The long axis of the femur was aligned at 11° in adduction to simulate single-leg stance (Cristofolini et al. 1996). A protractor, as well as laser levels, were used, aligning the midline of the femoral head (corresponding to the sagittal plane) over the midpoint of the medial condyle.

After bending testing was conducted (see Section 3.4.1), specimens were potted at the distal end in 4"x4" aluminum tubing with 1/8" wall thickness and an approximate height of 2". Square metal tubing was selected to simplify torsion testing. Specimens were potted to an approximate depth of 1.5" based on Saunders Potting Guide (Saunders 2015), covering the distal epiphysis of the femur completely with dental cement (Denstone Golden, Heraeus Kuler, South Bend, IN, USA). The cement was left undisturbed for 20 minutes, at which point it was moved to a nearby location and left to sit for several hours.

**Figure 3.2: Potting Images**

Potting alignment procedure, making use of laser levels and anatomical geometry (a) to set each specimen at 11° adduction without flexion/extension. Anterior (b) and lateral (c) views of the potted femurs prior to torsion testing demonstrate the consistency of the potting procedure.

3.2.3 Testing Protocols

Several testing protocols were developed in accordance with previous research to assess the mechanical properties of each femur. Testing was conducted using an Instron 5967 materials testing machine (Instron, Norwood, MA) with a 30 kN load cell. Testing protocols were first validated on a potted piece of lumber to ensure the program would behave as expected and to avoid damaging specimens. The specimens were tested in the same sequence: bending (in two planes, AP and ML), torsion, axial compression, screw pullout (Figure 3.3). Bending was completed first because it did not require the specimen to be potted. Torsion was second, being a non-destructive test that required potting to properly secure the specimen during testing. Axial compression was the third test conducted, finishing only after the specimen had fractured. Screw pullout was the final test, where the proximal and distal 30% were removed to facilitate placement in the testing fixture.

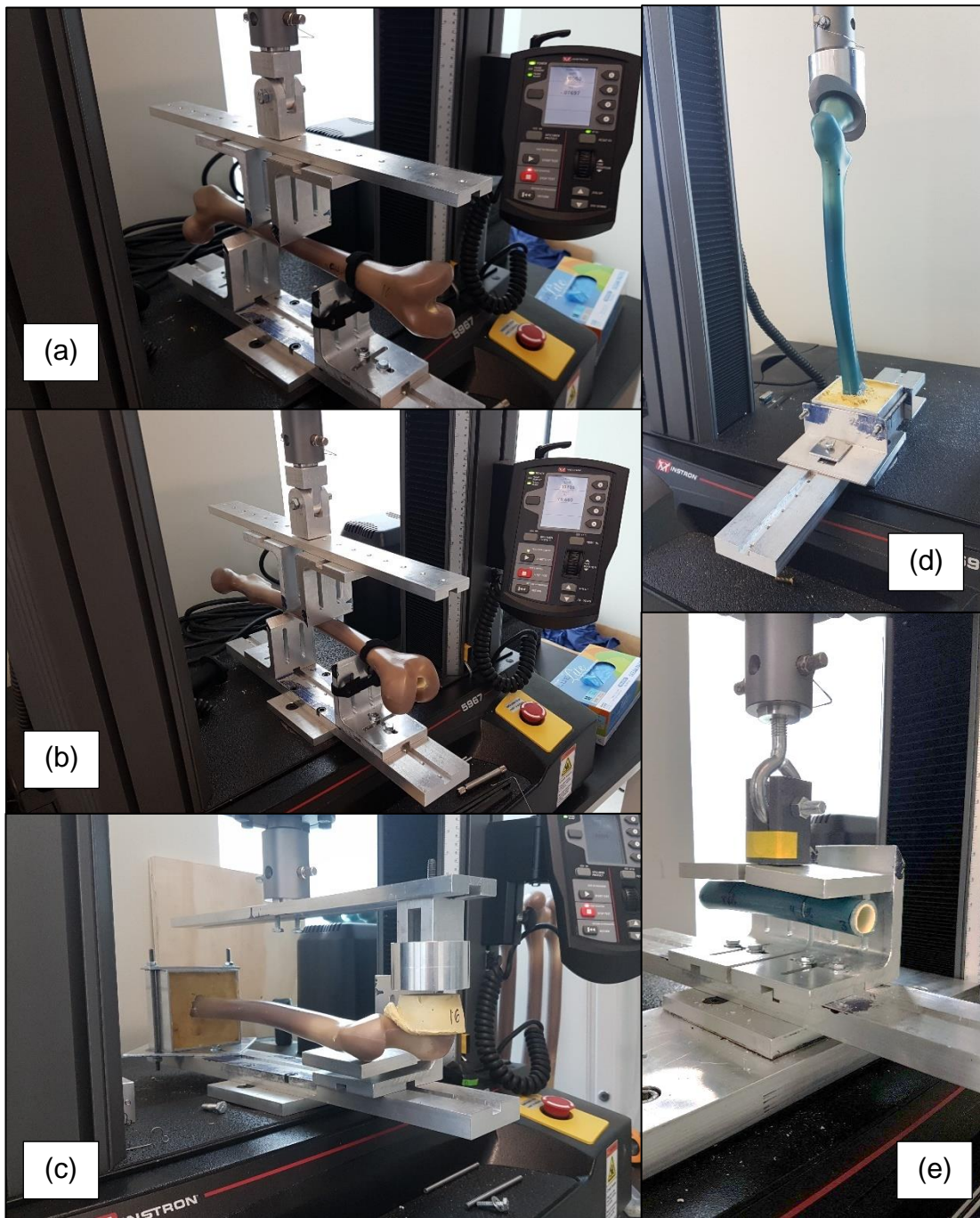


Figure 3.3: Testing Images

The images above represent the testing order, beginning with ML bending (a), AP bending (b), before torsion (c) and axial compression (d), then concluding with screw pullout (e).

3.2.3.1 Bending

Four-point bending tests were conducted using the apparatus described in Chapter 2 (Figure 3.2). The points of contact were spaced 62 mm apart, as was conducted by Cristofolini et al. (1996).

Specimens were tested in bending along two planes: medial-lateral (ML) with the posterior side in tension, and antero-posterior (AP) with the medial side in tension. Testing in the AP plane was conducted first. Each test was conducted five times, with five cycles per test: two cycles of preconditioning followed by three data collection cycles. The femur was secured using Velcro straps tightly wrapped around the diaphysis through the L-brackets, with the straps re-secured and the femur geometry re-adjusted after each test. The femur was aligned with the vertical slots of the L-bracket using the digital laser levels. A preload of 50 N was applied, and increased to a total of 550 N, half of the 1100 N total load used by Cristofolini et al. (1996), at a rate of 8 mm/min, corresponding to quasi-static loading with a 17.1 Nm maximum bending moment. This loading rate corresponded to a strain rate of $7.2 \times 10^{-4} \text{ s}^{-1}$. Each femur was visually inspected after each test for damage.

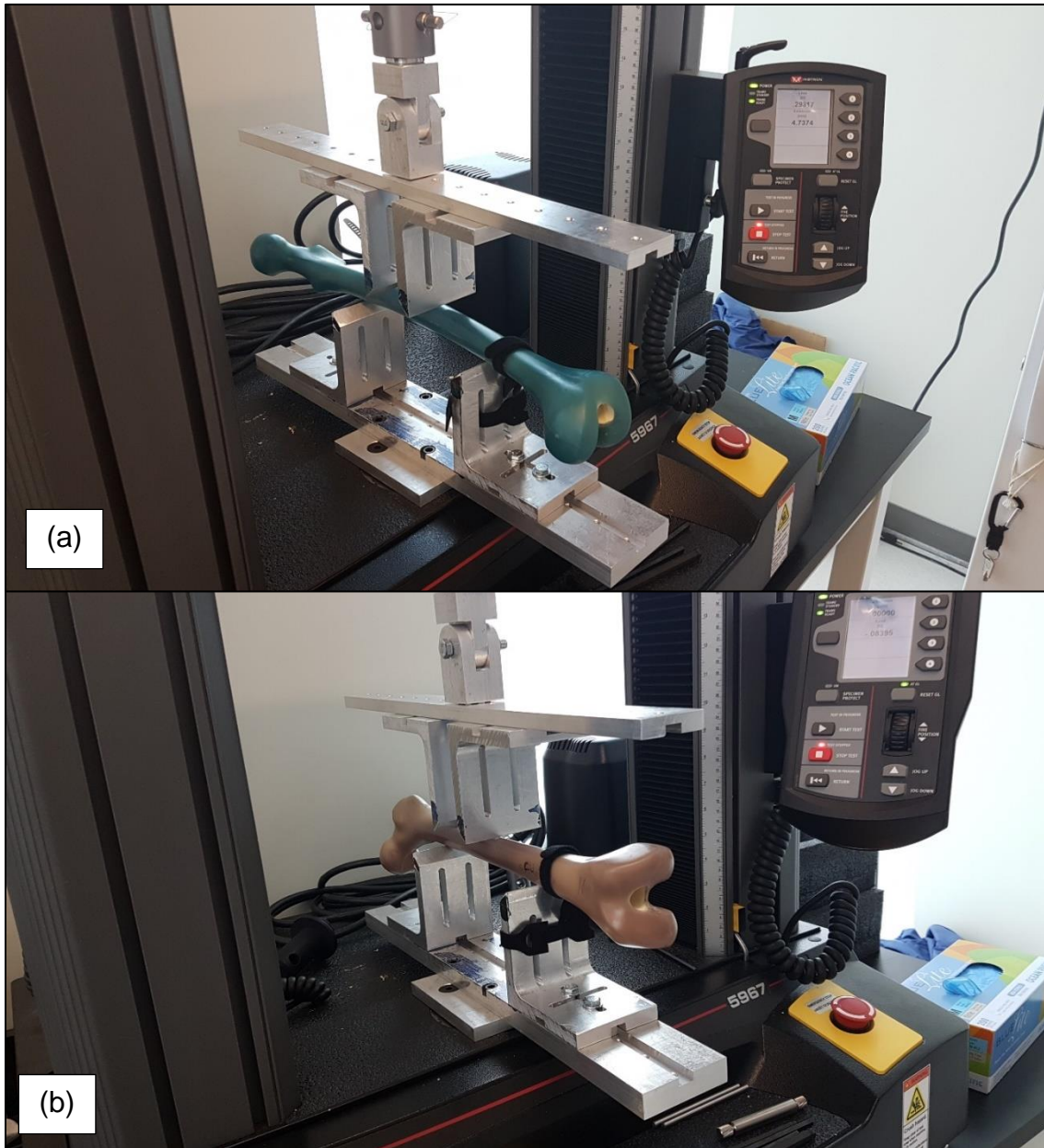


Figure 3.4: Bending Testing Photographs

A 3503 series bone in ML bending (a) and a 3403 series bone in AP bending (b). The top loading component was free to rotate within the sagittal plane (a) or the coronal plane (b) based on the loading configuration, and was implemented to evenly distribute the load applied by the Instron across any sloped geometry of the femoral diaphysis.

3.2.3.2 Torsion

Specimens were potted prior to torsional testing. Each specimen was laid horizontally (Figure 3.6) with the lesser trochanter supported by an aluminum plate.

The DXA scans provided by Science Care Inc. provided a calculated angle of inclination (angle between femoral neck and diaphysis) for each cadaveric femur. For synthetic specimens, an angle of inclination of 135° (Figure 3.1) was used.

A custom cast for each specimen was used to distribute force across the femoral head to prevent focal damage in testing. To create the cast, the femur was placed horizontally and a polystyrene cup was trimmed corresponding to the height of the midpoint of the femoral head. The trimmed cup was filled with dental cement and the anterior half of the femoral head was submerged; left to rest for one hour after pouring before the polystyrene was removed.

To conduct the test, each specimen was laid horizontally along the base fixture (Figure 3.6). The top bar, extending from the Instron crossbar, was equipped with a cylindrical head to transfer loading to the femoral head. The specimen was held with an aluminum plate set across the top surface of the pot with secured with threaded rods. Prior to testing, the height of the

support plate was adjusted to best fit the specimen, with the plate just below the lesser trochanter. Petroleum jelly was applied between the plate and the lesser trochanter with a cotton swab to reduce friction between the two surfaces, reducing noise in the data as the lesser trochanter slid during testing. Petroleum jelly was reapplied in this way before each test.

For the present study, a rate of rotation of 0.1 °/sec (based on Papini *et al.*, 2007) was translated to vertical movement based upon the distance between the diaphyseal axis and the centre of the femoral head. Given a measured 'radius of rotation' of approximately 34 mm for the synthetic femurs, a loading rate of 1.0 mm/min was employed. The loading rate was adjusted based upon the angle of inclination and distance from the long axis of the femur to the centre of the femoral head, to maintain a constant rate of rotation across all specimens (Figure 3.5, Table 3.2).

Similar to bending, five tests were conducted with five cycles per test; with each test consisting of two of preloading followed by three cycles of data collection.

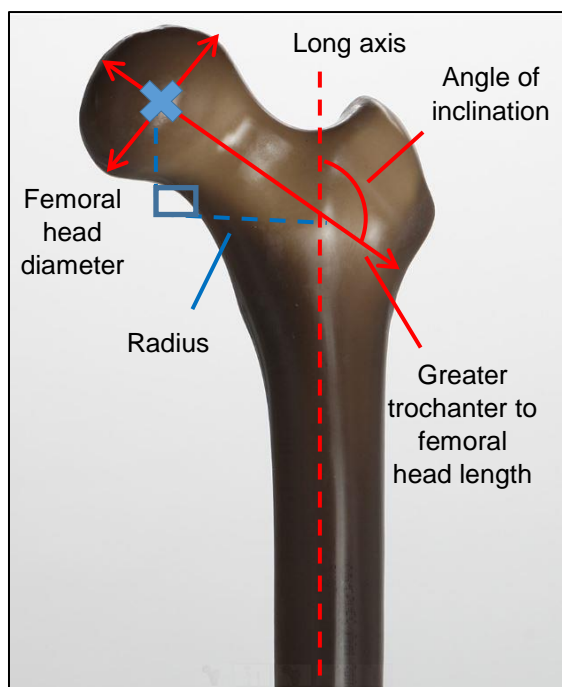


Figure 3.5: Radius of Rotation Calculation

The radius from the point of force application, X , to the long axis of the femur was calculated using the length between the greater trochanter and femoral head less half the diameter of the femoral head, made normal to the long axis using trigonometry based on the angle of inclination (Sawbones 2017). The loading rate was adjusted for each specimen based on the radius calculated, producing the same rate of rotation in all tests.

Table 3.2: Torsion Measurements

Specimens were measured with digital calipers to calculate the radius between the long axis of the femur and centre of the femoral head.

Specimen	Intertrochanteric Crest to Femoral Head (mm)	Femoral Head Diameter (mm)	Angle of Inclination (°)	Specimen Length (mm)	Moment Arm (mm)
3403	70	43	33	384	35.1
3503	70	43	33	384	35.1
161569	54	42	21	416	29.4
161607	57	43	30	438	27.9
171519	66	45	29	457	35.2
171987	57	44	31	422	26.8
172202	66	45	21	464	39.1

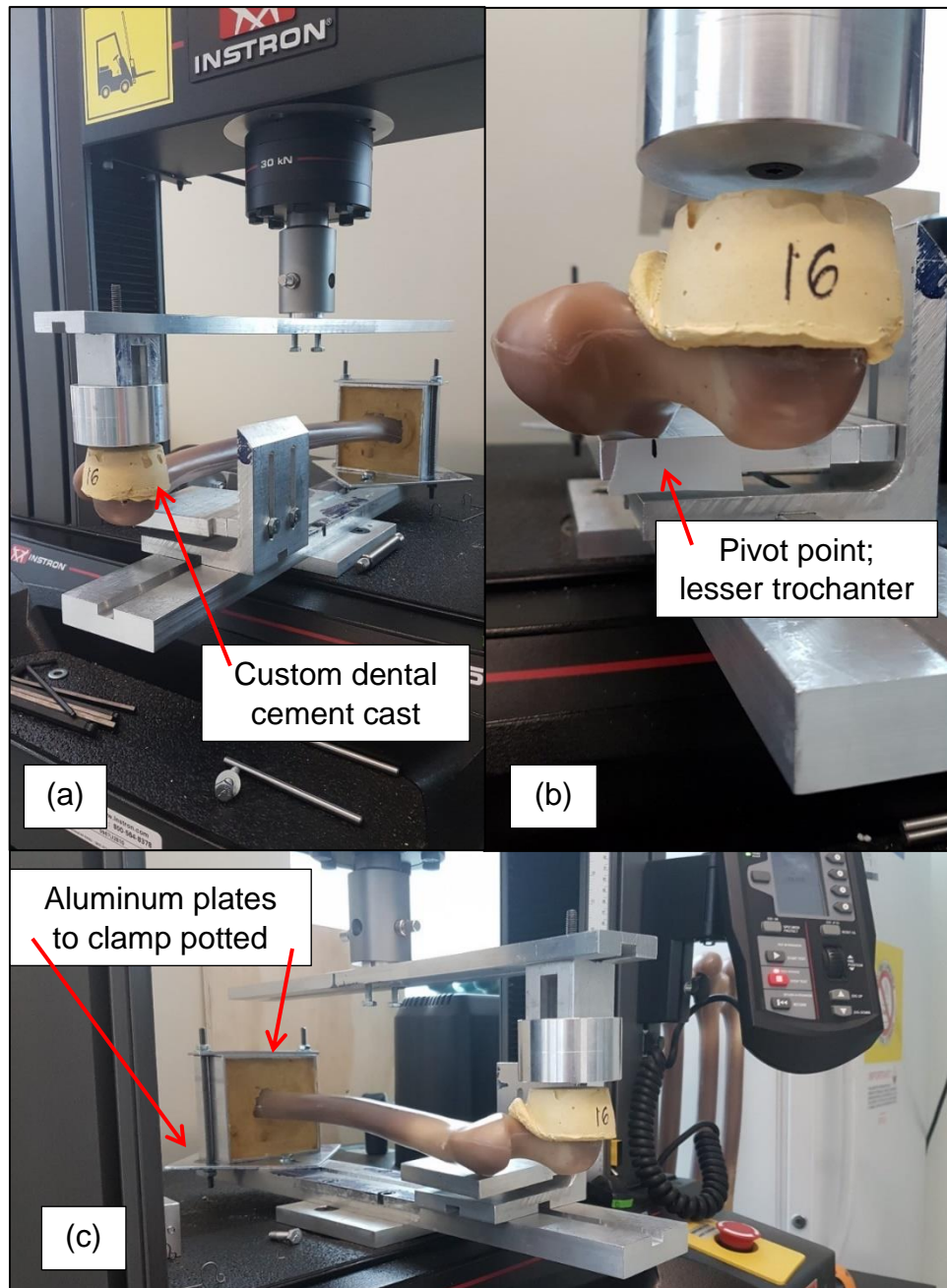


Figure 3.6: Torsion Testing Photos

Jig configuration for torsion testing, with the distal end secured with aluminum plates (a, c) and the lesser trochanter supported (b). The pivot point (marked with a line in the image) (b) was used to measure the distance of the lesser trochanter to the interior surface of the L-Bracket, used for data analysis in testing.

3.2.3.3 Axial Compression

Loads were applied to the femoral head using the aluminum cup described in Chapter 2, with the cup mounted to the Instron load cell, and the distal potting secured to the Instron base. Each specimen was visually aligned to the aluminum acetabular cup before being secured, with the centre of the cup overtop the most superior point of the femoral head (Figure 3.7). Two sets of tests were conducted, a first set of cyclic loading, and a second set of cyclic loading followed by loading to failure, defined as a load reduction of 40%. Each set of tests had the same initial parameters with a preload of 25 N, increasing to 200 N at a rate of 8 mm/min and unloading to 25 N at the same rate. The loading rate was adopted from testing previously conducted by Zdero et al. (2007) , but the magnitudes were reduced to 200 N (a 75% reduction in loading from the values used by Cristofolini et al. (1996)) to avoid damage to the femurs while still producing a linear segment from which stiffness could be calculated.

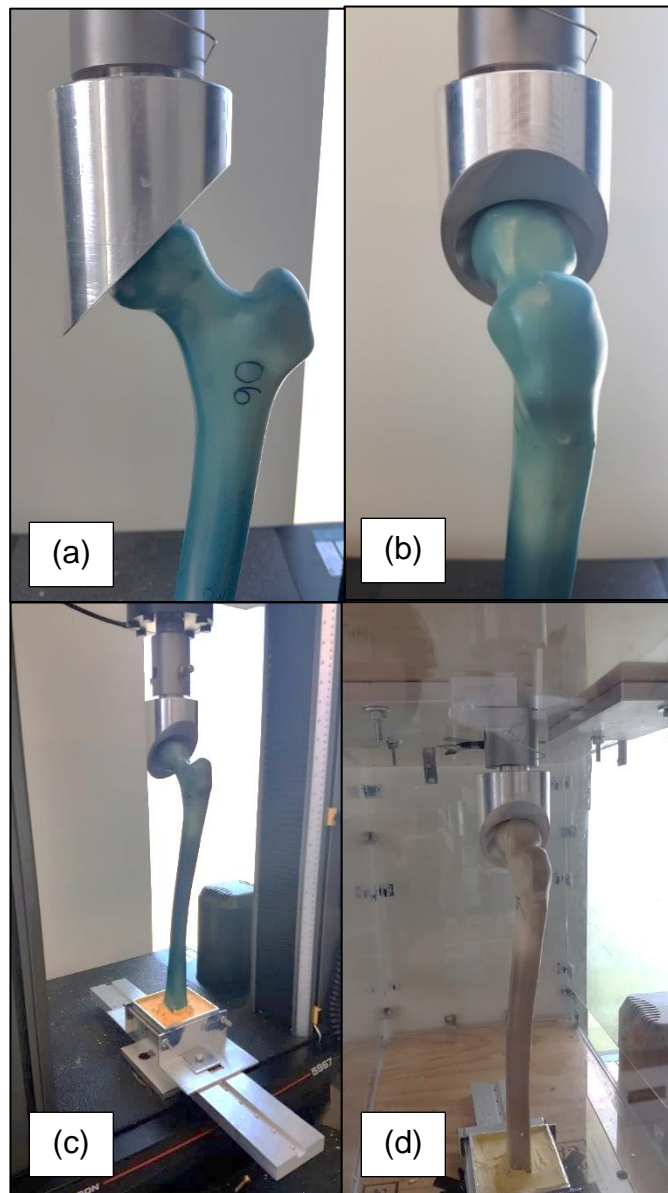


Figure 3.7: Axial Compression Photos

The axial compression jig configuration, demonstrating the acetabulum cup alignment in the anterior (a) and lateral (b) views. The specimen was secured to the base fixture with aluminum plates (c) and surrounded with blast shielding (d) to protect against high-velocity fragments as well as any biological aerosols, which could be then be properly exhausted through the top of the box, connected to the lab HVAC system.

3.2.3.4 Screw Pullout

A custom jig was also created for screw pullout testing, as described in Chapter 2. The jig was designed so that the screw was free to rotate in all axes except the long axis, causing failure to result from screw pullout instead of bending.

Each specimen was supported at the femoral head and restrained at the pot, then predrilled with a 3.2 mm bit and drill guide provided by DePuy Synthes (Synthes, Paoli, PA). The drill guide was inserted into a specially designed jig to create a pilot hole normal to the anterior surface of the midpoint of the bone (Figure 3.8). Each specimen was then trimmed, removing approximately the distal and proximal 30%, using a hacksaw and mitre box, to improve weight distribution during testing. Self-tapping cortical screws were provided by DuPuy Synthes (Synthes, Paoli, PA), with a major diameter of 4.5 mm and length of 38 mm. The screw was inserted through the U-Block and slowly penetrated into the cortical bone with the use of a hand drill. The first two threads of the screw tapped the hole and would therefore not be suitable to secure the screw to the bone. As such, screws were marked 9mm from the tip to indicate the minimum screw insertion length.

The screws were extracted using the Instron materials testing machine at a rate of 10 mm/min, with a preload of 50 N, recorded at 10 Hz. Each test was directed to stop after 12 mm of displacement or 12 kN of force read by the load cell.

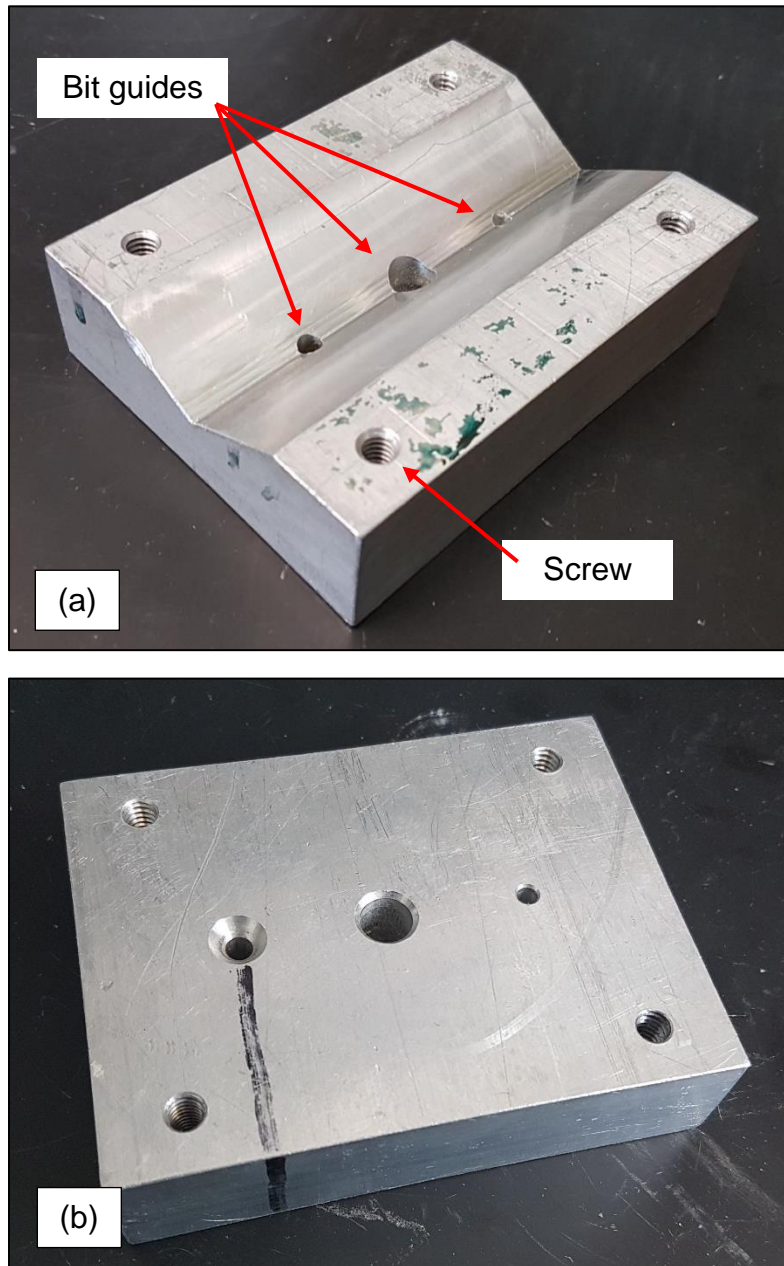


Figure 3.8: Predrill Guide Jig

The drill guide uses a v-shaped groove through its centre to rest upon the diaphysis of each specimen (a). A 0.25" screw was threaded through each of its corners to adjust jig alignment and provide stability. Three holes were drilled to identify which provided the most stability during screw predrilling, results indicated by the black line (b).

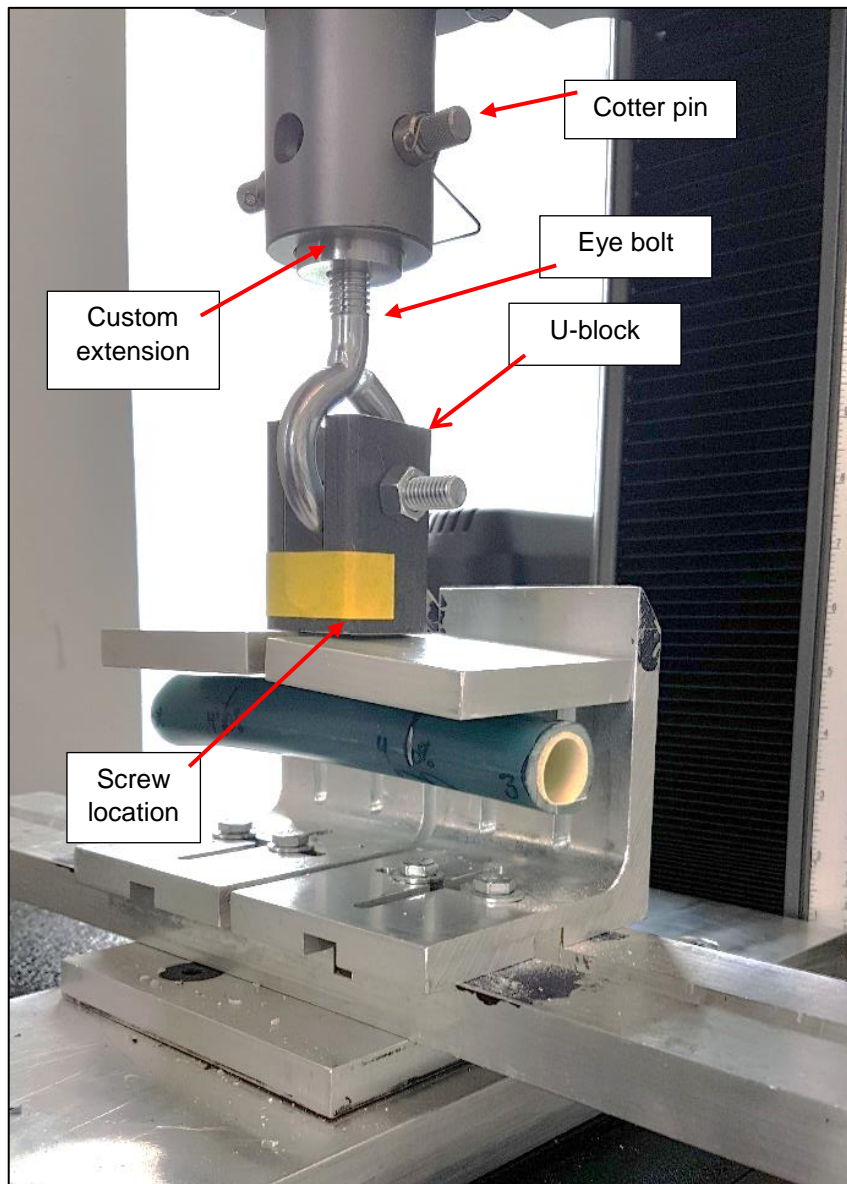


Figure 3.9: Screw Pullout Photos

The screw pullout jig configuration, shown from the inferior-lateral angle. Each specimen was trimmed, removing the distal and proximal 30%, and a unicortical screw was inserted through a hole in the U-block. The width of the U-block allowed for free rotation and some lateral movement relative to the eye-bolt, thus ensuring strictly normal loading was applied. The eye bolt connected to the load cell through a custom extension, secured with a cotter pin.

3.2.4 Analysis Methods

Stiffness values for bending and axial stiffness were calculated as force/normalized extension while torsional stiffness was calculated as torque/normalized extension, where torque was the force recorded multiplied by the length between the long axis of the femur and the centre of the femoral head; measured as the length from the greater trochanter to the femoral head minus the radius of the femoral head, using the angle between the long axis of the femur and the femoral neck to calculate the perpendicular distance from the long axis in the coronal plane (Figure 3.5, pg. 78). Bending and torsion stiffness values were averaged over the final three cycles of each test, while axial was averaged over the final five cycles.

Calculating flexural rigidity (EI , Equation 1.1) required the extension, y , the distance between the outer and inner support, a , as well as the total length between the outer supports, l . The force, F , was recorded through the load cell and divided by two for the two supports.

Torsional rigidity calculations (GJ , Equation 1.2) were calculated in a similar manner, with the length along the long axis between the potted cement and the centre of the femoral head, l , and the radius, r , from the centre of the long axis to the centre of the femoral head.

Flexural and torsional values were calculated over the entirety of the test. Axial rigidity (EA) was not calculated because it does not contain a length parameter. However, the equation was included for completeness (Equation 1.4).

To assess the screw pullout data, the maximum force recorded was defined as the screw extraction force or pullout load. The screw extraction force was divided by the shear area of the screw fully engaged in the bone, to calculate the screw extraction shear (Equation 1.5). With insertion into the diaphysis the screw was only engaged for the thickness of the cortical bone, l , measured after the test with calipers; and the pitch diameter of the screw, D_p , 3.9 mm.

All equations are reprinted with corresponding page numbers for convenience:

Pg. 20	$EI = \frac{Fa(4a^2 - 3L^2)}{24y_{max}}$	Equation 1.1: Flexural Rigidity
Pg. 22	$GJ = \frac{TL}{\theta} = \frac{FrL}{\theta}$	Equation 1.2: Torsional Rigidity
Pg. 24	$EA = \frac{FL}{d}$	Equation 1.4: Axial Rigidity
Pg. 26	$\tau = \frac{F}{A} = \frac{F}{\pi Dh}$	Equation 1.5: Screw Pullout

A one-way ANOVA ($\alpha = 0.05$) was conducted to determine differences between each series of femurs in all loading modes.

3.3 Results³

3.3.1 Bending

The mean (SD) bending stiffness in AP was 953.2 (133.2) N/mm for the 3403 series, 872.2 (98.7) N/mm for the 3503 series, and 763.8 (202.4) N/mm for the cadavers. No differences were found between the synthetic models ($p = 0.46$) or when compared to natural stiffness results ($p < 0.40$).

In ML bending, the mean (SD) stiffness was 1060.9 (23.9) N/mm for the 3403 series, 855.8 (30.9) N/mm for the 3503 series, and 592.5 (112.1) N/mm for the natural specimens. No significant difference was determined between the synthetic sets ($p = 0.08$) or between the 3503 set and natural specimens ($p < 0.07$). Difference was determined between the 3403 set and natural specimens ($p = 0.001$).

In ML bending, the mean (SD) stiffness was 1060.9 (23.9) N/mm for the 3403 series, 860.0 (30.5) N/mm for the 3503 synthetic series, and 592.5 (112.1) N/mm for the cadavers. The 3403 set was stiffer than the cadavers

³ Sample graphs for each test are available in APPENDIX D: Sample Test Data.

($p = 0.001$) but no significant difference was found between the 3503 series and cadavers ($p = 0.06$).

The mean (SD) flexural rigidity in AP was 105.2 (19.3) Nm^2 for the 3403 series, 96.2 (15.7) Nm^2 for the 3503 series, and 71.1 (20.0) Nm^2 for cadavers (Figure 3.10 (a)). Both series of synthetic femurs were statistically more rigid than the natural bones ($p < 0.046$), with no differences between the two models ($p = 0.51$). In ML bending, the mean (SD) flexural rigidity was 122.4 (4.1) Nm^2 for the 3403 series, 97.8 (4.9) Nm^2 for the 3503 series, and 69.1 (8.9) Nm^2 for the cadavers, again with differences between both synthetic models and the natural bones ($p < 0.035$) and differences between synthetic models ($p = 0.025$) (Figure 3.10 (b)).

The coefficient of variation in AP testing was substantially lower than that of ML testing, representing approximately 3-5%, rather than 16-18%, respectively, for the synthetic sets. In both orientations the cadaveric samples had high coefficients of variation (12.9-26.5%). The range of values for the bending testing conducted is listed (Table 3.3). Corresponding stiffness values were also calculated and included, for completeness.

Flexural rigidity values were used for further analysis; seen as more representative of the specimen and loading mode while also being better represented in literature.

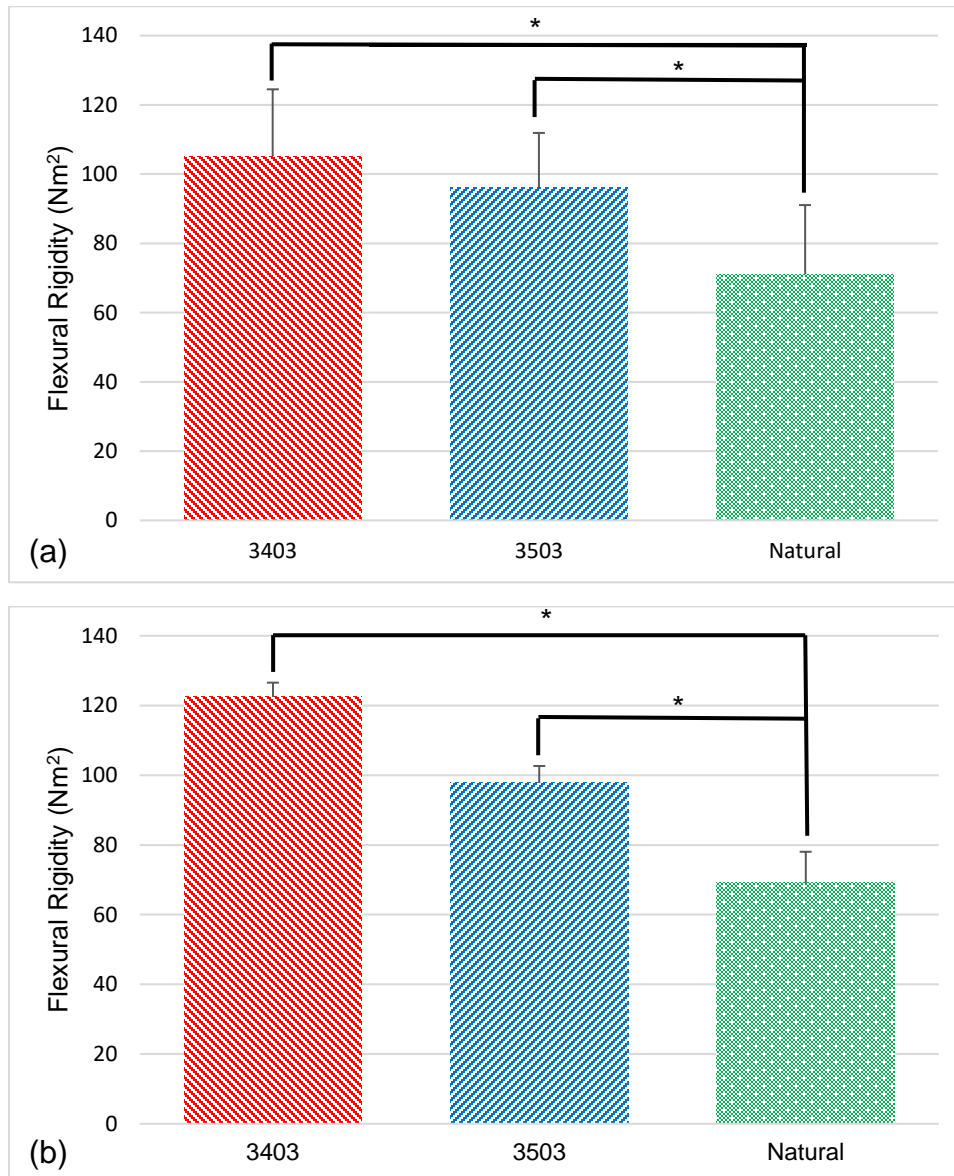


Figure 3.10: ML and AP Flexural Rigidity Graphs

Both sets of synthetic specimens demonstrated difference to cadaveric specimens in flexural rigidity in both AP (a) and ML (b) planes ($* < 0.05$).

Table 3.3: Minimum and Maximum Bending Stiffness and Flexural Rigidity Values

The minimum and maximum bending stiffness and flexural rigidity values are listed in both planes of four-point bending, demonstrative of a larger range in cadaveric response than either synthetic set.

Four-point Bending		ML			AP		
		Min	Max	SD	Min	Max	SD
Stiffness (N/mm)	3403	928.9	1158.1	23.9	538.3	1236.3	133.2
	3503	754.4	1025.0	30.9	642.0	1052.3	98.7
	Cadavers	108.9	1322.4	112.1	316.4	1019.1	202.4
Flexural Rigidity (Nm ²)	3403	107.1	136.6	4.1	52.9	144.7	19.3
	3503	76.3	120.9	4.9	62.6	124.6	15.7
	Cadavers	16.9	139.8	8.9	25.7	99.7	20.0

3.3.2 Torsion

Some seemingly inconsistent results were recorded for two synthetic specimens in each group, with values well below their respective averages. These specimens, specifically 3403-20, 3403-24, 3503-08, and 3503-10, were retested with new dental cement cups to examine this inconsistency (Table 3.4). Significant difference was calculated for the 3503 specimens, but not for the 3403 specimens retested. The first set was used for all calculations; the cause of the discrepancy is still unclear, so use of the second set could not be justified.

The mean (SD) torsion stiffness for the 3403 series was 106.1 (4.7) Nm/rad, 112.6 (3.5) Nm/rad for the 3503 series, and 38.2 (3.9) Nm/rad for natural specimens. No significant differences were found between the

synthetic sets ($p = 0.81$), but the natural specimens were significantly less stiff than both synthetic sets ($p < 0.003$).

The mean (SD) torsional rigidity values were 39.9 (1.6), 42.3 (1.3), and 16.8 (1.8) Nm^2/rad for the 3403, 3503, and cadavers, respectively. Significant difference was found between the cadaveric specimens and each synthetic set ($p = 0.002$, $p = 0.001$). The minimum and maximum values of torsional stiffness and torsional rigidity are listed (Table 3.5). Going forward, torsional rigidity values were used for the same reasons as used for selecting flexural rigidity.

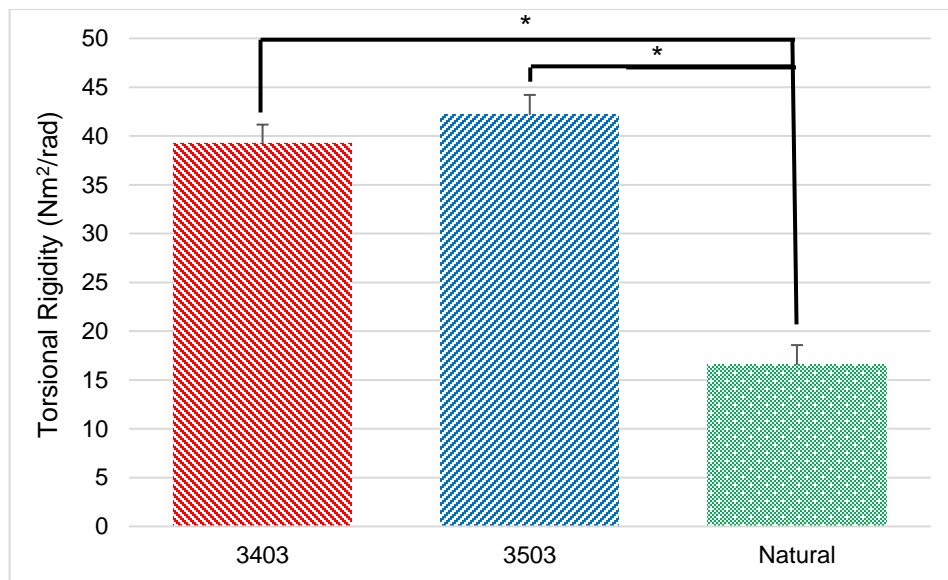


Figure 3.11: Torsional Rigidity Graph

Torsional rigidity for each specimen is presented with significant difference determined between both synthetic sets and cadaveric set (* < 0.05).

Table 3.4: Torsion Original and Retest Value Comparison Table

Four synthetic femurs were retested in torsion following results inconsistent with the rest of the respective group. Significant difference was determined using a paired t-test, indicating a reproducibility issue in torsion testing.

Torsion Retest		3403-20	3403-24	3503-08	3503-10
Stiffness (Nm/rad)	Original	56.1 (1.9)	62.2 (6.9)	61.0 (4.5)	60.5 (2.1)
	Retest	61.8 (3.0)	56.9 (1.3)	96.5 (4.3)	64.7 (2.3)
	T-test p-value	0.0076	0.1142	0.0006	0.0069
Torsional Rigidity (Nm ² /rad)	Original	22.0 (0.8)	22.4 (2.1)	23.5 (1.7)	23.5 (0.9)
	Retest	23.8 (1.0)	21.1 (0.5)	36.8 (1.4)	24.5 (0.9)
	T-test p-value	0.0088	0.2178	0.0006	0.0140

Table 3.5: Minimum and Maximum Torsional Stiffness and Torsional Rigidity Values

The minimum and maximum torsional stiffness and rigidity values are listed, indicating similar ranges between synthetic sets, both being significantly greater in magnitude than cadaveric responses.

Torsion		Min	Max	SD
Stiffness (Nm/rad)	3403	56.1	141.9	4.7
	3503	58.1	146.8	3.5
	Cadavers	28.4	53.5	3.9
Torsional Rigidity (Nm ² /rad)	3403	22.4	54.1	2.0
	3503	22.4	55.9	4.8
	Cadavers	11.5	24.5	2.0

3.3.3 Axial Compression

The mean (SD) stiffness values for the 3403 series was 683.8 (13.4) N/mm for the first set of testing and 556.9 (11.7) N/mm in the second set of testing. Similarly, the mean (SD) stiffness values for the 3503 series was 706.4 (56.6) N/mm and 555.1 (8.7) N/mm, for the first and second rounds, respectively. Mean (SD) cadaveric stiffness values were 499.3 (2.4) and 419.2 (4.6) for the first and second tests, respectively. There were no statistical difference among the groups ($p > 0.10$). The range of values is listed (Table 3.6).

Axial stiffness for cyclic and failure (the second round of axial testing) was used for further analysis. Given that the synthetic specimens have a common length and axial rigidity is equivalent to axial stiffness multiplied by that length, axial stiffness was chosen as it is more widely applicable and better represented in literature.

The mean (SD) failure loads were 2906.1 (693.0) N, 2895.1 (552.3) N, and 3316.2 (887.4) N, for the 3403, 3503, and cadavers, respectively, which were not significantly different ($p > 0.54$).

The mean (SD) failure load for the 3403 and 3503 series were 2906.1 (693.0) N and 2895.1 (552.3) N, respectively, with natural mean (SD) failure load at 3316.2 (887.4) N. No statistical significance was found between any

group in failure analysis ($p > 0.50$). There were four main fracture classifications, with natural specimens failing in two manners (Table 3.8). Fracture images for every specimen are available in APPENDIX E: Fracture Images.

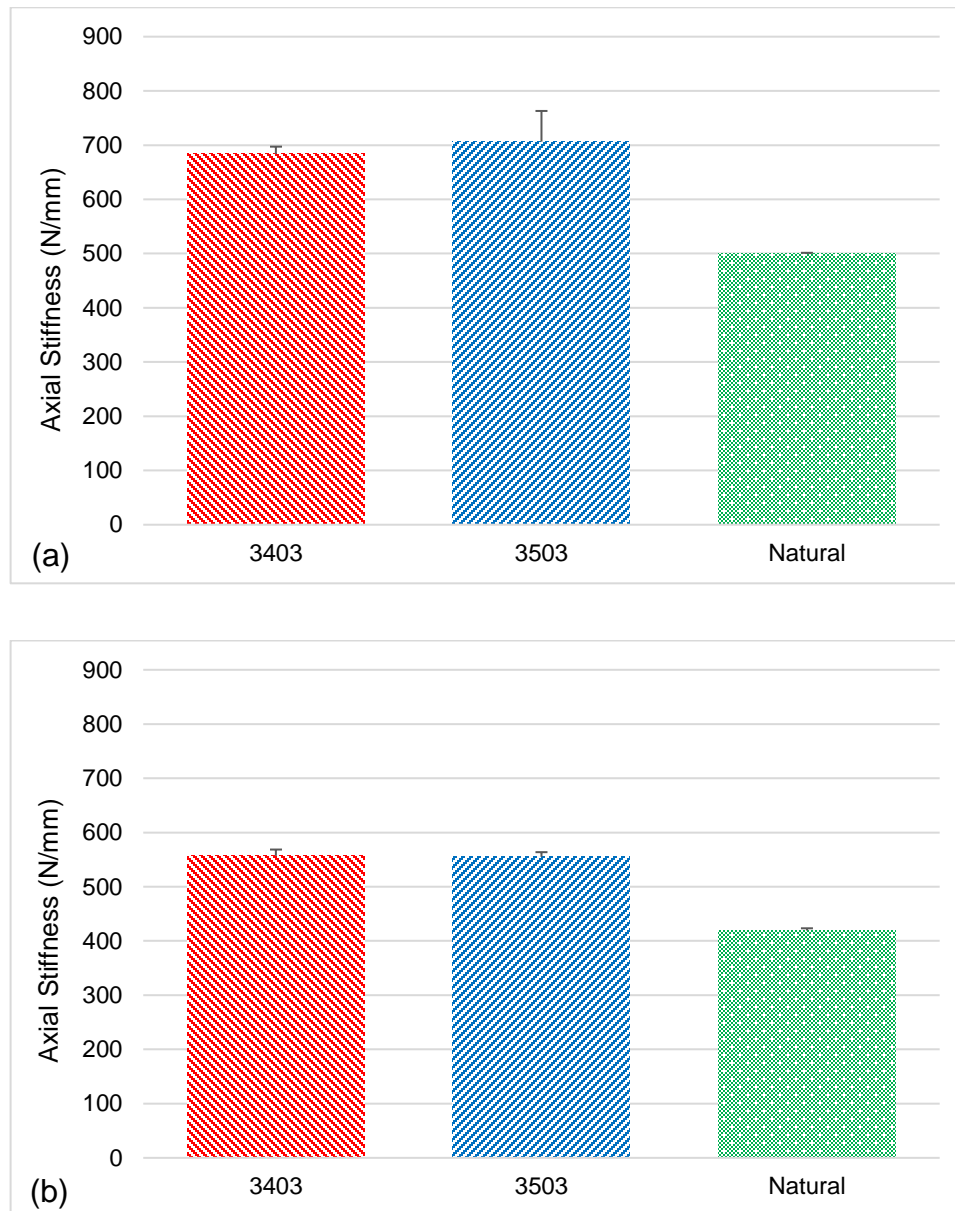


Figure 3.12: Axial Compression Results Graphs

In both cyclic axial compression tests, cyclic only (a) and cyclic to failure (b), no differences were found between either synthetic set and the natural femurs.

Table 3.6: Minimum and Maximum Axial Stiffness Values

Minimum and maximum stiffness values from both cyclic tests are presented, with the largest range observed in the 3403 cyclic only set, but the smallest range in cyclic and failure testing.

Axial		Cyclic Only			Cyclic and Failure		
		Min	Max	SD	Min	Max	SD
Stiffness (N/mm)	3403	168.3	960.3	11.7	476.7	639.9	13.4
	3503	376.0	834.7	8.7	461.6	659.1	56.6
	Cadaver	381.9	662.4	4.1	234.6	620.8	2.1

Table 3.7: Minimum and Maximum Axial Failure Load Values

The range of failure loads experienced by the synthetic and cadaveric sets indicated that the 3503 had the smallest range; however, cadavers failed at higher loads, with some crossover.

	Min. Failure Load (N)	Max Failure Load (N)	SD
3403	1684.7	3826.6	693.0
3503	1898.6	3665.4	552.3
Cadaver	2301.8	4723.5	887.4

Table 3.8: Experimental Fracture Types

Four main fracture types were observed during experimental testing, all localized to the femoral head and neck.

Fracture Type	Quantity - 3403	Quantity - 3503	Quantity - Natural	Total
Complete Transverse	2	5	0	7
Complete Femoral Head	1	2	2	5
Incomplete Transverse	1	0	0	1
Incomplete Femoral Head	4	1	3	8

3.3.4 Screw Pullout

The mean (SD) pullout load was 1896.3 (637.2) N, 2122.0 (351.6) N, and 835.3 (444.1) N, for 3403, 3503, and cadavers, respectively. The corresponding mean (SD) screw pullout stresses were 33.0 (9.1) MPa, 34.6 (5.2) MPa, and 11.0 (6.7) MPa, for 3403, 3503, and cadavers, respectively. The cadavers were significantly different to both sets of synthetic specimens ($p < 0.005$). Pullout stress values are scaled to load, and so are not included. Value ranges have been provided for completeness (Table 3.9).

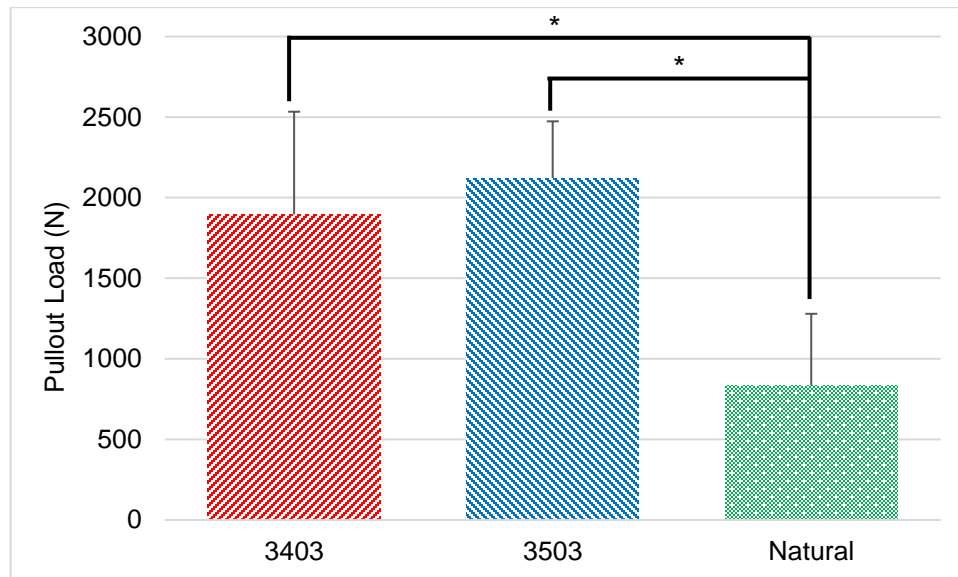


Figure 3.13: Screw Pullout Load Graph

Mean screw pullout loads were higher for both synthetic sets, which were significantly different to natural specimens ($p < 0.005$).

Table 3.9: Minimum and Maximum Pullout Load and Pullout Stress

Pullout loads and corresponding stresses were lower in cadaveric testing in almost all instances, when compared to synthetic data.

	Sample	Min	Max	SD
Pullout Load (N)	3403	1110.7	2852.7	637.2
	3503	1602.2	2568.1	351.6
	Cadavers	302.2	1203.3	444.1
Pullout Stress (MPa)	3403	20.9	46.9	33.0
	3503	27.2	42.9	34.6
	Cadavers	3.2	20.2	6.7

3.4 Discussion

This study examined the mechanical properties of synthetic femurs under a variety of loading mechanisms, including fracture and screw pullout. From previous research (*e.g.* Dickenson *et al.* 1981; Marcus *et al.* 2017), it was expected that osteoporosis would reduce the strength and stiffness exhibited by bone; driving the need for the development of new model representing an osteoporotic population. While many similar studies exist that have assessed the properties of Sawbones™ (*e.g.* Cristofolini *et al.* 1996; Dias Rodrigues *et al.* 2004; Schemitsch 2008; Zdero *et al.* 2009), this is the first study to examine the two new sets of Sawbones™ designed to replicate osteoporotic bones.

3.4.1 General Limitations

One limitation of the current testing was the order of tests was not randomized. Randomization was not possible with the destructive axial testing and epiphyses removal for screw pullout, and was highly impractical for torsion as bending would be severely complicated if conducted while the specimen was potted. Conducting the testing in one order meant any damage accumulated would be present in the following tests, weakening the specimens by an unknown amount. This limits comparison to previous literature, especially if multiple tests were conducted in a different order or with different methods. This limitation can be mitigated somewhat by

applying loading below yield stress, where deformations are predominately elastic. Given that the expected stress and strain values calculated during bending were below 20% of the corresponding yield values described in Dickenson et al. (1981), there should be marginal accumulated damage to the femur during testing. Similarly, torsion loading was below the same threshold yield percentage. Nonetheless, as this was a comparative study, any accumulated damage would be applied equivalently to all specimens.

It is unclear what DXA values the synthetic femurs are meant to replicate. It is possible the Sawbone characteristics were modelled at the diagnostic threshold t-score of -2.5, a score which none of the cadavers possessed. The cadaveric t-score range from -2.4 to -3.3. Such a range of values would likely influence the mechanical response of the femur most prominently in the torsion and axial compression testing. Mechanical properties were compared to t-score for all tests using a linear regression analysis, seen in Table 3.10. The results indicate that t-score was largely not a significant influence on bending but was moderately correlated with other tests such as axial stiffness and failure load.

There are several geometric distinctions between the synthetic and cadaveric specimens. One such difference is the hole in the distal end of the Sawbone through the cortical and cancellous bone. However, this

change likely did not significantly affect testing as loading was applied to the diaphysis or the proximal epiphysis while the distal end was potted in dental cement. However, this means that the response of the distal epiphysis has not yet been properly investigated. One other significant difference is the unchanged external geometry between the synthetic and 'healthy' Sawbones™. Age-related changes have been documented, altering bone geometry to better suit the loading with lower bone mass and density (Figure 3.14) (Karim et al. 2017). This is seen as an increase in bone diameter with a decrease in cortex thickness, effectively increasing the second moment of area of the bone without increasing mass. This may also be attributable to “preprogrammed behaviour” of the endosteal and periosteal bone cells (Karim et al. 2017). Regardless, such a change does not appear to have been incorporated into the design of the osteoporotic synthetic femurs being tested.

Only female (both right- and left-side) cadavers could be found that met the criteria for osteoporosis. Women are statistically more likely to suffer an osteoporotic fracture than men, estimated at one in three women compared to one in five men over fifty years old (International Osteoporosis Foundation 2017), indicating they are more likely to receive orthopaedics designed for osteoporosis. While industry safety standards are predominately based on 50th percentile male results, the use of female

cadavers may increase the overall effectiveness of the orthopaedics that result from them, making them more appropriate for more people.

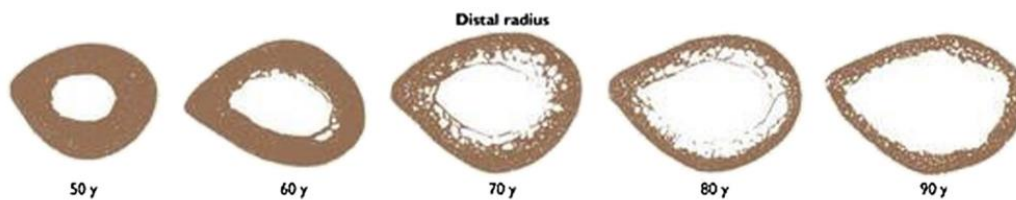
The limited availability of natural specimens has inhibited the sample size available for testing. However, the number included is in line with previous literature: Cristofolini *et al.* (1996), 4; Zdero *et al.* (2009), 6. While the addition of more natural specimens could improve results confidence, variation in some tests, such as ML bending and axial compression, was already quite low.

It was surprising to find no significant differences between the sets of synthetic specimens across several tests. Samples of the short fiber epoxy resin taken from the diaphysis after screw pullout testing were shipped back to Pacific Research Laboratories for analysis. The mean (SD) density of the 3403 specimens was revealed to be 1.65 (0.5) g/cc, in line with the standard material density of 1.64 g/cc expected. Results were not returned for the 3503 specimens.

Table 3.10: Linear Regression and Cadaver T-Score Comparison

A linear regression analysis conducted between the sample's t-score and corresponding testing results to assess the influence of bone mineral density.

	T-score	Flex. Rigidity – ML (Nm ²)	Flex. Rigidity- AP (Nm ²)	Torsional Rigidity (Nm ² /rad)	Axial Stiffness (N/mm)	Failure Load (N)	Screw Pullout Load (N)
Cadaver							
161569	-3.6	56.4	138.5	11.2	281.3	2301.8	1203.3
161607	-2.6	177.7	156.9	16.7	536.3	4723.5	404.5
171519	-3.0	270.8	140.2	21.3	240.4	2978.9	1076.6
171987	-2.4	65.2	115.2	13.9	619	3176.0	1189.8
172202	-2.7	97.6	160.1	19.7	527	3400.8	302.2
Regression Analysis	R ²	0.01	0.01	0.12	0.72	0.45	0.17

**Figure 3.14: Demonstration of Bone Cross-Sectional Geometry Change with Age**

With bone mass decrease with age, the structure of the cross-section adapts by expanding outward to maintain bending resistance (Karim et al. 2017).

3.4.2 Bending

As compared to the cadaveric specimens, the synthetic models presented were not suitable as surrogates for bending tests in either orientation.

Second generation synthetic model testing conducted by Cristofolini (1996) indicated a mean (SD) ML bending stiffness of approximately 2200 (100) N/mm and a mean (SD) AP bending stiffness of approximately 2300 (400) N/mm, approximately twice the mean values found in cadaveric specimens in this research. Fourth generation models tested by Heiner (2008) had a mean (SD) flexural rigidity of 241 (10.8) N/m² in the AP plane and 273 (15.8) N/m² in the ML plane, indicating a significant decrease in rigidity in the novel synthetic femurs in both planes, as expected.

Many values have been recorded concerning the bending modulus of bone, often unique to that type of bone. A range of 10.7 – 14.8 GPa was aggregated by Karim et al. (2017) for cortical bone in bending. Using a simplified hollow cylinder model based on the dimensions given by Sawbones and the 3503 flexural rigidity values determined experimentally, a modulus of 4.25 GPa was calculated, again indicating a significant reduction in modulus as compared to previous literature.

It was noted that the results from AP bending were significantly more consistent than those in ML. This was also seen in Cristofolini et al. (1996). This discrepancy may be attributed to the weight of the femoral head causing rotation during loading, which would not be present in the AP plane. Each specimen was re-secured and re-aligned between each set of testing, however, some rolling was noted during loading, possibly seen in the ‘kinks’ of the plotted graphs of APPENDIX D: Sample Test Data, notably specimens 3503-09, 3503-11, 3403-24, and 3403-26. Similar testing has employed the use of a metal vise-like clamp to secure the specimen. Velcro straps were used in this instance because they provided a precise fit for all geometries without damaging the surface of the bone.

3.4.3 Torsion

Both synthetic sets were shown to be inadequate for use as surrogates for natural testing. Previous literature on testing femurs under torsion has applied a broad range of maximum torques (15 Nm to 30 Nm) and loading rates (0.1 °/sec to 0.25 °/sec) (Cristofolini et al. 1996; Heiner and Brown 2001; Papini et al. 2007). As such, there appears to be no standardized method for torsion testing. It is also worth noting that those systems used an upright femur in a biaxial materials testing machine, capable of creating and recording torque, whereas the present study used a modified torque application method. As such, these tests would only assess torsion in the

diaphysis of the femur, rather than through the diaphysis and proximal end. Therefore, it is difficult to make direct comparisons to previous literature, given the significant differences in testing methodologies.

Research conducted by Papini et al. (2007) reported torsional stiffness values of 267 and 611 Nm/rad for cadaveric and 3rd generation synthetic femurs, respectively. Cristofolini et al. (1996) reported the average torsional stiffness over three runs for each femur, with a mean of approximately 8.5 Nm/degree for composite femurs, 4.5 Nm/degree for dried/rehydrated femurs, and 6.5 Nm/degree for frozen cadaveric femurs. These values equate to 487.0, 257.9, and 372.5 Nm/rad, respectively, and indicate that the synthetic femurs were too stiff in torsion. When compared to the present set of testing, which found torsional stiffness values of 106.1 and 112.6 Nm/rad for synthetic and 38.2 Nm/rad for natural femurs, indicative that the osteoporotic synthetic femurs tested are 16 – 40% as stiff as previously tested synthetics representative of the general population, while still being too stiff in torsion. This may be a result of the anisotropic material, where natural femurs adapt to accommodate axial loading, and would not be as resistant to torsion.

Heiner (2008) reported mean torsional rigidity values of 252.7 Nm²/rad for natural 'healthy' femurs and values of 123.2 and 183.9 Nm²/rad for 3rd

and 4th generation synthetic femurs, respectively [note: these values are converted from Nm^2/deg]. Compared to the values calculated in the present research, 39.2 and 42.2 Nm^2/rad , it is clear that the novel synthetic femurs tested herein have a significantly lower torsional rigidity than ‘healthy’ bone and its corresponding synthetic models. Similarly, the torsional rigidity calculated in natural osteoporotic specimens are 93.4% less rigidity than the natural specimens presented by Heiner (2008).

There were several limitations in the torsional testing conducted. Despite careful procedures in creating the dental cement cups (including a second round of casting, in some instances), there was often a noticeable angle between the loading jig and the flat of the dental cup, which would create a single point of contact over a small area. This issue was ignored due to the exact fit of the dental cement cup, which was thought to distribute any load over the entire femoral head. Testing was also limited by the instrumentation available, as previous research (e.g. Cristofolini et al. 1996; Papini et al. 2007) utilized instruments with the ability to create and measure rotation, which was not available with the Instron 5967.

It is unclear what the root cause of the discrepancies were in the 3403-20, 3403-24, 3503-08, and 3503-10 specimens. Aside from securing the models, no changes were made to the testing assembly or in the casting

process. After retesting these specimens, only one of the four specimens was not significantly different. It is unclear why the three specimens are so dissimilar to their respective sets. It is possible that the dental cement cup may not have adhered to these models as securely as others, causing the cup to tilt and apply a more concentrated load further from the axis of rotation. This would explain why casting new dental cement cup resolved the issue in three of the four specimens.

After testing had concluded, an error analysis was conducted to determine any leniency in the system which would alter results, specifically bending of the cantilevered lesser trochanter support and rotation of the top- fixture in the AP plane as the specimen was loaded. The system was reset, with a 12.6 mm x 25.4 mm x 127 mm steel beam placed with its long axis vertical between the cantilevered plate and the cylindrical torsion fixture. The beam was loaded to 30 N where the system extension was reset. The beam was then loaded to 80 N and the displacement of the system was recorded. A displacement of 0.5 mm was recorded, indicating some give in the system. This may explain the low torsional rigidity values recorded, increased the recorded displacement by up to 25% in some cases. This will limit the ability to compare the torsional results to future research, unless the data can be amended. However, every specimen was tested with this system, and reset between tests, with three tests averaged for a final result,

which limits any inherent variation in the set-up process, supported by the low coefficients of variation. Furthermore, the basis for comparison between synthetic sets and cadaveric specimens remains valid, given that the same apparatus (and corresponding configuration) was used for all tests.

A second error analysis was conducted regarding the specimen measurements used to calculate the moment arm of the torque applied around the long axis of the femur. Conducting five measurements of each of the principle lengths involved produced a maximum measuring error of 2.1%, corresponding to a maximum of approximately 8.8%. This maximum error is unlikely to occur, but would be more likely in the cadaveric specimens, where external geometry is not standardized. The significantly lower cadaveric results as compared to synthetic results (16.6 Nm²/rad vs 39.2 Nm²/rad, 42.2 Nm²/rad) indicate that this magnitude of measuring error would not have any effect on the determination of significant difference between the synthetic sets.

3.4.4 Axial Compression

Both sets of novel synthetic femurs were shown to be acceptable as a surrogate for testing, with the p-values calculated for axial failure loads being the highest across all comparisons, at 0.56 and 0.55 for the 3403 and 3503 sets, respectively.

Previous research conducted by Papini et al. (2007) reported a mean axial stiffness of 757 N/mm for cadaveric specimens and 1290 N/mm for 3rd generation synthetic femurs, using a similar loading jig but with free rotation of the femoral head. Cristofolini et al. (1996) reported only up to 0.8 kN of axial load, corresponding to an approximate mean stiffness of 1333, 1067, and 1333 N/mm for composite, dried/rehydrated, and frozen femurs, respectively. When compared to the experimental results (Table 3.6), the osteoporotic femurs tested herein are notably less stiff, representing approximately 31 – 66% of that listed previously, dependent on the amount of loading.

As expected, the first set of testing had a significantly higher cyclic stiffness than the second set. It was decided that cyclic axial compression and axial failure should be conducted in one continuous test; removing any result discrepancies occurring from specimen re-alignment between tests. Preliminary axial stiffness data were requested from PRL prior to the completion of the blast shielding, prohibiting failure testing due to safety concerns. It was then decided to conduct two rounds of cyclic axial compression tests. The consequence of an additional cyclic test may be seen in stress relaxation of the specimen, reducing stiffness and fracture load. The influence of this is mitigated by subjecting the natural specimens to the same procedure and the reduced load applied to the specimen.

Failure occurred in a number of locations within the samples (Table 3.8); the fracture mechanisms of the synthetic femurs tended to differ from those of cadaveric specimens. Natural specimens failed in only two modes, which were best represented by the 3403 series. The 3403 series were noted to fail by fracture in the cortical bone surrounding the femoral head, along the cast line in the coronal plane. The 3503 series tended to fracture horizontally across the diaphysis. It was noted that the 3503 series fractures tended to pass through the pilot hole in the lesser trochanter. Filling this hole and removing the stress concentration it produced may provide a more representative failure mode.

After testing was conducted, small regions of crush (approximately 20 mm²) were seen at the most proximal point of the femoral head (Figure 3.16). Scraping was also seen inside the axial jig, seeming to indicate movement of the contact point between the femoral head and the compression jig. This would correlate well to the noise seen in testing, notably specimens 3403-17, 3403-25, 3403-26, 3503-08, 3503-10, and 3503-11, as seen in APPENDIX D: Sample Test Data. This represents one of the major limitations involved in the present axial testing. Although built to specification, the diameter of the spherical cut-out was notably larger than the diameter of the femoral head. In this way, alignment between the femoral head and axial jig was imprecise.

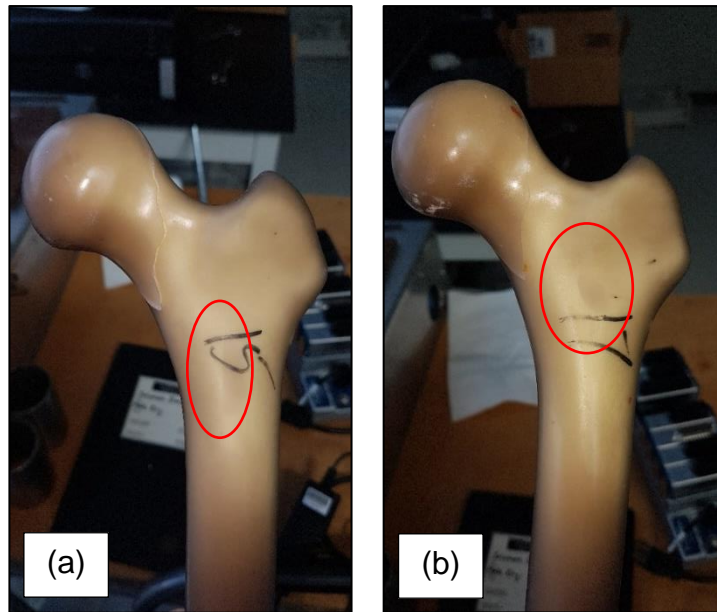


Figure 3.15: Sample Sawbones with Cancellous Bubbles

Bubbles below the surface of the epoxy resin were observed in the proximal ends of several specimens.

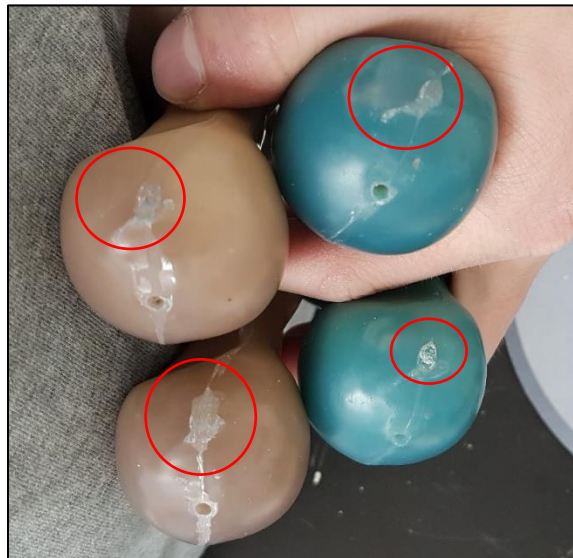


Figure 3.16: Femoral Head Crush After Axial Loading

Small regions of crush were noted at the contact point between the femoral head and axial loading cup.

3.4.5 Screw Pullout

Neither synthetic set was shown to be useable for screw pullout testing. This may be attributed to the failure mechanism of the short fiber epoxy resin, which failed with a distinct range of damage to the surrounding area, whereas the natural femurs failed without the area surrounding the screw sustaining any visible damage.

Two samples, 3403-25 and 3503-08, were visibly damaged while the screw was being inserted, denoted by a small discolored section adjacent to the screw (Figure 3.17). The pullout load for these damaged specimens, however, was not the minimum value for each set of testing, and so it is unlikely this affected the overall response under this testing mode.

Previous screw pullout tests conducted on fourth generation standard synthetic femurs had an aggregate (SD) pullout force of approximately 3000 (750) N, where human femurs had an aggregate (SD) pullout force of approximately 2500 (1500) N, with no significant differences between them ($p = 0.073$), or at different locations along the diaphysis ($p > 0.21$) (Zdero et al. 2009). These results indicate that the novel osteoporotic femurs tested, with mean (SD) pullout forces of 1896.3 (637.2) and 2122.0 (351.6) N, may provide a more accurate representation of screw pullout for the general

population than standard synthetic bones, in terms of pullout force, with lower variation.

It is worth noting that screws were pulled exclusively from the mid-diaphysis, as the epiphyses were significantly damaged or potted prior to this experiment. Previous literature (e.g. Zdero *et al.* (2009)) has conducted screw pullout at several locations along the diaphysis. Given that orthopaedic screws can be used *in vivo* in a variety of locations that may include or be dominated by trabecular bone, the response at the epiphyses may be worth investigating.

3.5 Conclusion

Both sets of synthetic femurs had mechanical responses significantly different to natural femurs in bending, torsion, and screw pullout. There are several possible components that may have contributed to this difference, including a different geometric distribution or an insufficient thickness reduction from the synthetic model representative of the normal population.

To improve upon the synthetic models provided, the modulus and distribution of epoxy resin should be investigated. Differences in flexural rigidity could be accommodated for in alterations to the epoxy modulus and/or distribution through the diaphysis. Such reductions could also help

improve the response in axial compression, which has a bending component previously noted. This may also be achieved by thinning the cortex in the proximal epiphysis, which may assist in reducing torsional rigidity.

Screw pullout was conducted only at the mid-diaphysis, however, this area was loaded repeatedly prior to screw pullout, and does not assess the influence of trabecular bone. It is recommended that further testing be conducted at the epiphyses to determine responses which may be more suitable for recommendations concerning a variety of screw insertions points.

With some minor modifications to density and/or geometry, it is likely that these novel synthetic femurs could be made representative of osteoporotic femurs. Such a model would provide a foundation for the development of orthopaedics optimized for the osteoporotic population, potentially improving surgical outcomes, lowering associated mortality, and increasing independence and quality of life for those who suffer osteoporotic fracture.

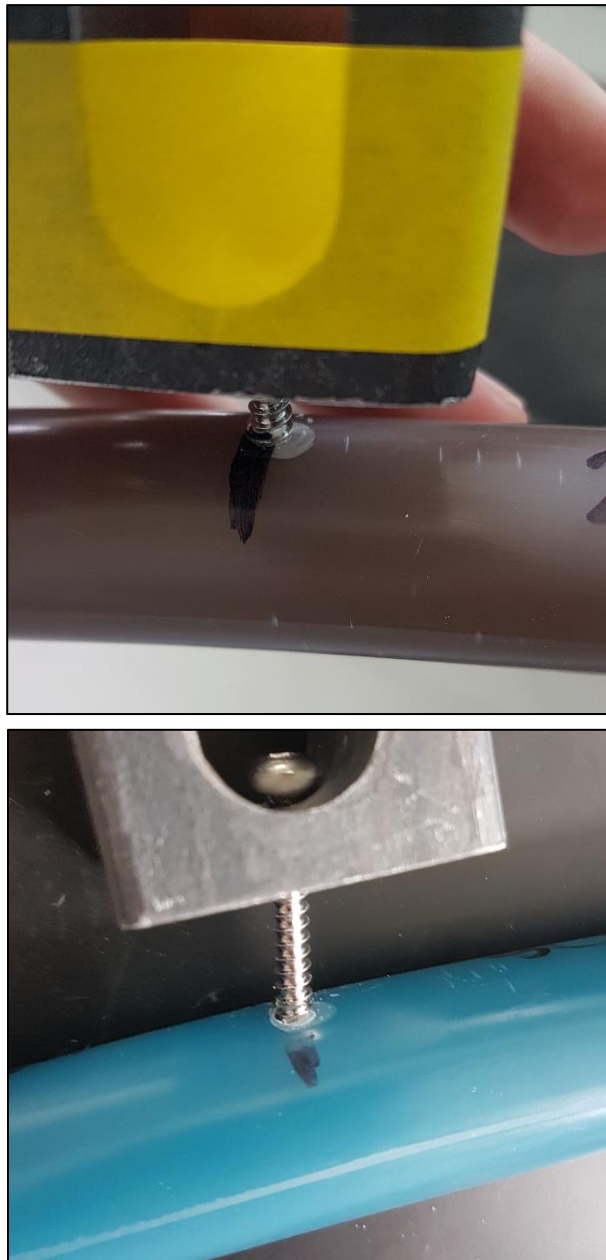


Figure 3.17: Screw Pullout Damage

Two instances of surface damage were observed after inserting the screw into the specimen.

3.6 References

Bayraktar HH, Morgan EF, Niebur GL, Morris GE, Wong EK, Keaveny TM. 2004. Comparison of the Elastic and Yield Properties of Human Femoral Trabecular and Cortical Bone Tissue. *J. Biomech.* 37:27–35. doi:10.1016/S0021-9290(03)00257-4.

Canadian Institute for Health Information. 2018. Hip and Knee Replacements in Canada, 2016-2017: Canadian Joint Replacement Annual Report. Ottawa, Ontario. [accessed 2018 Aug 27]. www.cihi.ca.

Cristofolini L, Viceconti M. 2000. Mechanical Validation of Whole Bone Composite Tibia Model. *Pergamon* 2:525–535. doi:10.1227/01.NEU.0000297048.04906.5B0.

Cristofolini L, Vicecontia M, Cappello A, Toni A. 1996. Mechanical Validation of Whole Bone Composite Femur Models. *J. Biomech.* 29:525–535.

Dias Rodrigues JF, Lopes H, de Melo FQ, Simoes JA. 2004. Experimental Modal Analysis of a Synthetic Composite Femur. *Exp. Mech.* 44:29–32. doi:10.1177/0014485104039745.

Dickenson RP, Hutton WC, Stott JRR. 1981. The Mechanical Properties of Bone in Osteoporosis. *Society* 63–B:233–238.

Heiner AD. 2008. Structural Properties of Fourth-Generation Composite Femurs and Tibias. *J. Biomech.* 41:3282–3284. doi:10.1016/j.jbiomech.2008.08.013.

Heiner AD, Brown TD. 2001. Structural Properties of a New Design of Composite Replicate Femurs and Tibias. *J. Biomech.* 34:773–781. doi:10.1016/S0021-9290(01)00015-X.

International Osteoporosis Foundation. 2017. Facts and Statistics. [accessed 2017 Dec 5]. <https://www.iofbonehealth.org/facts-statistics>.

Karim L, Hussein AI, Morgan EF, Bouxsein ML. 2017. The Mechanical Behavior of Bone. In: *Osteoporosis*. Fourth Edi. Elsevier. p. 431–452.

Li B, Aspden RM. 1997. Material Properties of Bone from the Femoral Neck and Calcar Femorale of Patients with Osteoporosis or Osteoarthritis. *Osteoporos. Int.* 7:450–456. doi:10.1007/s001980050032.

Marcus R, Dempster DW, Bouxsein ML. 2017. The Nature of Osteoporosis. In: *Osteoporosis*. Fourth Edi. Elsevier. p. 21–30.

MatWeb. 2017. Sawbones Fourth-Generation Simulated Cancellous Bone (Rigid Polyurethane Bone). [accessed 2017 Jun 13].

<http://www.matweb.com/search/datasheettext.aspx?matguid=42cd25dc7f414bfcb4432a8bcb969889>.

Papini M, Zdero R, Schemitsch EH, Zalzal P. 2007. The Biomechanics of Human Femurs in Axial and Torsional Loading: Comparison of Finite Element Analysis, Human Cadaveric Femurs, and Synthetic Femurs. *J. Biomech. Eng.* 129:12. doi:10.1115/1.2401178.

Saunders MM. 2015. *Mechanical Testing for the Biomechanical Engineer: A Practical Guide*. Enderle JD, editor. Morgan & Claypool Publishers.

Sawbones. 2017. Femur, Fourth Generation Geometry. [accessed 2017 Jul 11]. <https://www.sawbones.com/femur-medium-left-4th-generation-composite.html>.

Schemitsch EH. 2008. The Effect of Screw Pullout Rate on Screw Purchase in Synthetic Cancellous Bone. *J. Biomech. Eng.* 131:024501. doi:10.1115/1.3005344.

World Health Organization. 2004. WHO Scientific Group on the Assessment of Osteoporosis at Primary Health Care Level. In: Summary Meeting Report. Brussels, Belgium. [accessed 2017 Jun 13]. <http://www.who.int/chp/topics/Osteoporosis.pdf>.

Zdero R, Elfallah K, Olsen M, Schemitsch EH. 2009. Cortical Screw Purchase in Synthetic and Human Femurs. *J. Biomech. Eng.* 131:094503. doi:10.1115/1.3194755.

Zdero R, Rose S, Schemitsch EH, Papini M. 2007. Cortical Screw Pullout Strength and Effective Shear Stress in Synthetic Third Generation Composite Femurs. *J. Biomech. Eng.* 129:289–293. doi:10.1115/1.2540926.

CHAPTER 4 – DEVELOPMENT OF A FINITE ELEMENT MODEL TO INVESTIGATE FUTURE SYNTHETIC MODEL ITERATIONS

Overview: *This chapter details the development and evaluation of a finite element model of the novel synthetic femur tested in Chapter 3 under quasistatic, subfailure four-point bending and axial loading. The model was subsequently modified with combinations of reduced cortical thicknesses and reduced modulus values in an attempt to produce results more representative of the cadaveric osteoporotic femurs also tested in Chapter 3.*

4.1 Introduction

Finite element (FE) modelling is a powerful technique that has developed significantly over the last 50 years (Huiskes and Chao 1983) and become well-incorporated into biomechanical analyses and orthopaedics development (Burkhart et al. 2013). When properly evaluated, it acts as a reasonable alternative to *ex vivo* testing, without the direct expense or the complexities of biological testing. A major advantage of finite element testing is its ability to conduct repeatable testing with discrete changes,

which can then be used for predictive measures or to form recommendations for product modifications.

Very few finite element studies have focused on validating synthetic composite bones under various loading modes. Papini *et al.* (2007) developed a finite element model of a 3rd generation Sawbones™ synthetic bone, and tested it in axial loading using a range of modulus values. Results indicated good agreement between cadaveric specimens and the FE model using a cortical modulus of 4.5 GPa, within 1 SD of the cadaveric data collected.

The goal of the present study was two-fold: to develop a finite element model of the 3403 synthetic femur that agreed with experimental test results from Chapter 3, and then use it to parametrically evaluate the effect of cortical thickness and modulus changes based on stiffness outcomes, with the ultimate goal of defining recommendations that better match the cadaveric femur response.

4.2 Methods

4.2.1 Standard Model Development

One potted synthetic femur was scanned using Computed Tomography (CT) at 0.625 mm slice thickness. The 3403 and 3503 models shared similar geometry, so the 3403 model was chosen because the

material properties were more clearly defined by the manufacturer. The scan data were imported into Mimics (Materialise NV, Leuven, Belgium) for processing and model development. To construct the initial model, several masks were created using custom threshold values. The initial mask included both the trabecular and cortical surrogate materials, as well as the scanner bed below the specimen. The construct was then manually edited with the Edit Mask feature to remove the scanner bed. A second and third mask were then created, representative of the trabecular material and marrow cavity (empty space within the synthetic femur). The trabecular mask components were subtracted from the cortical mask, which then had the marrow component subtracted from them. The result was three final masks representing the cortical material and a superior trabecular and inferior trabecular component, which could then be region grown and turned into part files.

The part files were exported to 3-Matic (Materialise NV, Leuven, Belgium) to refine the models. Due to the very thin cortical material on the anterior surface below the inter-trochanteric line, as well as the voxel size used in scanning, several holes were present (Figure 4.1). These holes were isolated (Figure 4.2) and filled using the 3-Matic toolkit, which was then unified into one surface (Figure 4.3). Each component had a rough surface, derived from the voxel mesh of the original mask, which was refined in 3-

Matic using the 'smooth' and 'wrap' features. A surface mesh of the model was automatically generated in 3-Matic and refined using several preinstalled tools, such as uniform mesh generation.

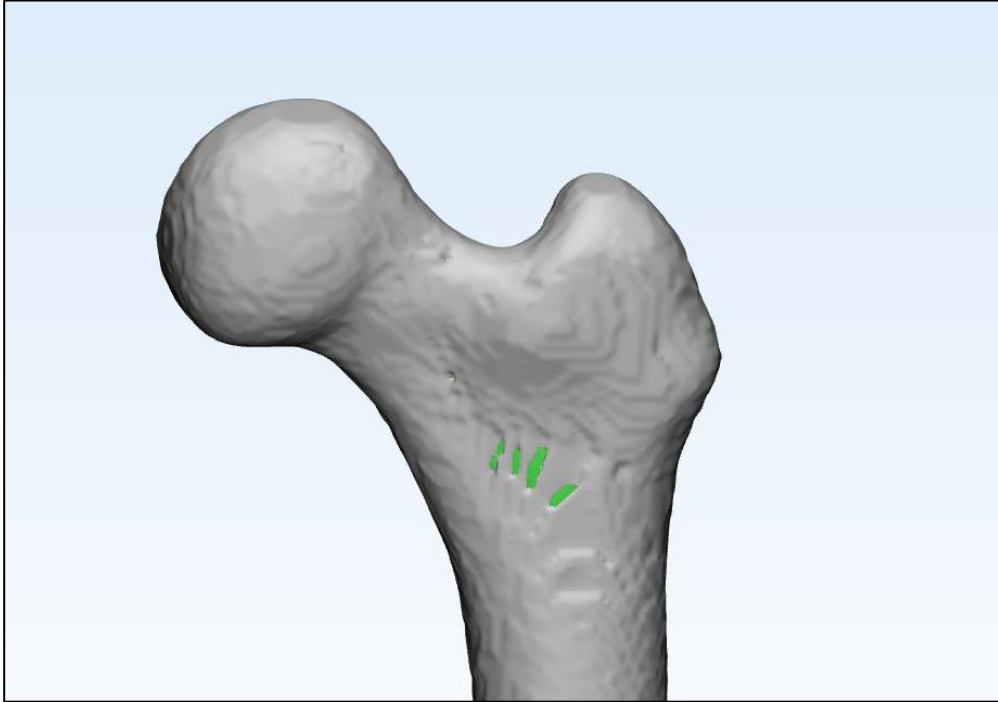
3-Matic and Mimics both contain the ability to export file information to Abaqus (Dassault Systemes, Velizy-Villacoublay, France), as STL and INP files. Unfortunately, these options all resulted in an orphan mesh - a mesh without any associated geometry - within Abaqus, which has a limited toolset associated with it. Attempts to convert the orphan mesh to a part file are outlined in APPENDIX F: Orphan Mesh to Part Conversion, all deemed unsuitable for this analysis.

4.2.2 Altered Cortical Thickness Model Development

To create the alternate models, the superior and inferior trabecular components were scaled by 3-Matic by 1.01 and 1.03 (a 1% and 3% overall growth in the trabecular components), henceforth referred to as the x101 and x103 models. The 3% scaling was the largest change possible without complete pop-out of the superior trabecular part through the cortical component. The 1% scaling was chosen to establish the influence of a minor reduction in cortical thickness. Scaling occurred from user-defined points to reduce pop through and more evenly distribute the cortical thinning. These points were located at the anterior surface below the

intertrochanteric line and at the most inferior plane for the proximal and distal trabecular components, respectively. The marrow cavity was scaled by the same amount for each model, with the same location specified in the distal trabecular scaling and used to reduce the diaphyseal thickness where no trabecular components were present. The cortical component was adjusted accordingly by converting the modified components to masks, using Boolean operations to remove the required 1-3% of cortical material from the inner cortex of the original cortical mask.

The new enlarged components (two trabecular components (Figure 4.4) and the marrow cavity) were transferred back to Mimics, converted to STL files, and then mask filled. A similar process to the first model creation was then implemented.

**Figure 4.1: Rough Surfaces in 3-Matic Import**

Model components imported from Mimics to 3-Matic maintained the shape and general geometry of the scan but had a rough texture. Due to the scan resolution and thin cortical shell on the proximal anterior surface of the synthetic model, gaps occurred that had to be filled manually.

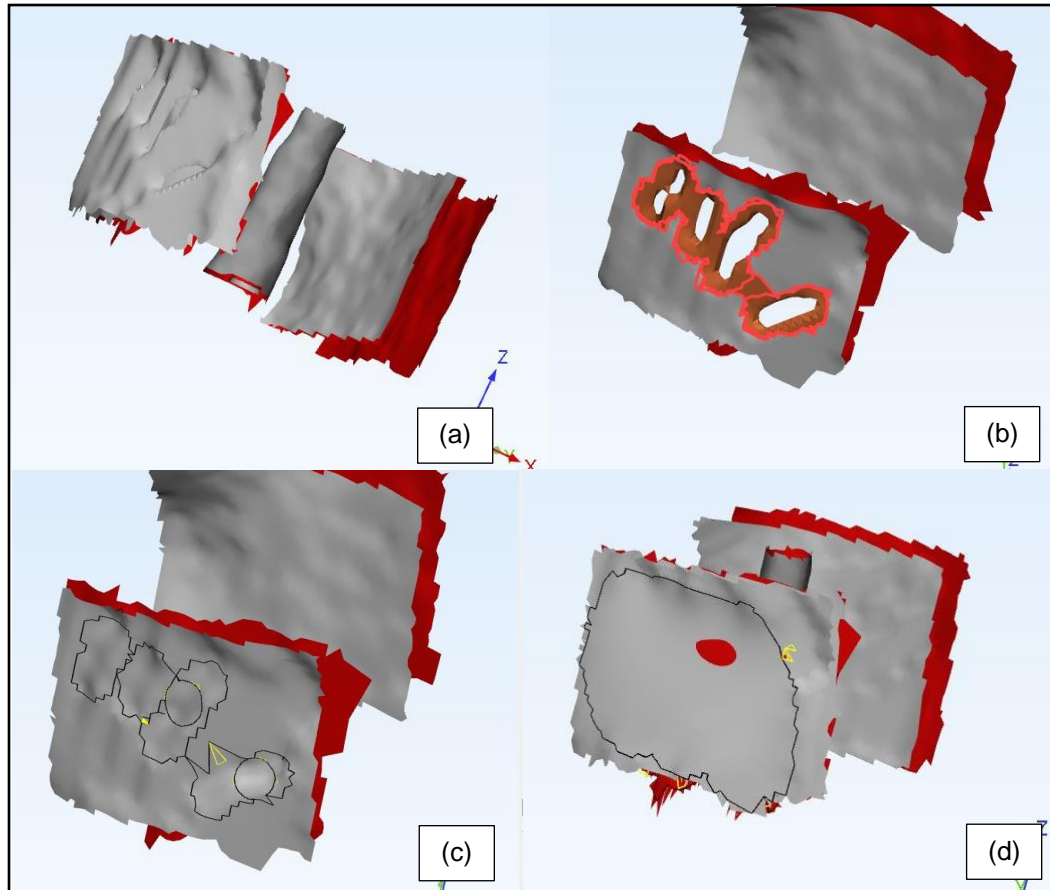
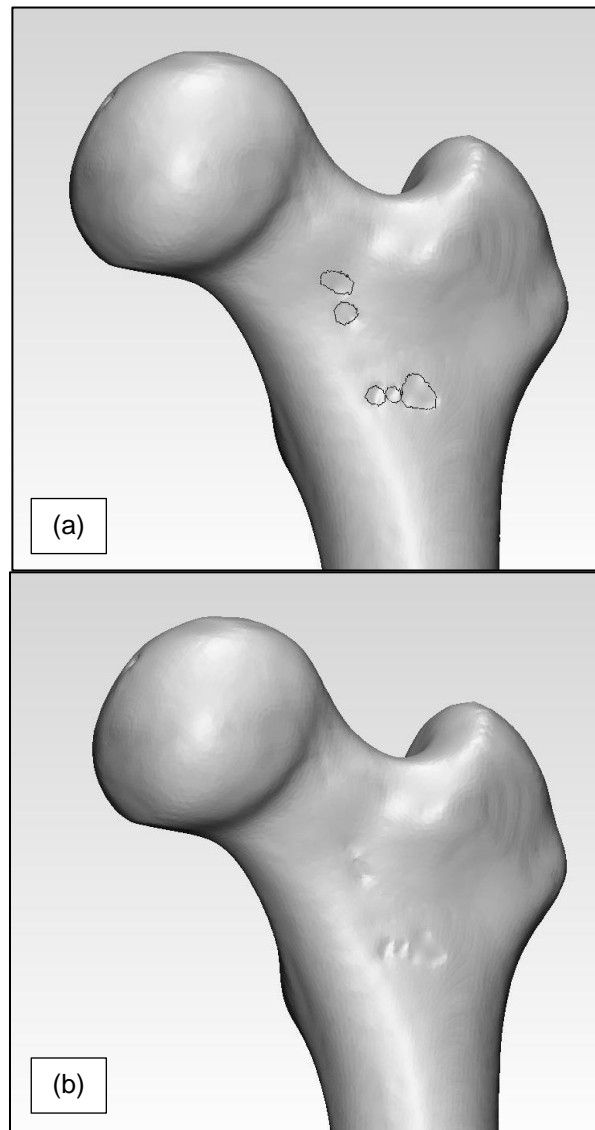


Figure 4.2: Cortical Gap Filling

To resolve any unwanted gaps in the model, small areas were isolated via viewing tools (a), with grey and red indicating exterior and interior surfaces, respectively. The surrounding areas were highlighted with the wave brush tool (b) and then deleted, to be filled with the 'fill hole freeform' feature (c). Large gaps had to be structured to create a uniform surface, otherwise, the fill feature would create gaps in the surface (d).

**Figure 4.3: Model Surface Unification**

After filling gaps (a), the resultant surfaces of the model were combined, then 'smooth' and 'wrap' tools were used to further reduce any inconsistencies, to create a surface more representative of the physical model.

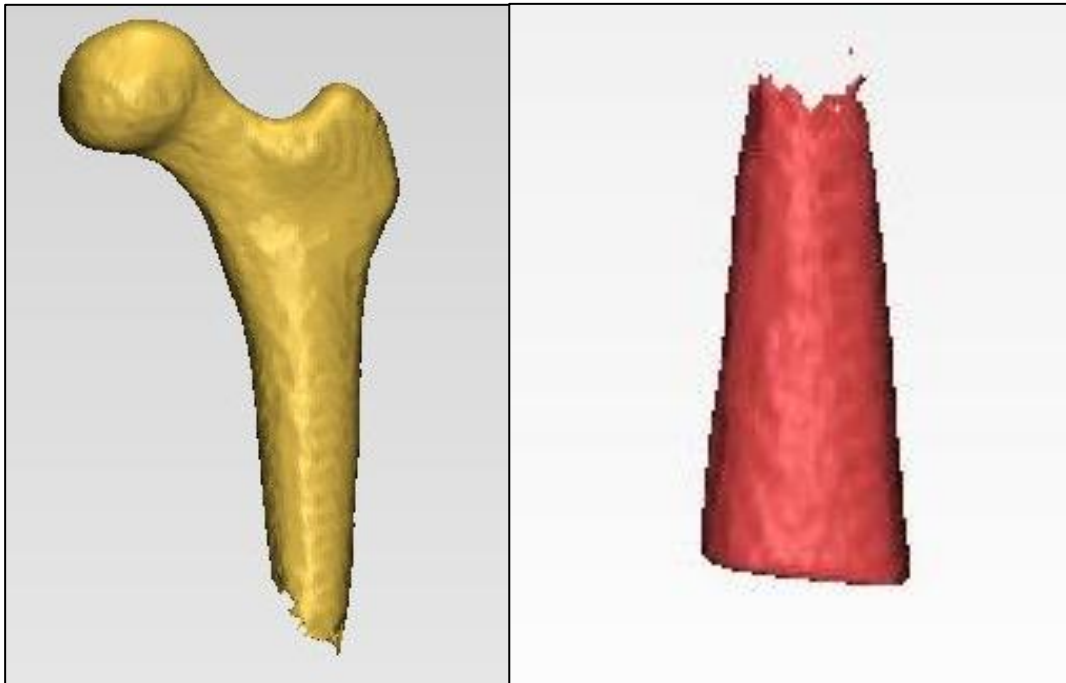


Figure 4.4: Trabecular Components in 3-Matic

The parts imported from Mimics to 3-Matic also had rough surfaces, and were smoothed and wrapped as the cortex part was.

4.2.3 Interior Contact

All parts were imported into Abaqus using the scale and alignment automatically generated from Mimics/3-Matic, eliminating the need for manual placement and/or orientation. Surface sets were assigned to the exterior surfaces of the trabecular components and to the corresponding interior surfaces of the cortical material. The cortical and trabecular components were put in contact using the 'Tie' constraint, with the cortical surface as the master. Surface-to-surface contact was defined, without tying rotational degrees of freedom.

4.2.4 Meshing

Two element shapes are typically used in biomechanical simulations, namely, tetrahedral and hexahedral, with hexahedral being the preferred choice for dynamic analysis (Burkhart et al. 2013). Hexahedral elements are noted to be more stable and less influenced by refinement; however, experimental strains measured in the proximal femur have been previously shown to be well correlated to simulated values using second order tetrahedral elements (Ramos and Simões 2006). Due to its acceptance for quasistatic simulations and the availability in 3-Matic, tetrahedral elements were selected. Hexahedral elements, also used in industry, are not available in Mimics or 3-Matic.

A linear tetrahedral mesh was generated automatically in Mimics and was refined in 3-Matic. The surface mesh was refined using the ‘uniform remesh’ option, replacing linear tetrahedral with quadratic tetrahedral elements. A maximum element length was also specified. A corresponding volume mesh was subsequently created.

4.2.5 Mesh Sensitivity Analysis

A mesh sensitivity analysis was conducted using volumetric models based on standard material properties (Table 4.1), with maximum edge lengths of 10, 7.5, 5.0, 4.0, 3.5, and 3.0 mm, generated in Mimics/3-Matic, with varying node and element numbers (Table 4.2). The analysis was conducted in axial compression only, one of the primary loading modes to be examined, to determine the minimum limit for acceptable results. The contacts, boundary conditions, and outputs are the same as those described in Section 4.2.8, unless otherwise specified.

Von Mises stress values were calculated at three key locations. Datum points were visually positioned on the anterior surface below the intertrochanteric line and on the medial and lateral mid-diaphysis. The absolute co-ordinates of these points were recorded and recreated in each model, using the nearest 1-3 elements for corresponding history analysis sets, depending on the position of the datum point on the mesh.

The resultant stress values at these elements were averaged and plotted against the associated number of total model elements (Figure 4.6). Accuracy was compared based on the values of the 3.0 mm model. A percentage difference of < 5 % was deemed an acceptable range for convergence, in line with previous studies (e.g. Jones and Wilcox 2008). As such, a 5 mm mesh size was used for all future simulations.

Table 4.1: Material Properties as Described by Sawbones™

The 3403 specimens had standard short fiber filled epoxy to represent cortical material and used 10pcf solid rigid polyurethane foam to represent trabecular material. Both sets of material properties were listed on the Sawbones™ website (Sawbones 2018). A density variation of $\pm 10\%$ was expected in the polyurethane foam based on personal communication with the company. Abaqus does not contain an option to model separate tension and compression modulus values simultaneously. Given the geometry of the femur and the loading vectors, there was no clear dominant loading mode – tension or compression – so an average value was used for the initial model. A Poisson's ratio of 0.26 was assumed for the solid rigid polyurethane foam used to represent the trabecular bone.

	Density (kg/m ³)	Tensile Modulus (GPa)	Compressive Modulus (GPa)	Modulus Used (GPa)	Poisson's Ratio
Short Fiber Filled Epoxy (Cortical)	1640	16	17	16.5	0.26
Solid Rigid Polyurethane Foam (Trabecular)	160	0.058	0.086	0.072	0.26

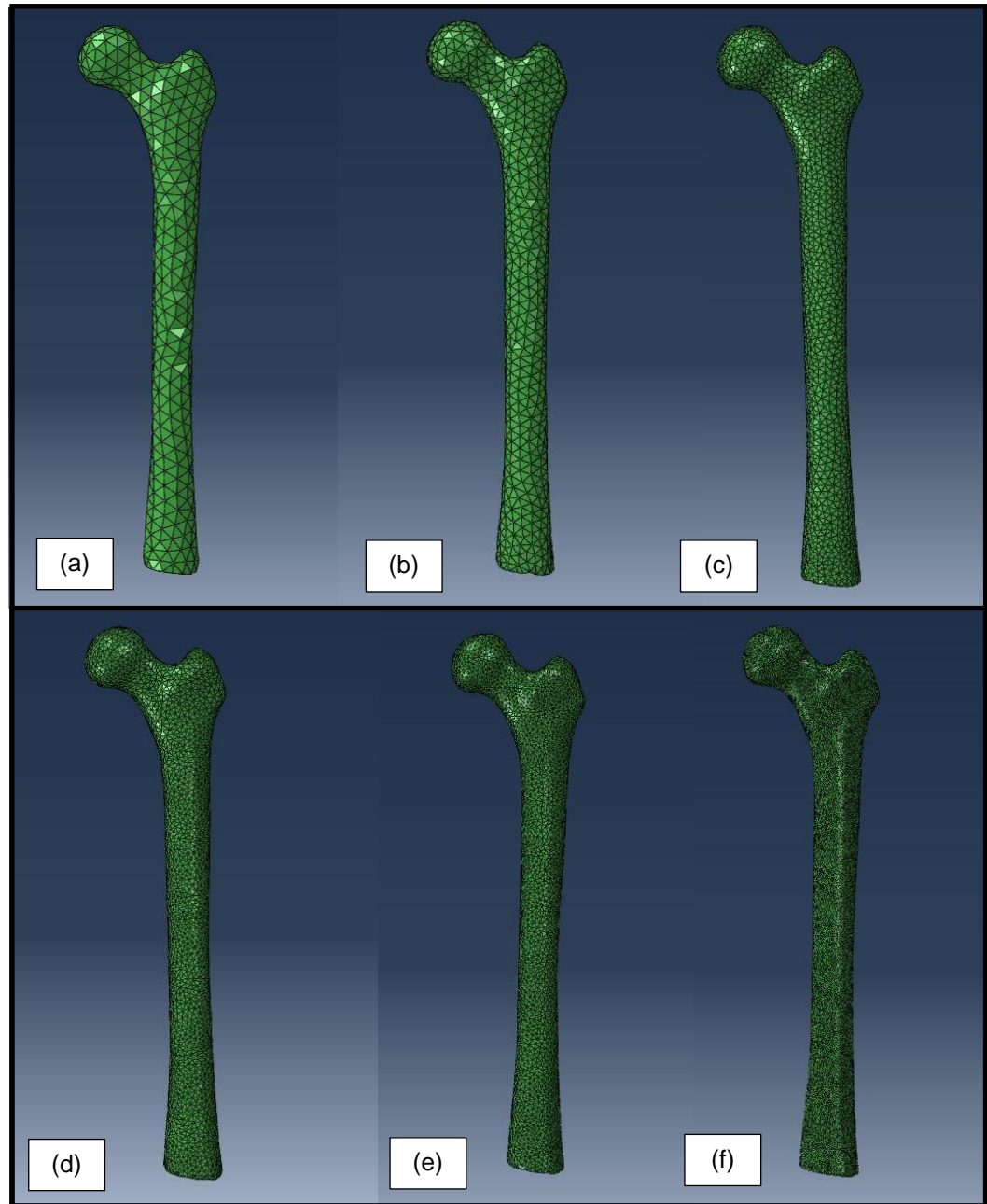


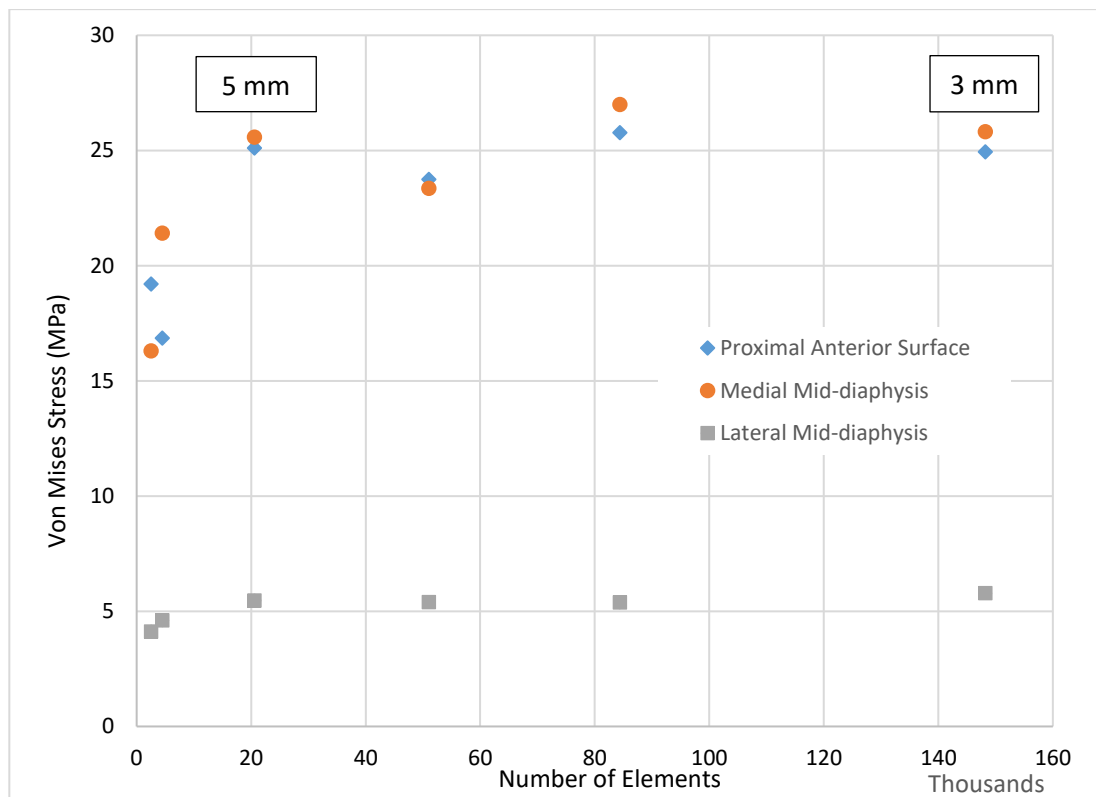
Figure 4.5: Levels of Cortical Mesh Refinement

Axial compression simulations were conducted on six levels of refinement, based on maximum element length, defined as: 10 mm (a), 7.5 mm (b), 5.0 mm (c), 4.0 mm (d), 3.5 mm (e), and 3.0 mm (f).

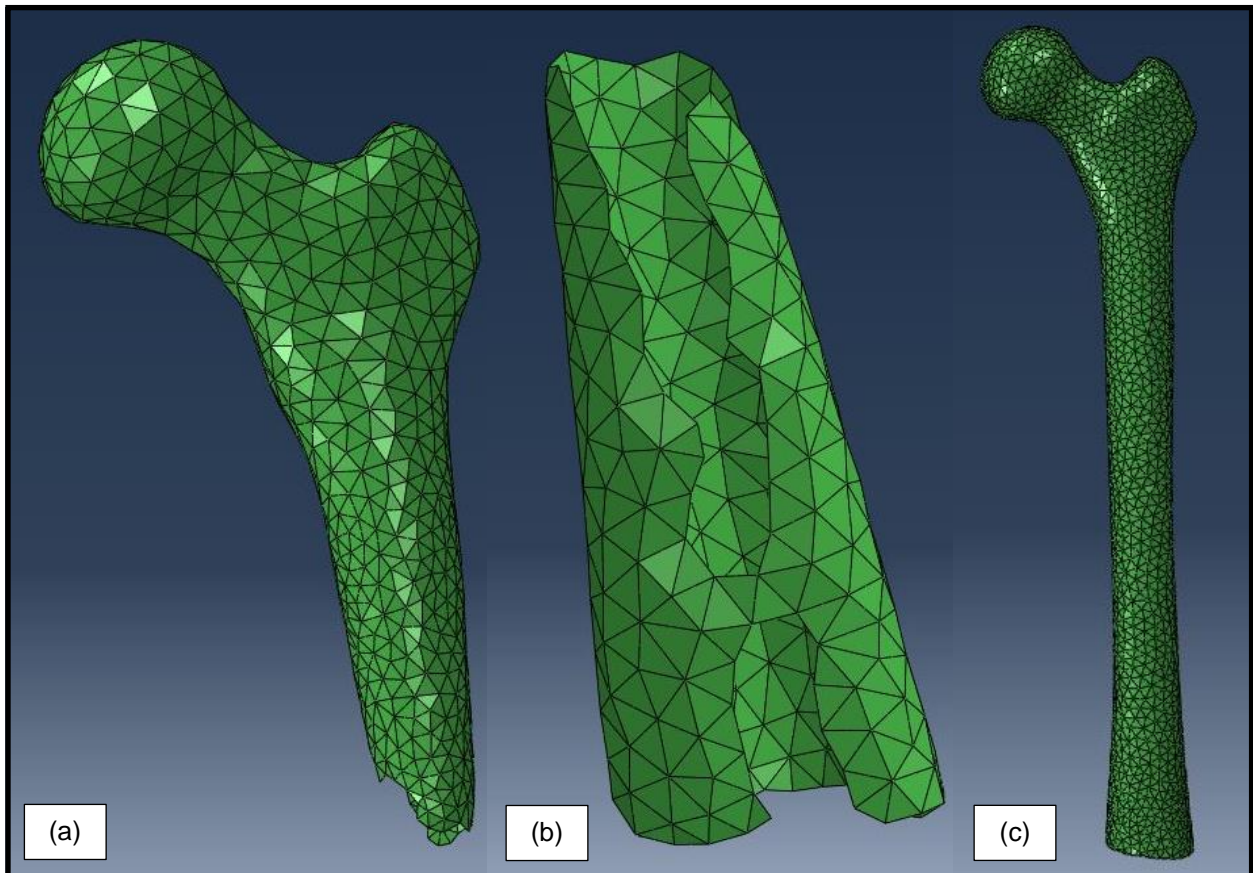
Table 4.2: Mesh Sensitivity Analysis Model Elements and Nodes

Meshes were created by specifying the maximum edge length in 3-Matic, with exponential increase in nodes and elements as maximum lengths were reduced.

Maximum Edge Length (mm)	Number of Nodes	Number of Elements	Computational Time (hours)
10.0	4955	2498	0.05
7.5	8831	4466	0.1
5.0	33711	20577	0.35
4.0	77327	51042	1.0
3.5	124403	84411	4.0
3.0	213081	148212	9.0

**Figure 4.6: Mesh Sensitivity Analysis Plot**

Comparing the Von Mises stress at three locations in the model indicated that the model reached convergence with the 5 mm element size.

**Figure 4.7: Final Mesh**

After conducting the mesh sensitivity analysis, the 5 mm model was selected, being the coarsest mesh that still provided suitably accurate results. In all test instances, all three parts were meshed with the same maximum element lengths. The corresponding superior (a) and inferior (b) trabecular components are shown, as well as the cortical (c) part.

4.2.6 Model Evaluation

After selecting the 5 mm model, the resultant stiffness was quantified to establish the suitability of the simulation for further analysis. No strain gauges were attached to the synthetic specimens during testing due to budget limitations, necessitating the use of stiffness values as the method of evaluation. The point of contact in the loading cup was used to create the displacement history output to record the exact displacement at each step, which was then combined with the measured load to compute stiffness – analogous to the Instron tests where the displacement was recorded via the movement of the crossbeam. A reference point was created inferior to the model, with a constrain interaction created between it and the inferior surfaces of the cortical and inferior trabecular parts (Figure 4.8). An encastre boundary condition was applied to the reference point, also constraining the corresponding inferior surfaces. A force history output was created using this reference point, recording the total force exerted on the model at a singular point.

Certain values were unknown *a priori* for the model; therefore, a series of studies were designed to investigate key values to ensure that the model matched experimental stiffness values before new models were tested. The unaltered model was adjusted using the cortical and trabecular modulus values, the friction value of the femur-cup interface, the initial position of the

cup, and total cup displacement. The force and displacement history output vectors were summed to create corresponding scalar total magnitude values and exported to Microsoft Excel as a force-displacement table. A total of 14 iterations were conducted (Table 4.3), with the cortical modulus being the most significant determinant of stiffness.

A modulus of 3 GPa gave the closest stiffness value to experimental results. Given that this value was so different from the 16.5 GPa listed by the manufacturer, isolated mechanical tests were conducted to verify the modulus of the 3403 specimens. The results of these tests are presented in Section 4.2.7.

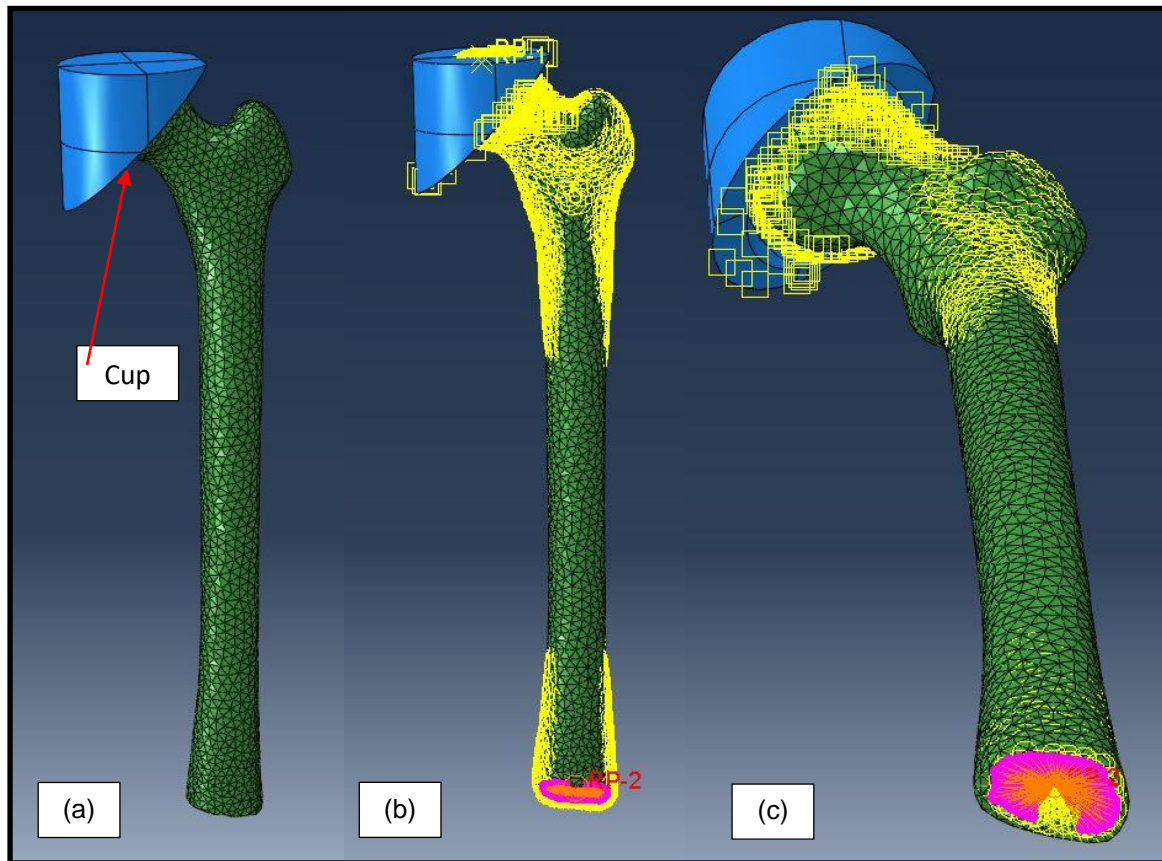


Figure 4.8: Axial Modelling Configuration

Primary analysis of the model was conducted in axial compression (a), with the femur model static and loading induced by displacement of the cup. Surface-to-surface interaction was defined for the cup and femoral head with a friction coefficient of 0.4. Trabecular components were tied to the interior cortical surface (b). A reference point was created distal to the bone, tied to the inferior surface and used as a boundary condition to facilitate force collection (c).

	Cortical Modulus (GPa)	Trabecular Modulus (MPa)	Friction Between Cup and Bone	Other	Stiffness (N/mm)	Percentage Error (%)
Natural	-	-	-	-	556.9	-
1*	16.5	72	0.4	-	3206.7	475.8
2	16.5	72	0.4	Cup Displacement at 1 mm	2996.6	438.1
3	15	72	0.4	-	2915.2	423.5
4	16.5	36	0.4	-	3206.7	475.8
5	16.5	72	0.1	-	3414.4	513.1
6	16.5	72	0.7	-	3215.9	477.5
7	16.5	108	0.4	-	3206.7	475.8
8	16.5	72	0.4	Cup Shifted (-3,1.5, -0.5)	3449.5	519.4
9	13.5	72	0.4	-	2623.7	371.1
10	10	72	0.4	-	1943.5	249.0
11	10	36	0.4	-	1943.5	249.0
12	5	36	0.4	-	971.7	74.5
13	5	10	0.4	-	971.7	74.5
14	3	10	0.4	-	583.0	4.7

* Model used for mesh sensitivity analysis

Table 4.3: Model Evaluation Table

The influence of cup displacement, modulus, cup-femur friction, and cup position was assessed and compared to 3403 cyclic stiffness calculated in Chapter 3. In trial 8, the cup was shifted to represent contact applied closer to the long axis of the femur. Highlighting is included to emphasize the target stiffness and the most representative model.

4.2.7 Material Property Selection

The diaphyseal remnants of five previously tested 3403 Sawbones™ were cut through the coronal plane with a band saw into a semicylinder. The samples were loaded into an Instron E1000 (Instron, Norwood, MA) materials testing machine equipped with a 2 kN load cell, in three-point bending configuration, with a distance of 7.0 cm between the bottom supports, where the shortest sample was approximately 7.5 cm in length (Figure 4.9). Samples were loaded at 10 mm/min with a preload of 20 N to a maximum of 300 N. One preconditioning cycle was conducted followed by two test cycles. The moment of inertia was calculated using the diameter and anterior/posterior thickness measured with a digital caliper, thus allowing the modulus to be calculated (assuming a constant thickness) based on the maximum force and displacement observed. Both sides of each specimen were tested and the cumulative average (SD) modulus of the ten tests (five samples, each with two sides) was 3.2 (0.5) GPa, with calculations presented APPENDIX G: Second Moment of Area Calculation on 3403 Mid-diaphysis Samples. This value was therefore used for all subsequent models (Table 4.4).

Modulus values of 2.56 and 2.88 GPa were selected as values for reduced modulus simulations, representing 80% and 90% of the experimentally measured modulus.

Table 4.4: Experimental Second Moment of Area and Modulus Values

Sections of the previously-tested 3403 specimen diaphyses were cut in half through the coronal plane and tested in three-point bending. The load and displacement were recorded, and the second moment of area was estimated based on diameter length and thickness measured by digital calipers, assuming a uniform thickness. The two second moment of area values were averaged and used to calculate a specimen modulus.

	Second Moment of Area (mm ⁴)			Modulus (GPa)
	Side 1	Side 2	Average	
3403-15	2529.1	2249.3	2389.2	3.64
3403-16	2850.0	1940.2	2395.1	2.45
3403-17	2576.9	2535.7	2556.3	3.36
3403-25	2611.8	1946.4	2279.1	3.58
3403-26	2532.5	2156.2	2344.4	2.87

Table 4.5: Simulated Material Properties

The final values used to define the material properties in Abaqus. Reduced modulus simulations were calculated as 80% and 90% of the cortical modulus listed.

	Modulus (GPa)	Density (kg/m ³)	Poisson's Ratio (-)
Short Fiber Filled Epoxy (Cortical)	3.2	1640	0.26
Solid Rigid Polyurethane Foam (Trabecular)	0.072	160	0.26



Figure 4.9: Three-Point Bending

A series of three-point bending tests were conducted to assess the modulus of five 3403 specimens, with approximately 20% of the length above or below the mid-diaphysis. Each specimen was cut in half with a bandsaw, with both halves tested and their derived modulus values averaged.

4.2.8 Axial Compression

The axial cup created in AutoCAD Inventor was imported into Abaqus and modified slightly to simplify the geometric complexity, though the contact surface remained unaltered (Figure 4.8 (a)). The cup was established as a Discrete Rigid part, eliminating the need for an aluminum material assignment but requiring meshing. General surface-to-surface contact was defined between the interior surface of the axial cup and the superior surface of the femoral head, as master and slave surfaces, respectively. A friction coefficient of 0.4 was used based on iterations in Section 4.2.6. Orientation of the displacement of the cup was defined based on the line between the point of contact and the lateral inferior surface, approximating the adduction seen in the physical specimen. Displacement with a magnitude of 1.5 mm along this line was used to load the model. Boundary conditions and other interactions were the same as those listed in Section 4.2.6.

4.2.9 Four-Point Bending

To conduct four-point bending, simplified models of the supports were constructed using discrete rigid shells. The geometry of the contact points remained the same, using a 1 mm radius cylinder instead of the rounded head. The bottom supports were spaced 186 mm apart, with a part-specific datum point positioned over a corresponding cortical datum point,

representing the experimental application location (Figure 4.10 (a,b)). A surface-to-surface interaction was defined with the support as the master surface.

A reference point was created below the specimen and tied to the two bottom supports (Figure 4.10 (c,d)). Encastre was applied to this reference point and used to create a history output for the total force in the model.

The top two supports were spaced 62 mm apart, again positioned to corresponding anatomical landmarks. A reference point was created above the model, with its movement tied to the top supports. Rotation in the x-axis was not restricted, similar to physical testing, allowing the load to be evenly distributed over the two points of contact. Displacement of the reference point was recorded at each interval to provide exact displacement values for stiffness calculations. Finally, a boundary condition representative of the straps used in experimental testing was implemented on the top surface of each model above the distal bottom support, restricting rotation in the long axis of the femur and translational movement along the axis of the support.

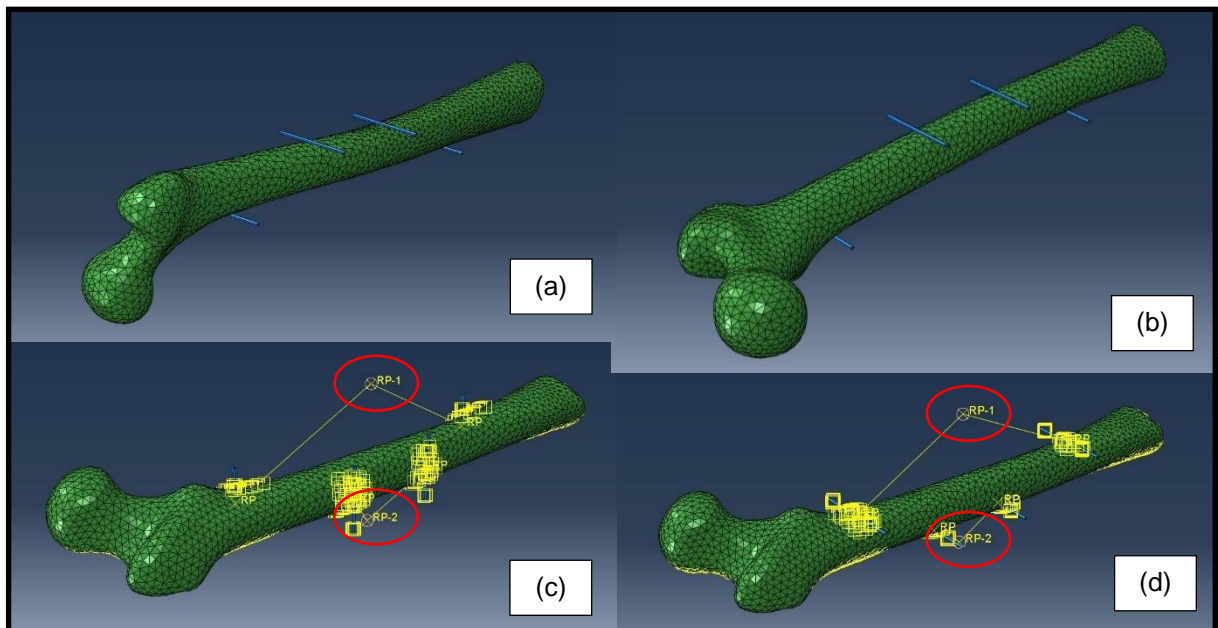


Figure 4.10: Bending Model Configuration

Four-point bending in ML (a) and AP (b) configurations are shown with blue lines representing the pivot points. Calculations were simplified by directing all forces through reference points (RP). The two pivot points were each coupled to these RPs (c, d; circled), with the RPs set as boundary conditions, used to calculate total force in the model.

4.3 Results

4.3.1 Axial Compression

The unaltered model (most representative of the experimental test specimens, with a 3.2 GPa modulus) produced a stiffness value of 641.3 N/mm, which was greater than the 556.9 N/mm stiffness recorded for 3403 synthetic experimental data (Chapter 3). The x100 with 90% modulus produced a stiffness of 578.8 N/mm, which was within 4% of the experimental data (Table 4.6, Figure 4.13).

The reduced cortical thickness was expected to decrease the resultant stiffness of the model. Experimental cadaveric data from Chapter 3 had a mean (SD) axial stiffness of 419.2 (4.1) N/mm. The closest stiffness to the cadaveric osteoporotic femurs calculated in the present series of models was the x103 model with a modulus of 2.56 GPa, with a stiffness of 455.4 N/mm (Table 4.6, Figure 4.8), which was 8.6% greater than the experimental results. The x101 model had a minimum stiffness of 550.9 N/mm, 31.4% greater than cadaveric experimental results.

4.3.2 Bending

The unaltered model produced a stiffness of 601.4 N/mm in AP, approximately 37% below the mean (SD) experimental 3403 response of 955.2 (23.9) N/mm (Chapter 3). The most representative model was the

x101 at 80% experimental modulus (2.56 GPa), which resulted in a stiffness of 1139.9 N/mm, roughly 20% greater than the synthetic experimental mean.

The mean (SD) natural stiffness in AP bending found in Chapter 3 was 763.8 (202.4) N/mm, best represented by the unaltered model at 601.4 N/mm, 21.3% below the natural experimental data collected. All other models showed an increase in stiffness, ranging from 1139.9 N/mm in the x101 model at 2.56 GPa to 1723.2 N/mm in the x103 model at 3.2 GPa (Table 4.7, Figure 4.14a). Only the unaltered model was within 1 SD of the natural experimental data.

In ML bending, the unaltered model produced a stiffness of 1116.8 N/mm, within 6% of the average 3403 response at 1056.3 N/mm; the best match of all models tested.

The mean (SD) natural experimental stiffness in ML bending was 592.5 (112.1) N/mm, best represented by the x101 model at 2.56 GPa with a stiffness values of 594.5 N/mm. The x100 model was too stiff across all modulus values, with a minimum stiffness of 893.5 N/mm. Four models fell within 1 SD of the natural experimental results: x101 at 2.56 and 2.88 GPa; and x103 at 2.88 and 3.2 GPa (Table 4.7, Figure 4.14 (b)).

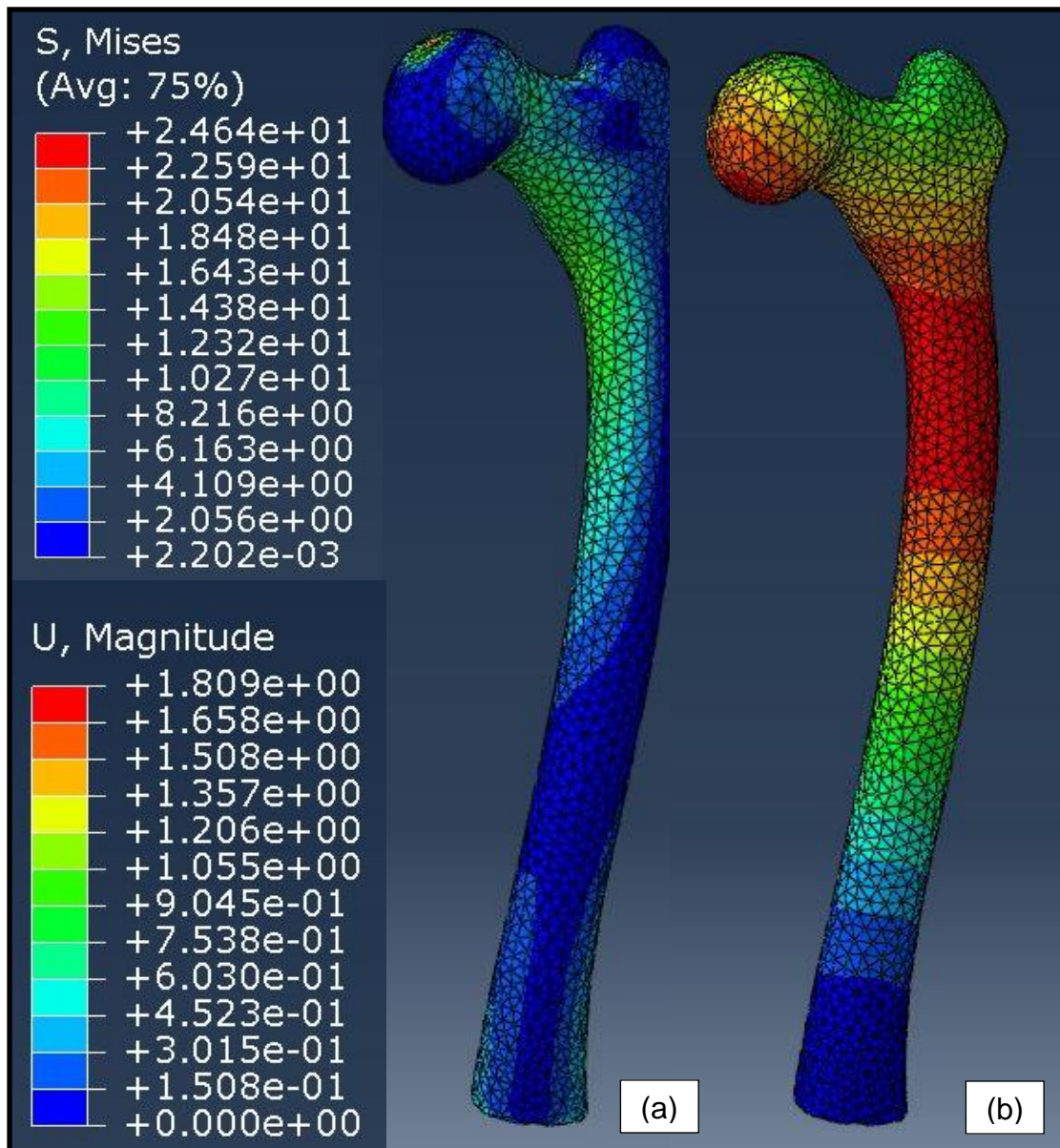


Figure 4.11: Axial Compression Fringe Plots

The fringe plots corresponding to Von Mises stress in MPa (a) and magnitude of displacement in mm (b) throughout the model in axial compression with the cup removed for clarity. Model distortion is visually exaggerated in all images.

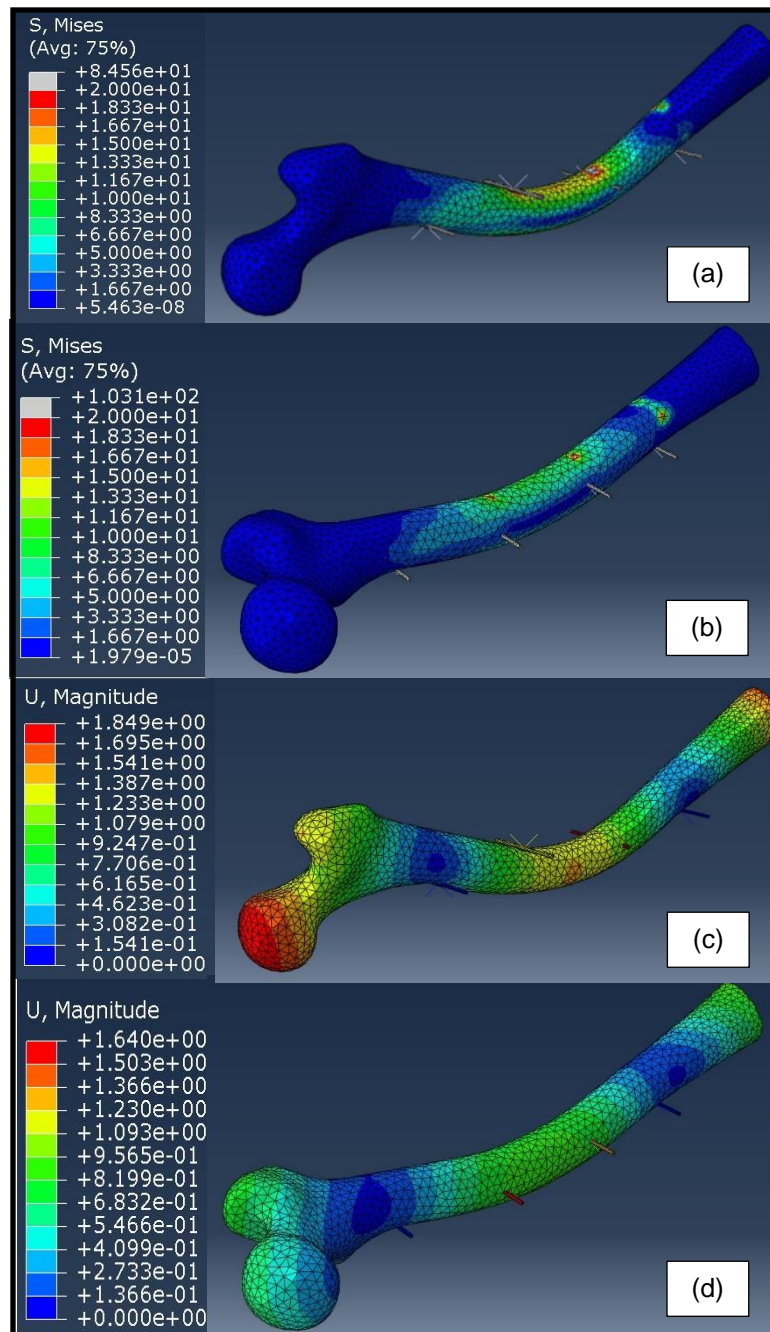


Figure 4.12: AP and ML Bending Fringe Plots

Sample fringe plots from the x100 model in both planes of bending, demonstrating Von Mises stress in MPa (a, b) and displacement magnitude in mm (c, d) distribution throughout the model at peak loading. Model distortion is visually exaggerated in all images.

Table 4.6: Axial Compression Stiffness Results and Percentage Error
Results from the nine simulations indicated that the best axial compression approximation occurred in the x103 model at 80% modulus (highlighted), which ended up being 8.6% stiffer than the natural specimen average.

		Stiffness (N/mm)	Cadaveric Percentage Error (%)
Experimental	Cadaver	419.2	-
x100	E80	516.3	23.2
	E90	578.8	38.1
	E100	641.3	53.0
x101	E80	550.9	31.4
	E90	617.3	47.3
	E100	683.6	63.1
x103	E80	455.4	8.6
	E90	504.7	20.4
	E100	556.6	32.8

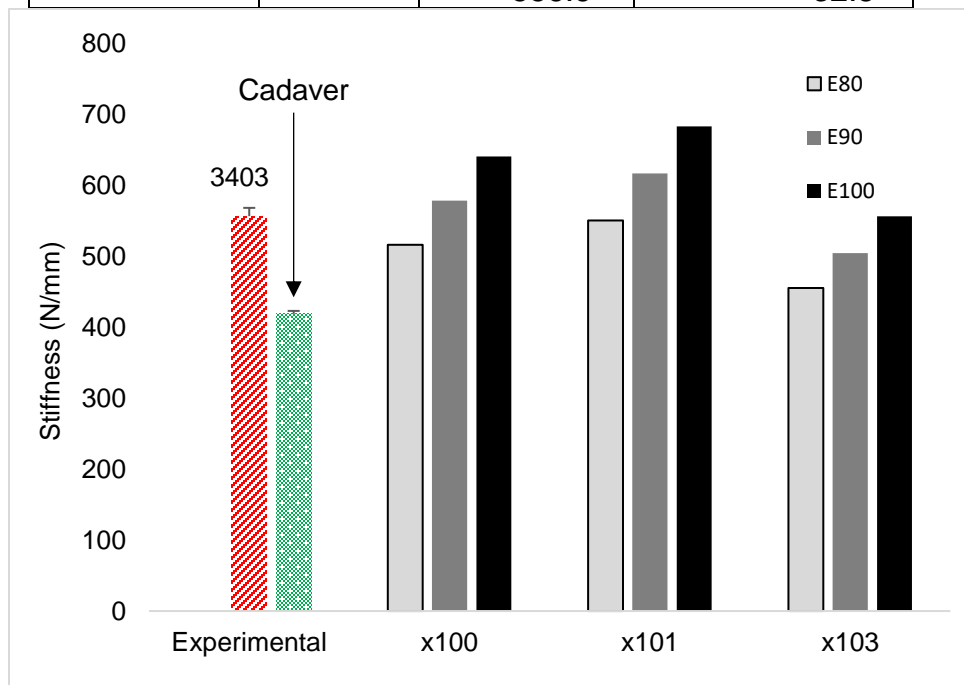


Figure 4.13: Axial Compression Stiffness Results

The calculated stiffness of each model with 80, 90, and 100 % of the 3.2 GPa base cortical modulus derived, as compared to the 3403 model (red) and cadaveric results (grey dotted).

Table 4.7: AP and ML Bending Stiffness Results

The resultant stiffness values in four-point bending in AP and ML planes across all nine simulations conducted. Resulting stiffnesses were compared against cadaveric experimental stiffness in the corresponding plane, with the target value and closest model results highlighted and bolded.

		AP		ML	
		Stiffness (N/mm)	Cadaveric Percentage Error (%)	Stiffness (N/mm)	Cadaveric Percentage Error (%)
Experi-mental	Cadaver	763.8	-	592.5	-
x100	E80	481.1	37.0	893.5	50.8
	E90	540.0	29.3	1005.1	69.6
	E100	601.4	21.3	1116.8	88.5
x101	E80	1139.9	49.2	594.5	0.3
	E90	1282.3	67.9	668.8	12.9
	E100	1424.8	86.5	743.1	25.4
x103	E80	1378.5	80.5	401.3	32.3
	E90	1550.8	103.0	451.5	23.8
	E100	1723.2	125.6	501.7	15.3

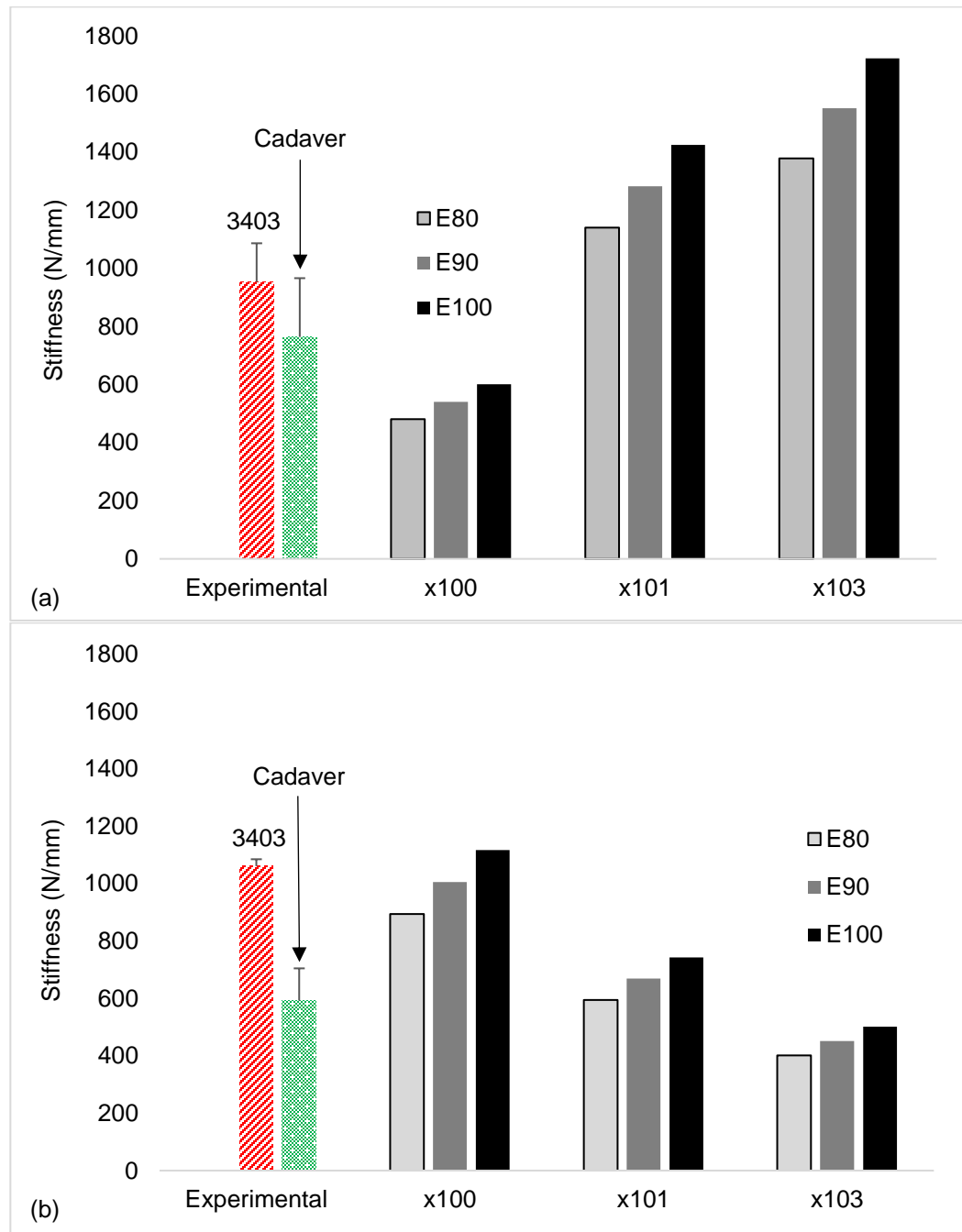


Figure 4.14: AP and ML Bending Stiffness Results

The resultant stiffness values recorded in four-point bending in the AP (a) and ML (b) planes, compared to the 3403 experimental results (solid red) and cadaveric experimental results (dotted grey).

4.4 Discussion

This study has been a preliminary and systematic analysis of possible revisions to the 3403 synthetic model, facilitated by attempting combinations of reduced cortical modulus and cortical thickness. A model was developed that is largely representative of the experimental response of 3403 synthetic osteoporotic femurs in axial compression and ML bending but produced larger errors in AP bending. No one model was created that was optimal for all loading configurations, and what might produce highly similar results in one orientation was less than optimal in others.

While the cortical modulus listed by Pacific Research Laboratories was 16 GPa, the synthetic femurs received had reduced epoxy resin properties, with 3.2 GPa shown to be more representative in experimental tests and through model evaluation. The 3.2 GPa is also in line with Papini (2007), who used a modulus of 4.5 GPa for synthetic femurs in axial compression that produced results within one standard deviation of the average of cadaveric data. This value was well matched to the series of axial studies conducted herein, but was not representative of experimental results in AP bending. The reason for this discrepancy is currently unclear.

Result analysis indicated an increase in the second moment of area between unaltered and adjusted models, most notably a significant increase

in AP bending from $2.2 \times 10^{-8} \text{ m}^4$ in the standard model to 5.3×10^{-8} and $5.7 \times 10^{-8} \text{ m}^4$ in the x101 and x103 models, respectively. It is worth noting that the approximate second moment of area for the synthetic model was $2.1 \times 10^{-8} \text{ m}^4$ as measured using BoneJ based on CT scan data at the mid-diaphysis. Component volumes for each part (Table 4.8) indicate that the cortical component did not decrease in volume, as expected, while the trabecular components' volumes increased substantially. Total model volumes (Table 4.9), demonstrating the magnitude of the change. It is likely that the change in cortical geometry occurred from the multiple import/exports between Mimics and 3-Matic, possibly during mask creation and cavity fill. It is also possible a combination of the model modifications derived from the marrow cavity or that the trabecular components did not scale as intended. The geometric alterations may also have occurred from the 'wrap' and 'smooth' tools; however, without the use of these tools, the model was unlikely to produce reasonable results. Although the model was not altered as intended, the alterations provided a more representative response in AP bending than would have otherwise occurred, as the base model stiffness was already below the desired response and would only decrease further with a reduced second moment of area. Similarly, the ML response proved very accurate to experimental results. In a future iteration, use of a dedicated computer-aided design (CAD) program, rather than

Mimics/3-Matic, would provide greater control over model iterations and help resolve this issue.

In AP and ML bending, the major influencer of stiffness was the adjusted cortical thickness, representing a 136-187% increase in AP and a 33-55% decrease in ML. A 10% change in modulus represented an 11% change in stiffness, which was also seen in axial compression. Decreasing the cortical thickness in axial compression produced a 6% increase in the x101 model, but a 13% decrease in the x103 model. It is possible this was also influenced from the unintended second moment of area increases in the diaphysis; due to the morphology of the bone, bending is inescapable in axial compression testing, presenting itself as a bowing in the AP plane. The decrease seen in the x103 model was expected from the effects of the very thin cortical shell overwhelming the effect of the increased moment of area, while the opposite was true for the x101 model.

Given the relatively linear relationship between cortical modulus and resultant stiffness in all modes, a unique modulus value could be used in each mode to produce an ideal stiffness to represent the natural experimental results in the unaltered model. The optimal representation for axial stiffness could be produced with a modulus of 2.06 GPa. A modulus of 1.70 GPa would be ideal for ML bending, while a modulus of 4.08 GPa

would be most effective for AP bending. However, targeting different models and moduli to different modes is not an ideal approach, so a single modulus that provided results that were within an acceptable range and could be tied with localized cross-section adjustments to achieve the desired response is the recommended method moving forward.

A key limitation of this work was the mesh sensitivity analysis, which was conducted in axial compression alone, and therefore did not guarantee sufficient convergence in either plane of bending testing. While additional analyses could have been conducted, it was decided that one mesh quality with unified material properties would be used across all tests to allow for comparisons between models and tests without caveats or relative numbers. Further, the response of the model chosen proved very accurate when compared to the finest mesh tested. No information about the number nodes or elements was included in Papini *et al.* (2007); however, the mesh was visibly more coarse than what was used in this research. Research conducted by Taddei *et al.* (2006) used a mesh of 10-noded tetrahedral elements, constituting 76,026 elements and 118,970 nodes, approximately 2.25x greater than the 33,711 elements and 20,577 nodes in the 5 mm model used in this research; however, this model was based on a natural femur and no mesh sensitivity analysis was documented. It is difficult to make recommendations for future studies based on this mesh sensitivity

analysis. The distal end was not included in the mesh, which reduced the number of elements and nodes created. While convergence was demonstrated across different meshes (representing several magnitudes of difference in element and node number), this model was developed from a synthetic femur, with uniform and anisotropic properties. This model may serve as a landmark for similar, future synthetic studies, or possibly as an initial estimate for cadaveric studies.

Another limitation occurred from the 3-point bending tests. The hemicylindrical specimens were unrestrained laterally during testing, so it is possible that transverse expansion occurred under loading, which would reduce the resultant modulus calculated. A reduced modulus would reduce the associated model stiffnesses to an unknown extent in bending. Further tests were not conducted, given that the modulus value calculated was similar to that determined during model evaluation, similar as compared to previous studies (e.g. Papini *et al.* 2007), and the models produced results similar to experimentally determined values in axial and ML bending, indicating that the influence of the transverse expansion was likely insignificant.

Torsional testing, while conducted in Chapter 3, was omitted from the finite element analysis conducted. This is due, in part, to the complications

arising from the orphan mesh geometry, which prevented the development of a matching cup for loading. Attempts were made to simulate analogous loading with the use of distributed moments and loads, but was not pursued due to the number of assumptions and simplifications required. Similarly, the method used in torsion testing is relatively novel, and would be difficult to contrast to previous literature, limiting its efficacy in future analysis.

One other parameter that was unknown *a priori* was the friction factor between the head and the aluminum acetabulum cup used for testing; an initial value of 0.4 was selected. The aluminum cup contact surface was polished, but was not lubricated during experimental testing in Chapter 3. During that synthetic testing, noise in the load signal and a squeaking sound was noted, indicating potential movement between the femoral head and the cup. Scratches were found inside the cup corresponding to synthetic femoral head displacement after experiments had finished. Other frictional coefficients were examined in evaluating the model but did not significantly influence the resultant stiffness in axial compression.

While not a precise replication in this respect, using an average modulus value was deemed acceptable, given that the trabecular modulus was largely irrelevant, similar to statements from Papini (2007), and as illustrated during the parametric initial investigation. Osteoporosis will reduce the

properties of trabecular bone; however, in this study reductions to the trabecular modulus were shown to not influence the overall model stiffness.

Screw pullout has been investigated in fourth generation synthetic femurs (Sawbones™) and cadaveric femurs using finite element modelling (Zdero *et al.* 2008). A finite element model was developed, and the experimental screw pull-out forces were used as input variables to develop shear stress values at the screw-bone interface. The finite element analysis of solid rigid polyurethane foam results were within 1 standard deviation compared to human femur shear stress values, even though of the six cadaveric specimens tested, two were osteopenic and three were osteoporotic, indicating that the polyurethane foam is better matched to poorer quality bone. While not feasible in this work, the numerical model constructed could be improved with the addition of non-linear material properties, which would allow axial failure and screw pullout to be assessed.

Moving forward, it is recommended that the model be adjusted with computer-aided design (CAD) software, such as AutoCAD or SolidWorks, rather than Mimics/3-Matic. A model created and modified in this way could be used to produce a numerical model representative of the torsion loading cup, allowing torsion testing to be conducted. Using design-based software would also be more effective in maintaining the exterior geometry of the

model and assist in producing the right alterations. The cross-section of the x101 and x103 models should be analyzed to determine the new cross-section, which can be correlated to the bending and axial stiffness results presented here. These differences from the unaltered model can be used as guides, alongside cortical modulus values, in producing a revised model that better represents all three natural stiffness results. This model will serve as the basis of a second prototype, governing its associated geometries, materials, and sensitivity to variation in these parameters. With minor modifications, the models produced in this work can be used to provide insight into more optimal geometric and material properties in future Sawbones™ models.

Table 4.8: Component Volume Analysis Across Different Models
Automatically generated volumes for each component using 3-Matic.

	Model	Volume (mm³)
Cortical	x100	182 813
	x101	195 841
	x103	184 776
Superior Trabecular	x100	98 102
	x101	125 383
	x103	130 409
Inferior Trabecular	x100	15 078
	x101	21 649
	x103	22 595
Canal	x100	59240
	x101	61053
	x103	66715

Table 4.9: Total Model Volume
Combined volumes by model from data found in Table 4.8.

Model	Total Volume (mm³)
x100	295 993
x101	342 873
x103	337 780

4.5 References

- Burkhart TA, Andrews DM, Dunning CE. 2013. Finite Element Modeling Mesh Quality, Energy Balance and Validation Methods: A Review with Recommendations Associated with the Modeling of Bone Tissue. *J. Biomech.* 46:1477–1488. doi:10.1016/j.jbiomech.2013.03.022.
- Huiskes R, Chao EYS. 1983. A Survey of Finite Element Analysis in Orthopedic Biomechanics: The First Decade. *J. Biomech.* 16:385–409. doi:10.1016/0021-9290(83)90072-6.
- Jones AC, Wilcox RK. 2008. Finite Element Analysis of the Spine: Towards a Framework of Verification, Validation and Sensitivity Analysis. *Med. Eng. Phys.* 30:1287–1304. doi:10.1016/j.medengphy.2008.09.006.
- Papini M, Zdero R, Schemitsch EH, Zalzal P. 2007. The Biomechanics of Human Femurs in Axial and Torsional Loading: Comparison of Finite Element Analysis, Human Cadaveric Femurs, and Synthetic Femurs. *J. Biomech. Eng.* 129:12. doi:10.1115/1.2401178.
- Ramos A, Simões JA. 2006. Tetrahedral Versus Hexahedral Finite Elements in Numerical Modelling of the Proximal Femur. *Med. Eng. Phys.* 28:916–924. doi:10.1016/j.medengphy.2005.12.006.
- Sawbones. 2018. Materials Selection - Sawbones. [accessed 2018 Jul 29]. <https://www.sawbones.com/biomechanical/material-selection/>.
- Taddei F, Cristofolini L, Martelli S, Gill HS, Viceconti M. 2006. Subject-Specific Finite Element Models of Long Bones: An In Vitro Evaluation of the Overall Accuracy. *J. Biomech.* 39:2457–2467. doi:10.1016/j.jbiomech.2005.07.018.

CHAPTER 5: GENERAL DISCUSSION AND CONCLUSIONS

Overview: *This chapter reviews the objectives and hypotheses established in Chapter 1 and the experimental and computational work conducted in this thesis. The overall strengths and limitations of this work are discussed, concluding with future directions.*

5.1 Summary

Testing biomedical devices is often conducted with cadaveric specimens. However, bone is immensely complex, as demonstrated by its unique and variable properties influenced by factors such as age, gender, exercise level, and diet, further complicating testing due to the need for special handling, storage, and disposal. Synthetic models resolve many of these issues by being engineered materials and offering a much lower variability due to standardized material properties and geometry. Synthetic models have also been shown to replicate the mechanical response of femurs from the general population in loading modes such as bending, torsion, and axial compression (e.g. Cristofolini et al. 1996; Heiner and Brown 2001). Unfortunately, such analogues also come with their own disadvantages present in the form of simplified material properties,

dissimilar fracture mechanics, manufacturing artefacts, and a similar geometry often being used to represent the entire population, making synthetic bones useful in many situations given their limitations are understood and accounted for.

Another type of analogue is numerical modelling, which uses pre-defined conditions and interactions to approximate stress and strain values throughout a digital model, ideal for irregular geometries where an exact mathematical model would be impossible or impractical. Models can be used to recreate the same test with minor alterations, providing a strong basis for comparison purposes; however, digital models must be thoroughly evaluated before experimental comparisons can be made (Burkhart et al. 2013). Numerical modelling is also limited by simplifications and assumptions made while creating the model, such as a uniform interaction and loading conditions.

Disease can alter the properties and behaviours of bone by influencing attributes like density. Osteoporosis is one such affliction prevalent in older populations, significantly increasing bone porosity and thus fracture risk. Osteoporosis-related fractures are quite common, which can significantly reduce independence and quality of life. Orthopaedic devices such as plates and screws are often used to help treat such

fractures, though joint replacements (another orthopaedic device) are also common in older populations. Both types of orthopaedic implants are typically designed for the general population, and may perform differently in patients with poorer bone quality (Bukata 2017). Development of osteoporotic-focused orthopaedic implants would be greatly assisted by a model that recreates the response of osteoporotic bone; however, to date, no model has been demonstrated to do so.

The overall purpose of this study was to assess the mechanical response of novel synthetic femurs for representing osteoporotic bone, and to make recommendations to the material and geometric properties via finite element modelling to improve response accuracy.

Two sets of ten synthetic femurs with reduced wall thickness and cortical stiffness were tested and compared against five osteoporotic natural femurs stripped of soft tissue in four-point bending, torsion, axial compression to failure, and screw pullout, using custom jigs developed and manufactured in-house (*i.e.*, Objective 1, Chapter 3). Specimens were tested using methods adapted from previous research, with the exception of torsion, which required the development of a novel method. Both sets of synthetic specimens demonstrated lower variability than the cadavers in all

tests except axial compression, where all coefficients of variation were below 2.5% (*i.e.*, Hypothesis 1 accepted).

Results from the synthetic and cadaveric specimens were compared using a one-way ANOVA with Tukey post-hoc analysis. Significant differences were identified between both sets of synthetic femurs and natural specimens in bending, torsion, and screw pullout (*i.e.*, Hypothesis 2 rejected). There were several possible causes for these differences, such as modulus and cortical thickness, which were explored using numerical analyses.

Simulations recreating axial compression and four-point bending in the anteroposterior and mediolateral planes were developed in Abaqus to establish a basis for recommendations on the cortical thickness and modulus to produce a more accurate synthetic osteoporotic femur.

An experimental synthetic femur was scanned with Computed Tomography (CT) and modelled using Materialize Mimics and 3-Matic. The mesh was evaluated over six levels of varying refinement to determine that convergence was achieved along with an associated minimum mesh quality. The model was then evaluated, again in axial compression, to determine the influence of cortical and trabecular modulus, friction coefficient, and cup alignment on stiffness. The predominant model

influence was determined to be the cortical modulus, with good experimental result approximation at 3 GPa. This modulus was confirmed by conducting three-point bending tests on a set of diaphyseal cross sections from the previously tested 3403 models.

Two new models were created by increased the trabecular components and empty space of the model by 1 % and 3 %, using Boolean operators to reduce the cortical thickness. These models were substituted for the unaltered model, maintaining the same orientation as the original, with minimal adjustment to the complementary components required. Three modulus values were tested at 2.56, 2.88, and 3.20 GPa, corresponding to 80, 90, and 100 % of the experimental modulus, resulting in a total of 27 simulations.

While good representation was found for axial compression and ML bending, with results within 10% of the cadaveric experimental research conducted, the closest AP bending result was over 20% larger than the experimental response. Moving forward, no single model presented itself as ideal for any combination of loading modes. An unexpected increase in cross-section occurred from the creation procedure while exporting between 3-Matic and Mimics. This was especially prominent in AP testing,

but presents an opportunity to better understand the geometry and material properties that would produce ideal results.

5.2 Limitations and Strengths

Limitations on the evaluation of the mechanical response of these synthetic femurs include the use of a small sample size of female cadaveric specimens, where the external geometry of the synthetic femurs was based on 50th percentile male femurs. It is probable that the primary effect of this was seen in the distribution of cortical bone in the diaphysis of the femur, likely most influential in bending. While most biofidelic analysis is based on a 50th percentile male, women are more likely to suffer an osteoporosis fracture than men – estimated at one in three women versus one in five men, over the age of fifty (International Osteoporosis Foundation 2017). As such, an argument can be made that a model representative of female osteoporotic femur response would provide better overall outcomes in the development of associated orthopaedics.

Another testing limitation was the method employed for torsion testing. Previous research has used a controlled rotation effected by the testing system. This method was not possible with the equipment available, instead opting for a controlled displacement of the femoral head with the lesser trochanter supported and the distal end potted and secured. The

displacement rate was adjusted for each specimen to ensure that each specimen was tested at the same rate of rotation. This limitation has been mitigated by conducting the same test on natural specimens, confirmed to be osteoporotic, rather than comparing to previous literature.

One limitation in modelling was conducting the mesh sensitivity analysis and model evaluation solely in axial compression. While not ideal, six models with differences of several magnitude in terms of node and element number were assessed, with the model chosen producing the closest Von Mises stress values in all three assessment locations to the finest mesh model. Further, the model was evaluated using five different criteria over 14 tests, demonstrating the influence (or lack thereof) of these components, and producing a recommended modulus that corresponded to original experimental testing, was within 5 % of the stiffness value determined in additional three-point bending testing, and was reasonable in regards to past literature (eg. Papini et al. 2007) – a value notably different to the one expected by the manufacturer. These tests are typically under-defined or entirely absent in biomechanics literature (Burkhart et al. 2013).

Differences in cortical thickness, predominantly in the superior anterior surface and diaphyseal cross-section, have been noted while analyzing the specimens in Chapter 3. While these differences may be

apparent now, the synthetic models provided were produced by Pacific Research Laboratories, Inc. (PRL) in a small batch, so any inconsistencies between synthetic models will likely be reduced in a mass production setting.

This limitation may be extended to the use of one synthetic femur providing the basis of all digital models used in this study. It may also be advantageous to develop new models derived from the idealized original, rather than using modified CT scan data. As stated previously, it is likely that the model were not adjusted as originally intended. This could be a consequence of conducting the model alterations in Mimics/3-Matic, tasks these programs are not optimized to do, and could thus be mitigated with the use of dedicated computer-aided design (CAD) software, which would allow for more precise measurements and model refinements. Regardless, this unexpected increase in ML bending resistance produced values closer to experimental data than would have otherwise occurred. The models produced could serve as a basis for the refinement of future versions by serving as a guide for cortical distribution in the diaphysis.

Several simplifications were made when producing the axial and four-point bending models, and when executing the loading parameters. No conditioning criteria were established in Abaqus, thus, each model was only

loaded once to produce a resultant stiffness. Similarly, no fatigue or fracture criteria were outlined, eliminating the possibility of fracture load and screw pullout analyses. Torsion testing models were omitted due to complications in modelling accurate loading, as well as the limited comparative basis to previous literature, reducing results confidence and restricting the ability to make recommendations.

The model evaluation and recommendation basis could have been strengthened with the use of strain analysis at key locations. Strain data were collected in cadaveric samples during testing; however, strain data were not anticipated to be a source of model verification in synthetic models, and were thus not collected on the synthetic femurs during testing. The lack of comparable data weakens the basis for comparison, and so were excluded. These data have been stored, however, and could be used in further analysis, such as on revised models of the synthetic femur.

A major strength of this work was the use of natural specimens in all testing modes, in the same order, at the same magnitude and loading rate. Many methods were developed based on previous literature (eg. Cristofolini et al. 1996; Heiner 2008), thus allowing for direct comparisons. The tests conducted were comprehensive, with results compared to cadaveric femurs

verified to be osteoporotic, rather than simply modifying experimental results by a percentage or another means.

As stated previously, mesh sensitivity analysis and model evaluation were both conducted to support the consistency and accuracy of the finite element analysis. Additional experimental testing demonstrated the correctness of the model, with the unaltered model representative of two loading responses.

5.3 Future Directions

There are several future directions for this research. One such direction is the development of new models drawing from the results of the FEA conducted, concerning geometry and modulus. This may be better facilitated with the use of dedicated modelling software and being founded from an idealized model, rather than scan data, which would be more accurate in large production runs.

The trabecular components involved in the finite element testing did not appear to produce any significant effect on the resulting stiffness. Efforts should be made to adjust the trabecular bone such that it produces some influence on the digital model, and by extension, the synthetic model, as it

may be a useful tool to adjust mechanical response in torsion or axial compression without compromising the response of four-point bending.

While a major strength of the work was the number of different tests conducted, screw pullout could be expanded. Fracture can occur in a variety of modes and locations in the human femur. To help repair the damage and reinforce the bone, orthopaedics and associated screws are inserted at multiple angles and locations across the femur, including the proximal and distal ends. To better replicate osteoporotic bone, several locations should be assessed with screw pullout to facilitate the analysis of stability and strength in osteoporotic orthopaedic fixation and implant devices with respect to trabecular bone. Surgeons should also be consulted in regards to the ‘feel’ of inserting the screws and the cutting response of the synthetic femurs, making them more effective as a training tool.

5.4 Significance

This work represents the first study to assess the mechanical response of synthetic femurs attempting to replicate osteoporotic bone. The finite element models developed have been analyzed and evaluated and can now be used to create recommendations for revisions to the osteoporotic model. It is hoped that the results of this work can be used to improve the accuracy of the osteoporotic synthetic femurs produced,

creating a foundation for the development of orthopaedic implants more suited to osteoporotic bone, reducing the consequences of osteoporotic fracture and improving quality of life for those affected.

5.5 References

- Bukata S V. 2017. Orthopedic Aspects of Osteoporosis. In: Osteoporosis. Fourth Edi. p. 1641–1648.
- Burkhart TA, Andrews DM, Dunning CE. 2013. Finite Element Modeling Mesh Quality, Energy Balance and Validation Methods: A Review with Recommendations Associated with the Modeling of Bone Tissue. *J. Biomech.* 46:1477–1488. doi:10.1016/j.jbiomech.2013.03.022.
- Cristofolini L, Vicecontia M, Cappello A, Toni A. 1996. Mechanical Validation of Whole Bone Composite Femur Models. *J. Biomech.* 29:525–535.
- Heiner AD. 2008. Structural Properties of Fourth-Generation Composite Femurs and Tibias. *J. Biomech.* 41:3282–3284. doi:10.1016/j.jbiomech.2008.08.013.
- Heiner AD, Brown TD. 2001. Structural Properties of a New Design of Composite Replicate Femurs and Tibias. *J. Biomech.* 34:773–781. doi:10.1016/S0021-9290(01)00015-X.
- International Osteoporosis Foundation. 2017. Facts and Statistics. [accessed 2017 Dec 5]. <https://www.iofbonehealth.org/facts-statistics>.
- Papini M, Zdero R, Schemitsch EH, Zalzal P. 2007. The Biomechanics of Human Femurs in Axial and Torsional Loading: Comparison of Finite Element Analysis, Human Cadaveric Femurs, and Synthetic Femurs. *J. Biomech. Eng.* 129:12. doi:10.1115/1.2401178.

Appendices

APPENDIX A: Glossary of Medical Terms

This section contains explanations of medical terminology used throughout this document to assist the layperson (taken from Dorland's Illustrated Medical Dictionary⁴).

Acetabulum: The large cup-shaped cavity in which the femur articulates

Anterior: Situated in front of or in the forward part of an organ

Cancellous: Any structured arranged like a lattice

Cartilage: A specialized, fibrous connective tissue

Coronal Plane: A longitudinal plane or section passing through the body at right angles to the median plane, see. Frontal Plane

Cortex: An external layer

Cortical: Pertaining to or of the nature of a cortex or bark

Diaphysis: The portion of the long bone between the ends or extremities

Distal: remote; farther from any point of reference

Epicondyle: An eminence upon a bone, above its condyle

Epiphysis: The end of a long bone, usually wider than the shaft

⁴ Friel, J. 1974. Dorland's Illustrated Medical Dictionary. 25th ed. Philadelphia: W. B. Saunders Co.

Ex vivo: Out of living

Extension: The movement by which the two ends of any jointed part are drawn away from each other; a movement which brings the members of a limb into or toward a straight line

Femur: the bone that extends from the pelvis to the knee, being the longest and largest bone in the body

Fibula: The outer and smaller of the two bones of the leg

Flexion: the act of bending or condition of being bent

Frontal Plane: Any plane passing through the body, at right angles to the median plane, dividing the body into front and back parts

In situ: In its normal place

In vivo: Within the living

Lateral: Denoting a position farther from the median plane or midline of the body

Ligament: A band of fibrous tissue that connects bones or cartilage or holds together a joint

Marrow: The soft organic material that fills the cavities of the bones

Medial: Pertaining to the middle, closer to the median plane or the midline of a body or structure

Median Plane: The plane dividing the body into left and right halves

Medullary Canal: The central cavity in long bone shafts where marrow is stored

Orthopaedic: The branch of surgery which is especially concerned with the preservation and restoration of the function of the skeletal system, its articulations, and associated structures

Osteopenia: Reduced bone mass due to a decrease in the rate of osteoid synthesis to a level insufficient to compensate normal bone absorption

Osteoporosis: Abnormal rarefaction of bone, seen most commonly in the elderly.

Patella: A bone about 5cm. In diameter, situated at the front of the knee

Pelvis: the lower portion of the trunk of the body

Porous: Penetrated by pores and open spaces

Posterior: Situated in back of, or in the back part of

Proximal: Nearest, closest to any point of reference

Sagittal Plane: Vertical plane that divides the body in left and right portions, see Medial Plane

Shank: Leg

Tendon: A fibrous cord by which a muscle is attached

Thigh: The portion of the lower extremity situated between the hip above and the knee below

Tibia: The shin bone: the inner and larger bone of the leg below the knee

Trabecula: A little beam; a general term for a supporting or anchoring strand of connective tissue

Trabecular Bone: Spindles of cancellous bone, which form a lattice

Transverse Plane: A horizontal plane dividing the body into upper and lower portions

Trunk: The main part of the body, to which head and limbs are attached

APPENDIX B: Technical Drawings

Continuing on the next page, this section contains the technical drawings for the parts used in Chapter 3. Due to export limitations, they are no longer to scale.

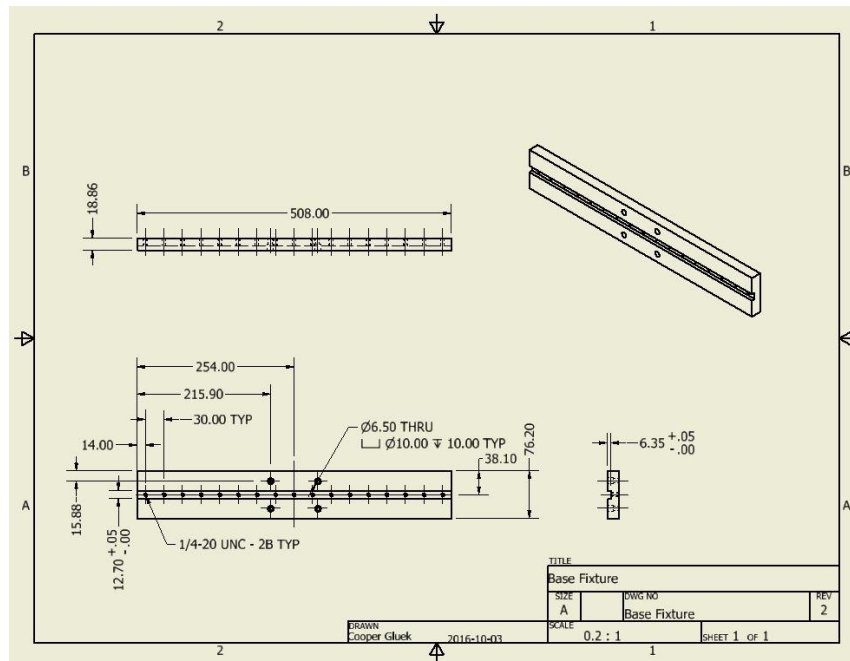


Figure B.1: Dimensional Drawing of Base Fixture
All dimensions in mm, made of aluminum.

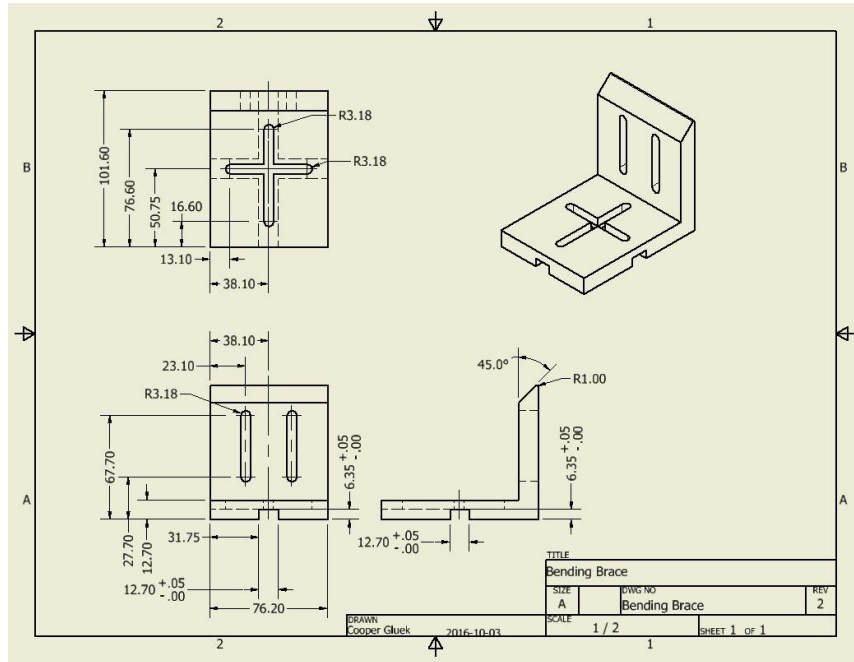


Figure B.2: Dimensional Drawing of Bending Brace L-Bracket
All dimensions in mm, made of aluminum.

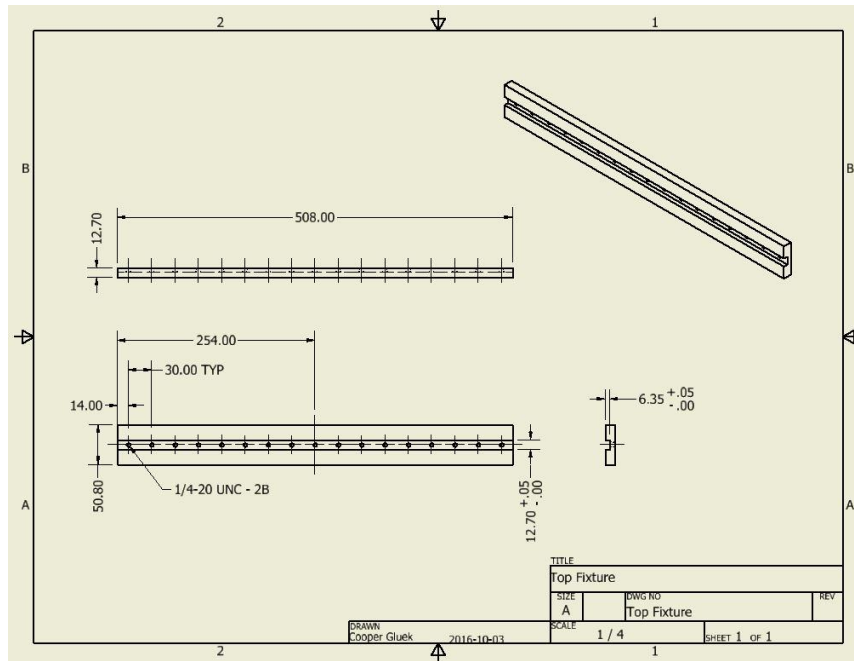


Figure B.3: Dimensional Drawing of Top Fixture
All dimensions in mm, made of aluminum.

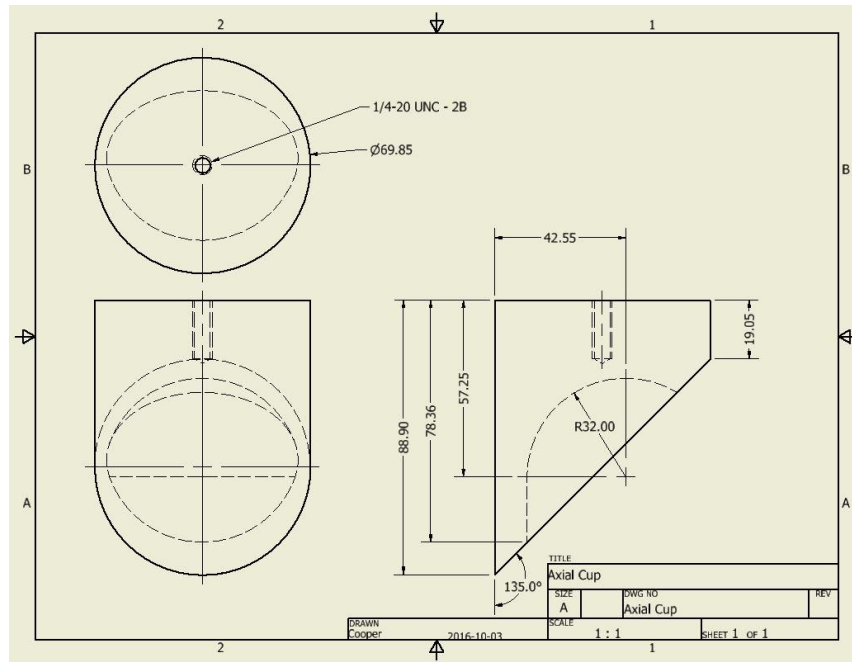


Figure B.4: Dimensional Drawing of Axial Cup
All dimensions in mm, made of aluminum.

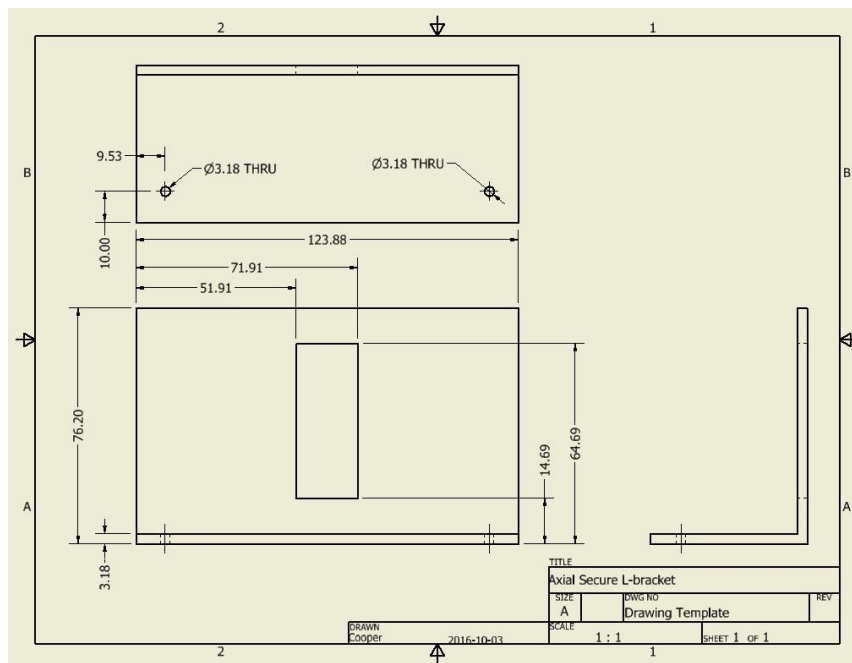


Figure B.5: Dimensional Drawing of Axial Secure L-Bracket
All dimensions in mm, made of aluminum.

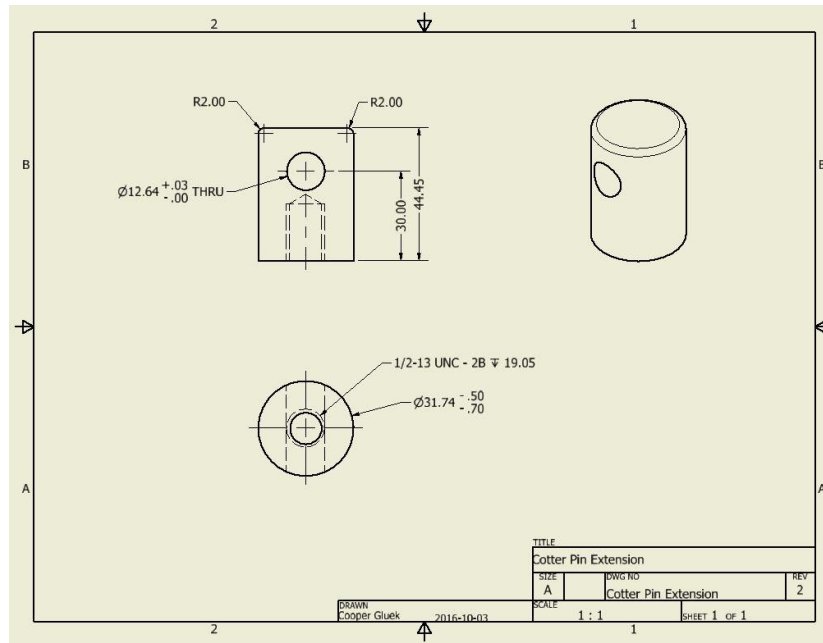


Figure B.6: Dimensional Drawing of Cotter Pin Extension
All dimensions in mm, made of aluminum.

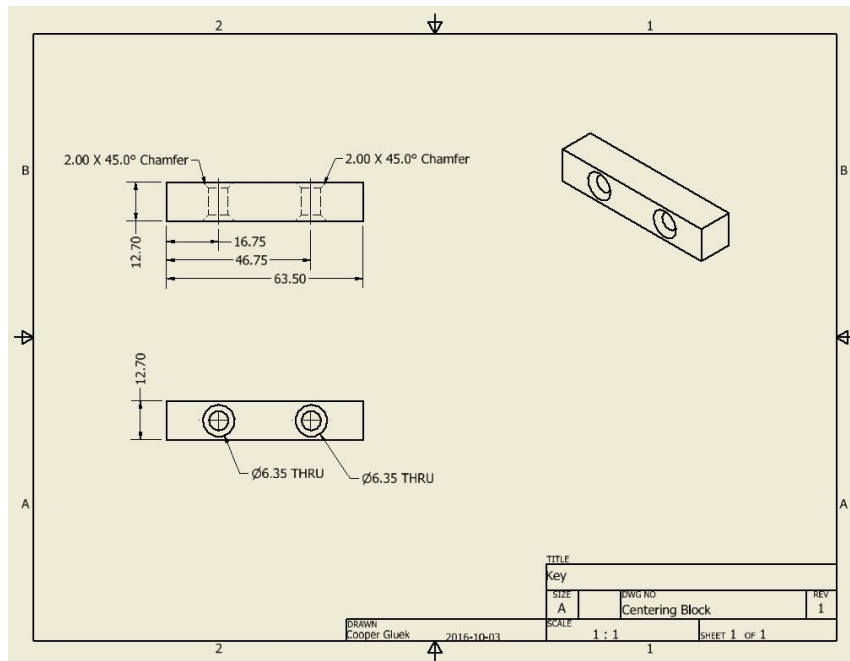


Figure B.7: Dimensional Drawing of Key
All dimensions in mm, made of aluminum.

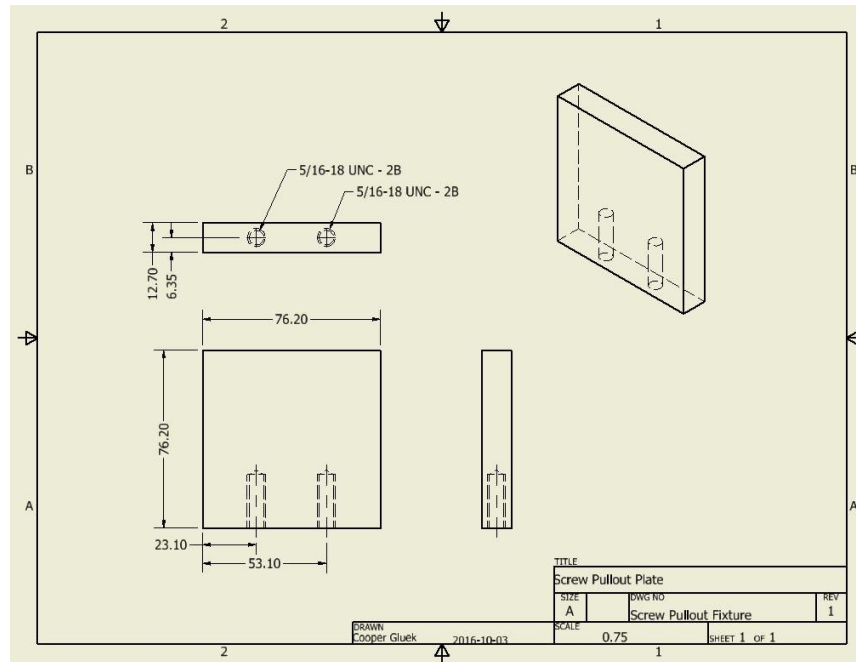


Figure B.8: Dimensional Drawing of Aluminum Plate
All dimensions in mm, made of aluminum.

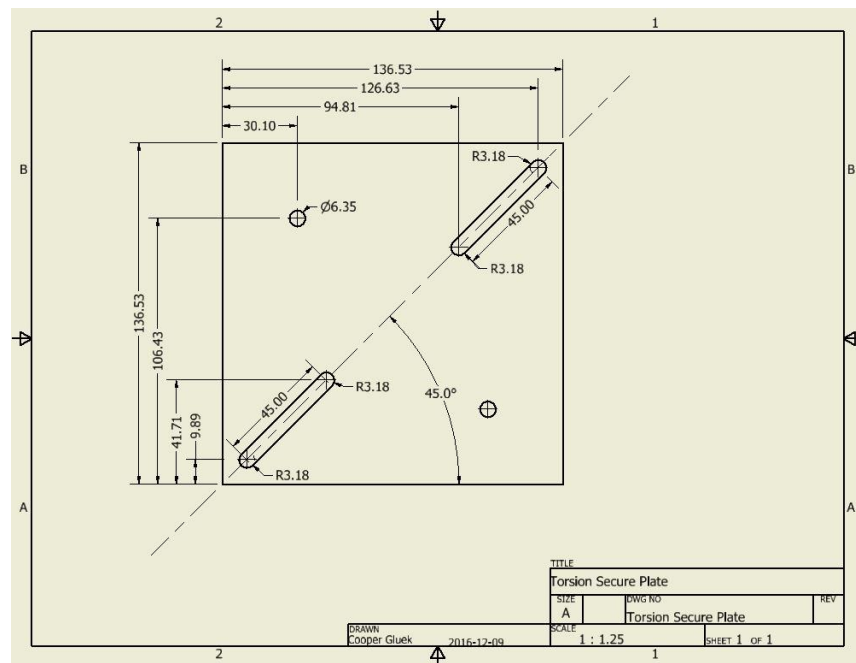


Figure B.9: Dimensional Drawing of Torsion Secure Plate
All dimensions in mm, made of aluminum.

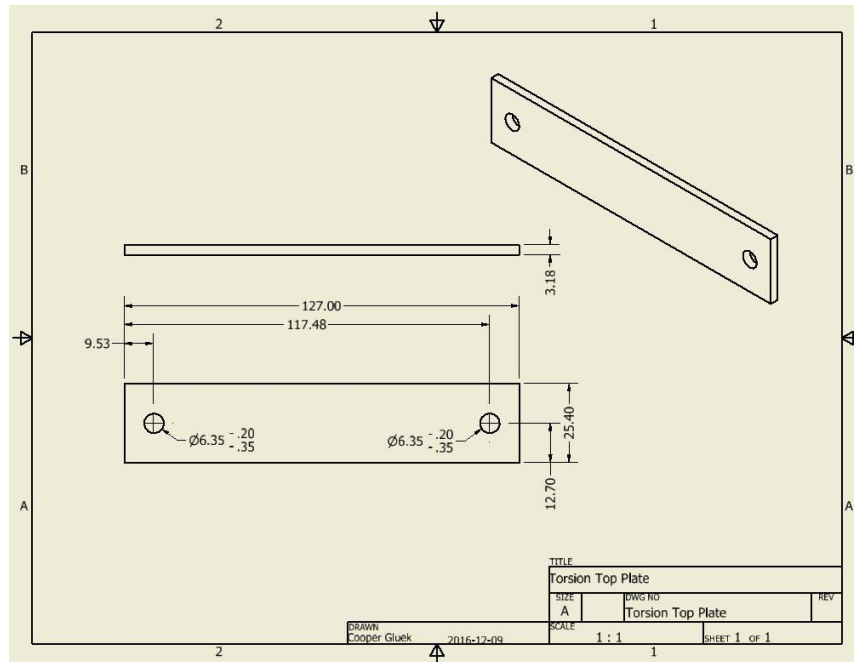


Figure B.10: Torsion Secure Complementary Plate
All dimensions in mm, made of aluminum.

APPENDIX C: DXA Scan Data

The following document excerpts were received from Science Care Inc.

Name: L161569, BON03L Patient ID: DOB: June 06, 1922	Sex: Female Ethnicity: White	Height: 64.0 in Weight: 125.0 lb Age: 94
------------------------------------------------------------	---------------------------------	------------------------------------------------

Referring Physician:

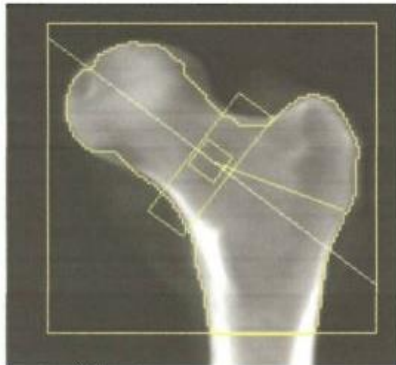


Image not for diagnostic use
k = 1.196, d0 = 85.3
106 x 101
NECK: 49 x 15
HAL: 97 mm

Scan Information:

Scan Date: March 29, 2017 ID: A0329170E
Scan Type: a Left Hip
Analysis: March 29, 2017 15:56 Version 13.6.0.1:7
Hip
Operator: LFG
Model: Horizon C (S/N 200442)
Comment:

DXA Results Summary:

Region	Area (cm ²)	BMC (g)	BMD (g/cm ³)	T-score	Z-score
Neck	5.04	1.89	0.376	-4.3	-1.7
Total	33.75	16.85	0.499	-3.6	-1.3

Total BMD CV 1.0%, ACF = 1.010, BCF = 0.978, TH = 0.155
WHO Classification: Osteoporosis
Fracture Risk: High

Name: L161607, BONE03L Patient ID: DOB: October 09, 1935	Sex: Female Ethnicity: White	Height: 65.0 in Weight: 180.0 lb Age: 81
----------------------------------------------------------------	---------------------------------	------------------------------------------------

Referring Physician:

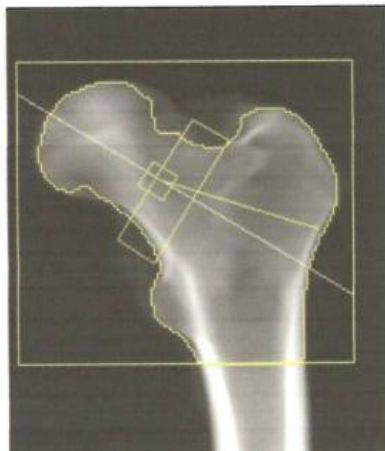


Image not for diagnostic use
k = 1.199, d0 = 85.1
112 x 102
NECK: 49 x 15
HAL: 99 mm

Scan Information:

Scan Date: March 29, 2017 ID: A0329170C
Scan Type: a Left Hip
Analysis: March 29, 2017 15:51 Version 13.6.0.1:7
Hip
Operator: LFG
Model: Horizon C (S/N 200442)
Comment:

DXA Results Summary:

Region	Area (cm ²)	BMC (g)	BMD (g/cm ³)	T-score	Z-score
Neck	5.27	2.83	0.537	-2.8	-0.4
Total	41.75	26.27	0.629	-2.6	-0.4

Total BMD CV 1.0%, ACF = 1.010, BCF = 0.978, TH = 0.103
WHO Classification: Osteoporosis
Fracture Risk: High

Name: L171519, BONE03L Patient ID: DOB: February 15, 1941	Sex: Female Ethnicity: White	Height: 64.0 in Weight: 124.0 lb Age: 76
-----------------------------------------------------------------	---------------------------------	------------------------------------------------

Referring Physician:

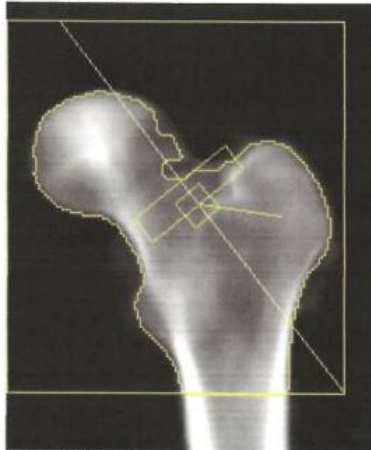


Image not for diagnostic use
k = 1.202, d0 = 86.8
116 x 128
NECK: 41 x 11
HAL: 63 mm

Scan Information:

Scan Date: July 25, 2017 ID: A07251709
Scan Type: x Left Hip
Analysis: July 25, 2017 12:20 Version 13.6.0.1:7
Hip
Operator: AB
Model: Horizon C (S/N 200442)
Comment:

DXA Results Summary:

Region	Area (cm ²)	BMC (g)	BMD (g/cm ²)	T - score	Z - score
Neck	3.65	1.24	0.339	-4.6	-2.4
Total	59.34	34.48	0.581	-3.0	-1.1

Total BMD CV 1.0%, ACF = 1.010, BCF = 0.978, TH = 0.058
WHO Classification: Osteoporosis
Fracture Risk: High

Name: L171987 Patient ID: DOB: February 17, 1918	Sex: Female Ethnicity: White	Height: 62.0 in Weight: 66.0 lb Age: 99
--------------------------------------------------------	---------------------------------	-----------------------------------------------

Referring Physician:

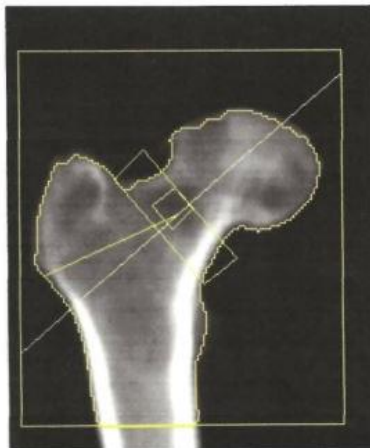


Image not for diagnostic use
k = 1.204, d0 = 86.3
112 x 130
NECK: 49 x 15
HAL: 97 mm

Scan Information:

Scan Date: October 09, 2017 ID: A10091704
Scan Type: x Right Hip
Analysis: October 09, 2017 15:28 Version 13.6.0.1:7
Hip
Operator: AB
Model: Horizon C (S/N 200442)
Comment:

DXA Results Summary:

Region	Area (cm ²)	BMC (g)	BMD (g/cm ²)	T - score	Z - score
Neck	5.30	2.71	0.511	-3.0	-0.5
Total	41.60	27.13	0.652	-2.4	0.0

Total BMD CV 1.0%, ACF = 1.010, BCF = 0.978, TH = 0.083
WHO Classification: Osteopenia
Fracture Risk: Increased

Name: L172202, CADV01 Patient ID: DOB: February 10, 1932	Sex: Female Ethnicity: White	Height: 66.0 in Weight: 170.0 lb Age: 85
----------------------------------------------------------------	---------------------------------	------------------------------------------------

Referring Physician:

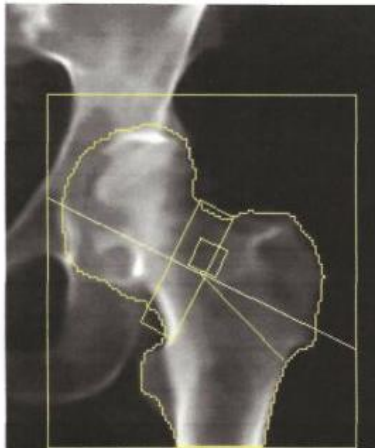


Image not for diagnostic use
k = 1.143, d0 = 52.6
105 x 120
NECK: 47 x 14
HAL: 95 mm

Scan Information:

Scan Date: October 30, 2017 ID: A10301703
Scan Type: a Left Hip
Analysis: October 30, 2017 06:43 Version 13.6.0.1:7
Hip
Operator: AG
Model: Horizon C (S/N 200442)
Comment:

DXA Results Summary:

Region	Area (cm ²)	BMC (g)	BMD (g/cm ²)	T - score	Z - score
Neck	5.29	3.47	0.656	-1.7	0.8
Total	35.99	22.10	0.614	-2.7	-0.4

Total BMD CV 1.0%, ACF = 1.010, BCF = 0.978, TH = 5.969
WHO Classification: Osteoporosis
Fracture Risk: High

The following DXA images were created at McMaster Children's Hospital

Hamilton Health Sciences Nuclear Medicine
McMaster Hospital
Hamilton, Ontario

Name: 161569 Patient ID: DOB: January 16, 1923	Sex: Female Ethnicity: White	Height: Weight: 56.8 kg Age: 94
------------------------------------------------------	---------------------------------	---------------------------------------

Referring Physician:

106 x 104
NECK: 54 x 15

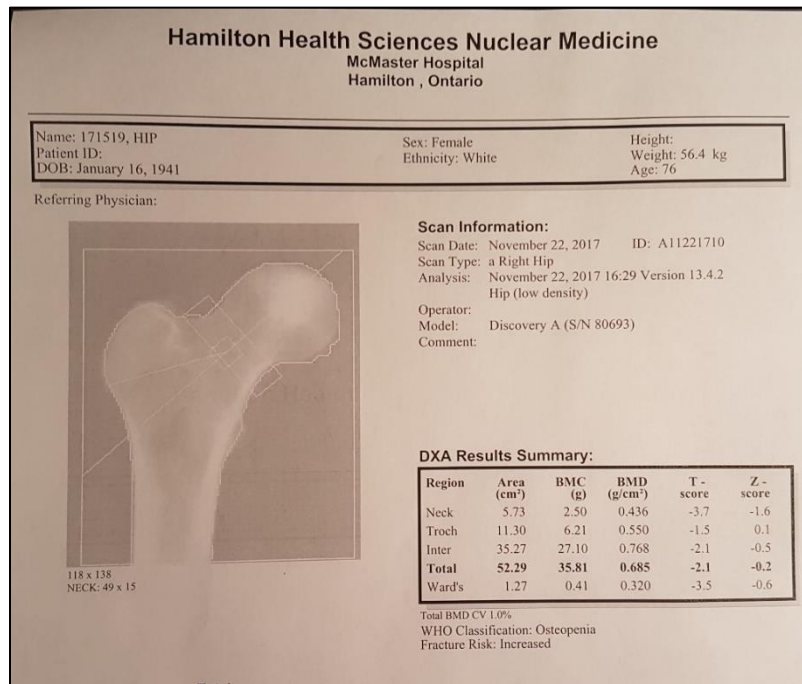
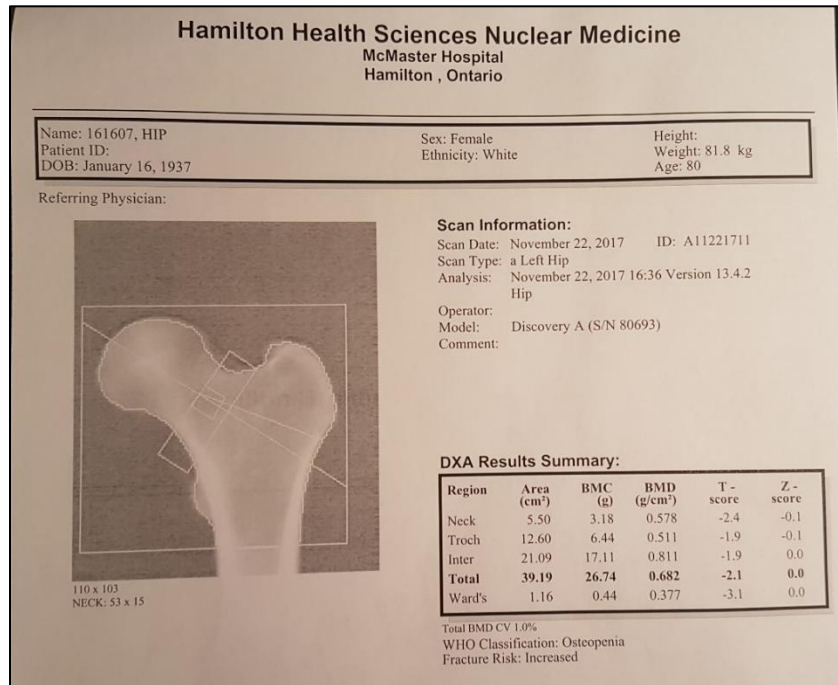
Scan Information:

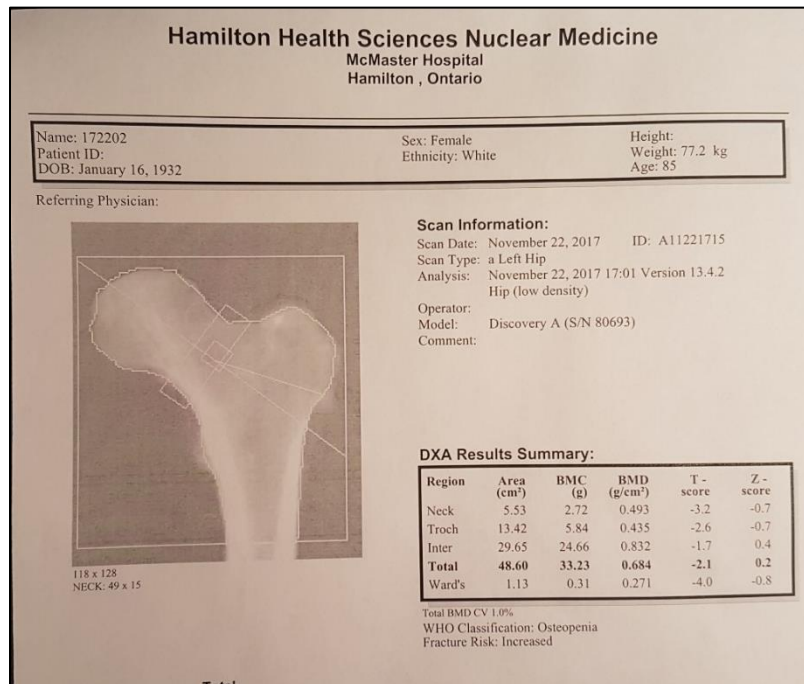
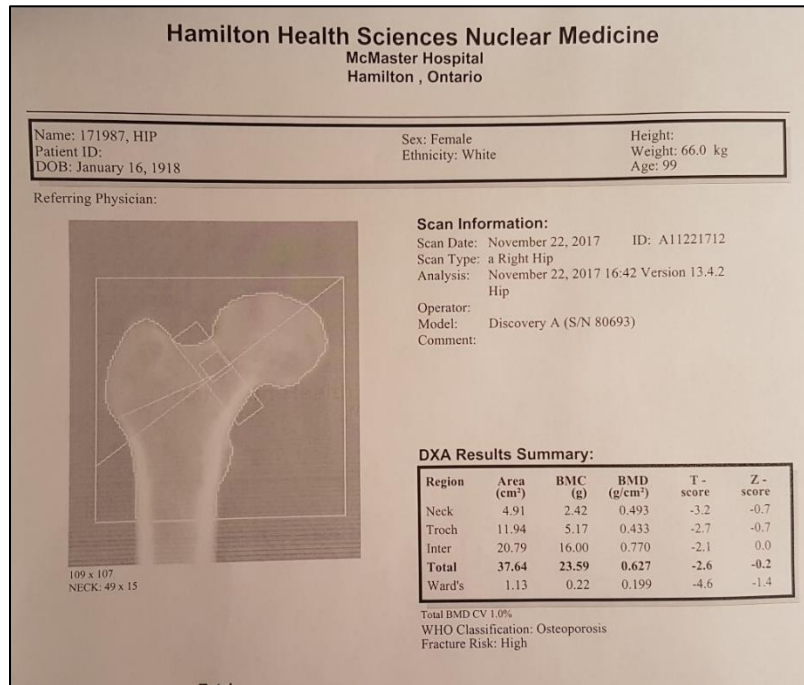
Scan Date: November 22, 2017 ID: A11221714
Scan Type: a Left Hip
Analysis: November 22, 2017 16:52 Version 13.4.2
Hip
Operator:
Model: Discovery A (S/N 80693)
Comment: WITHOUT WOODEN HOLDER

DXA Results Summary:

Region	Area (cm ²)	BMC (g)	BMD (g/cm ²)	T - score	Z - score
Neck	5.61	2.25	0.401	-4.0	-1.5
Troch	10.49	5.03	0.480	-2.2	-0.2
Inter	18.97	12.10	0.638	-3.0	-0.9
Total	35.06	19.38	0.553	-3.2	-0.9
Ward's	1.13	0.35	0.309	-3.6	-0.4

Total BMD CV 1.0%
WHO Classification: Osteoporosis
Fracture Risk: High





APPENDIX D: Sample Test Data

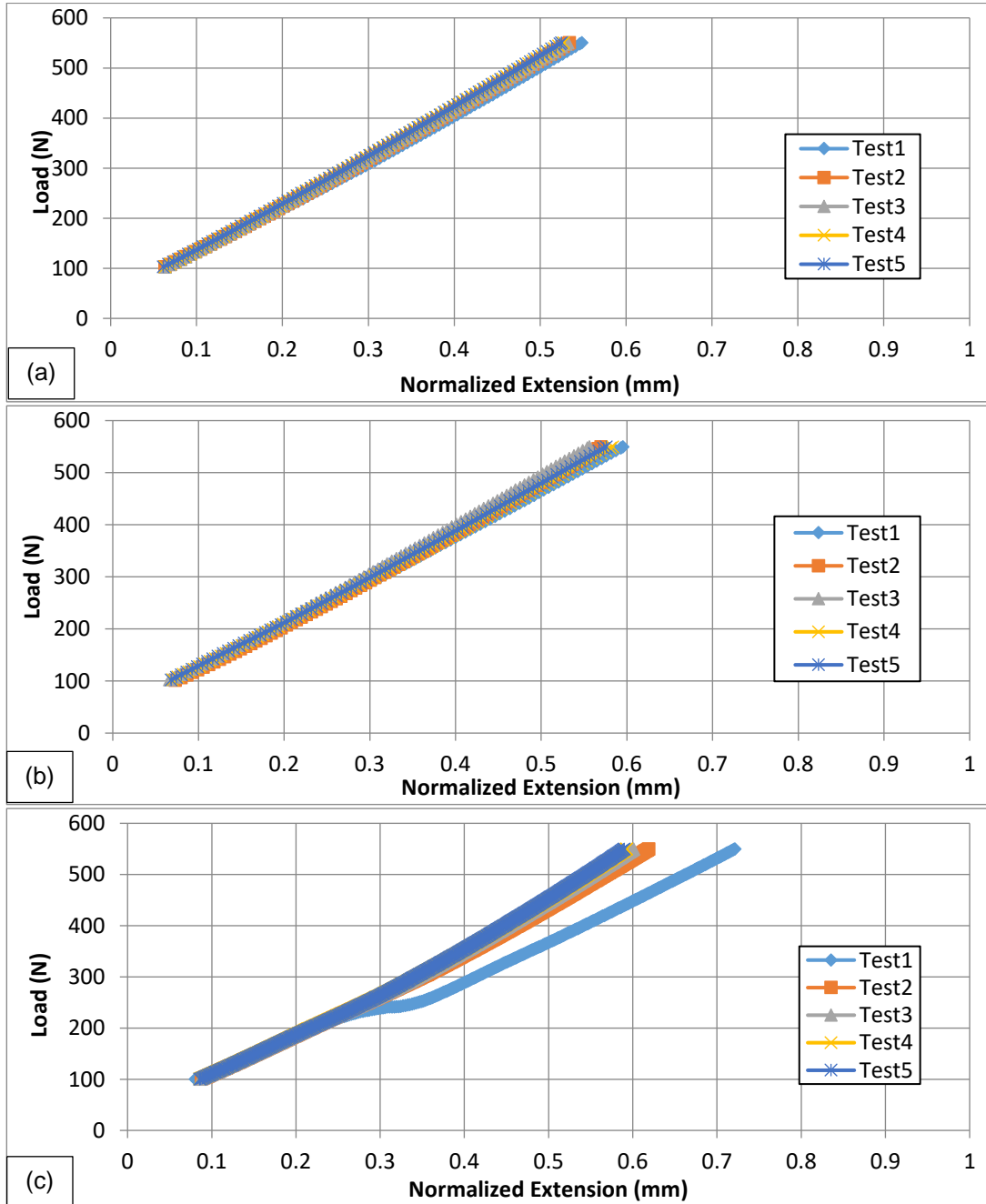


Figure D.1: AP Bending Sample Test Data
 Representative test data from the 3403-21 (a), 3503-11 (b), and 161607 (c).

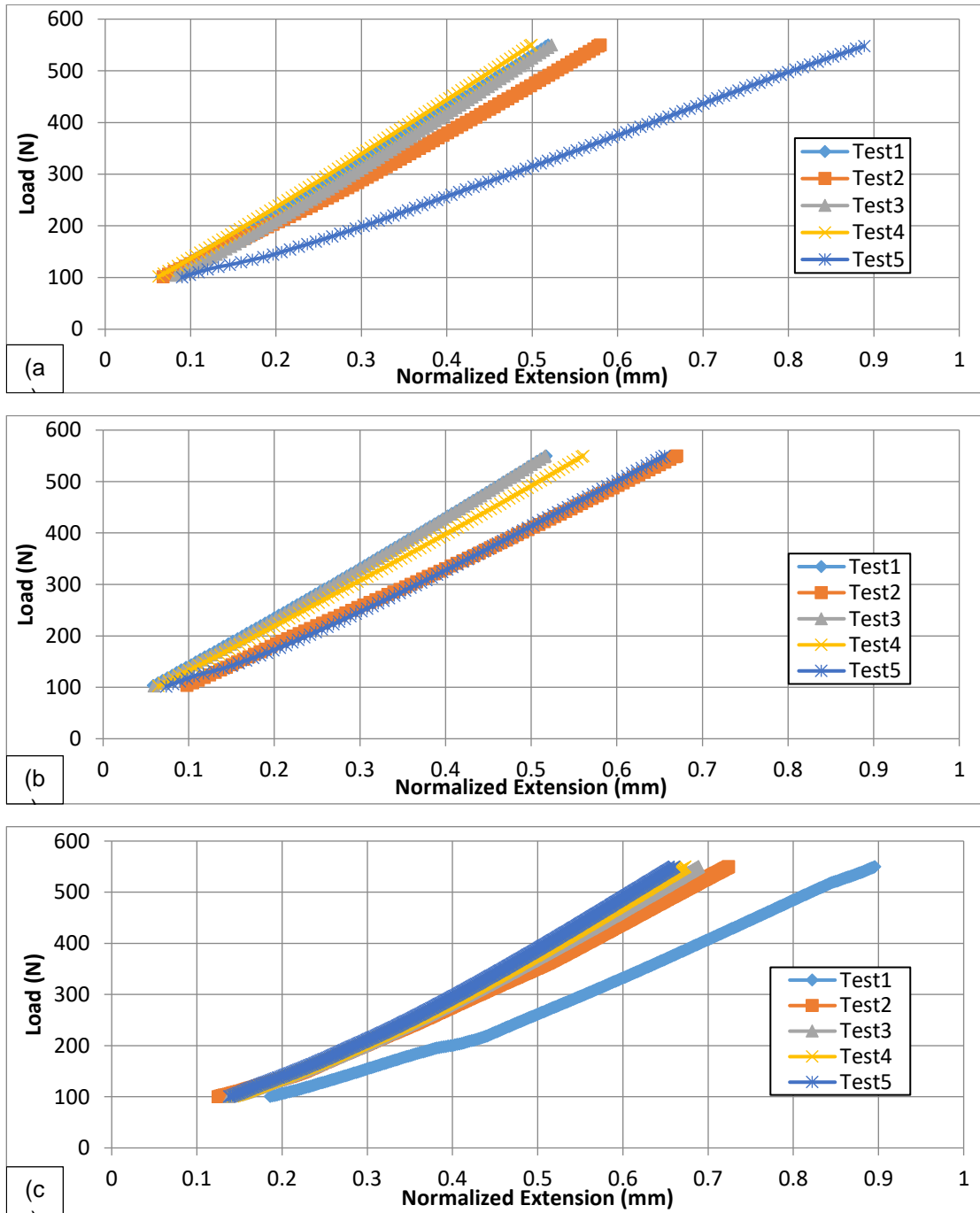


Figure D.2: ML Bending Sample Test Data
 Representative test data from the 3403-16 (a), 3503-07 (b), and 161569 (c).

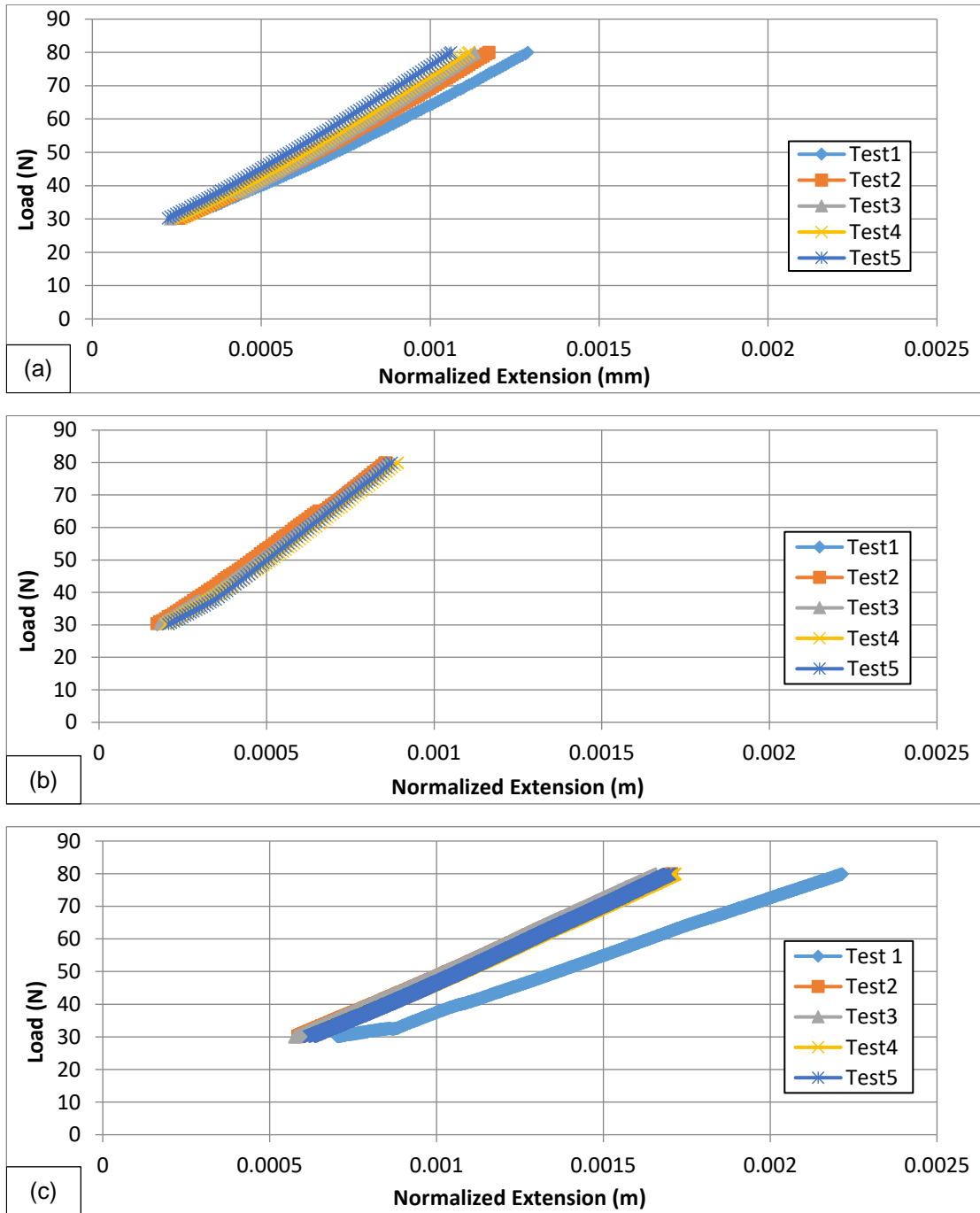


Figure D.3: Torsion Sample Test Data
 Representative test data from the 3403-23 (a), 3503-07 (b), and 171987 (c).

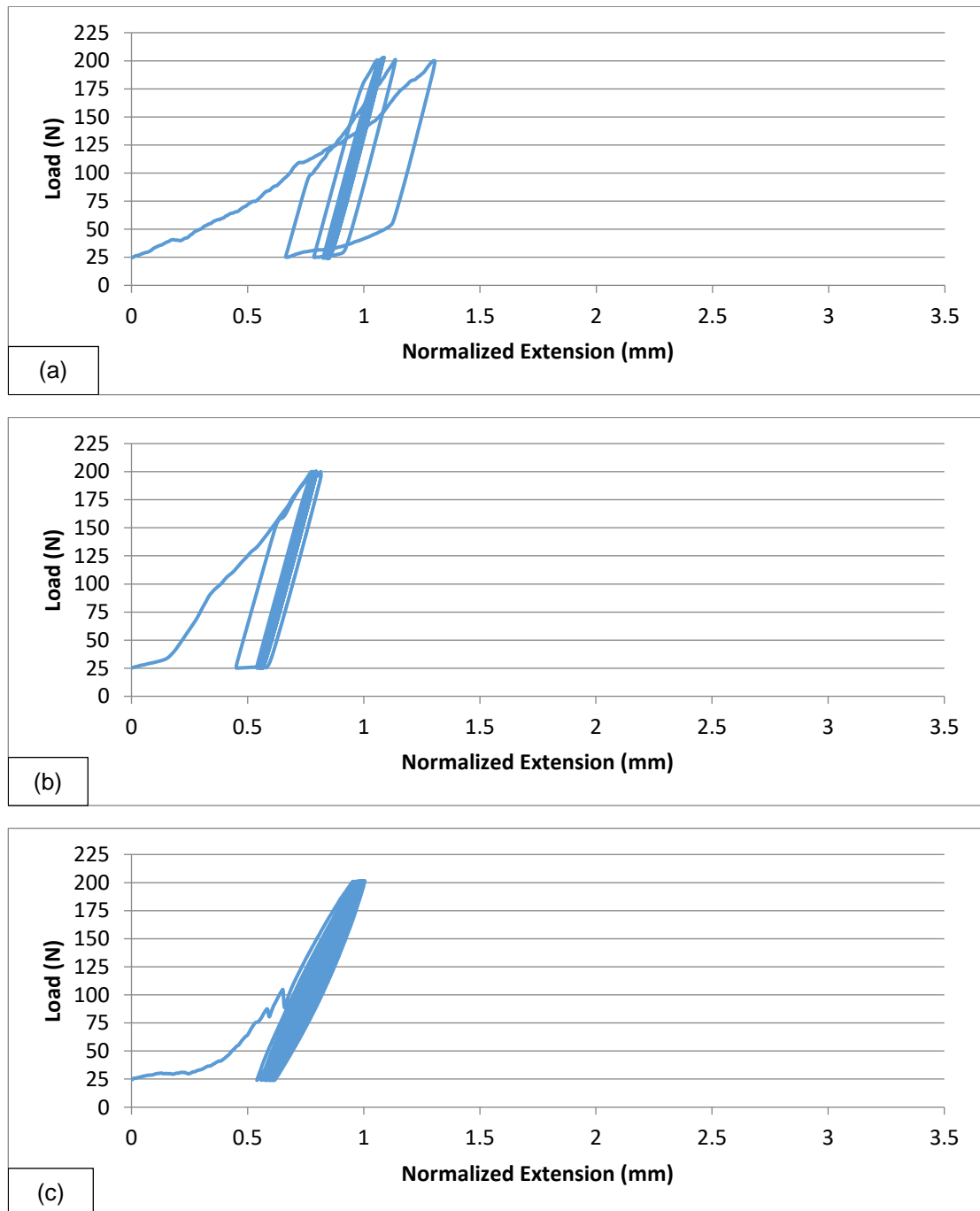


Figure D.4: Axial Compression Sample Test Data

Representative test data from the 3403-20 (a), 3503-08 (b), and 161569 (c).

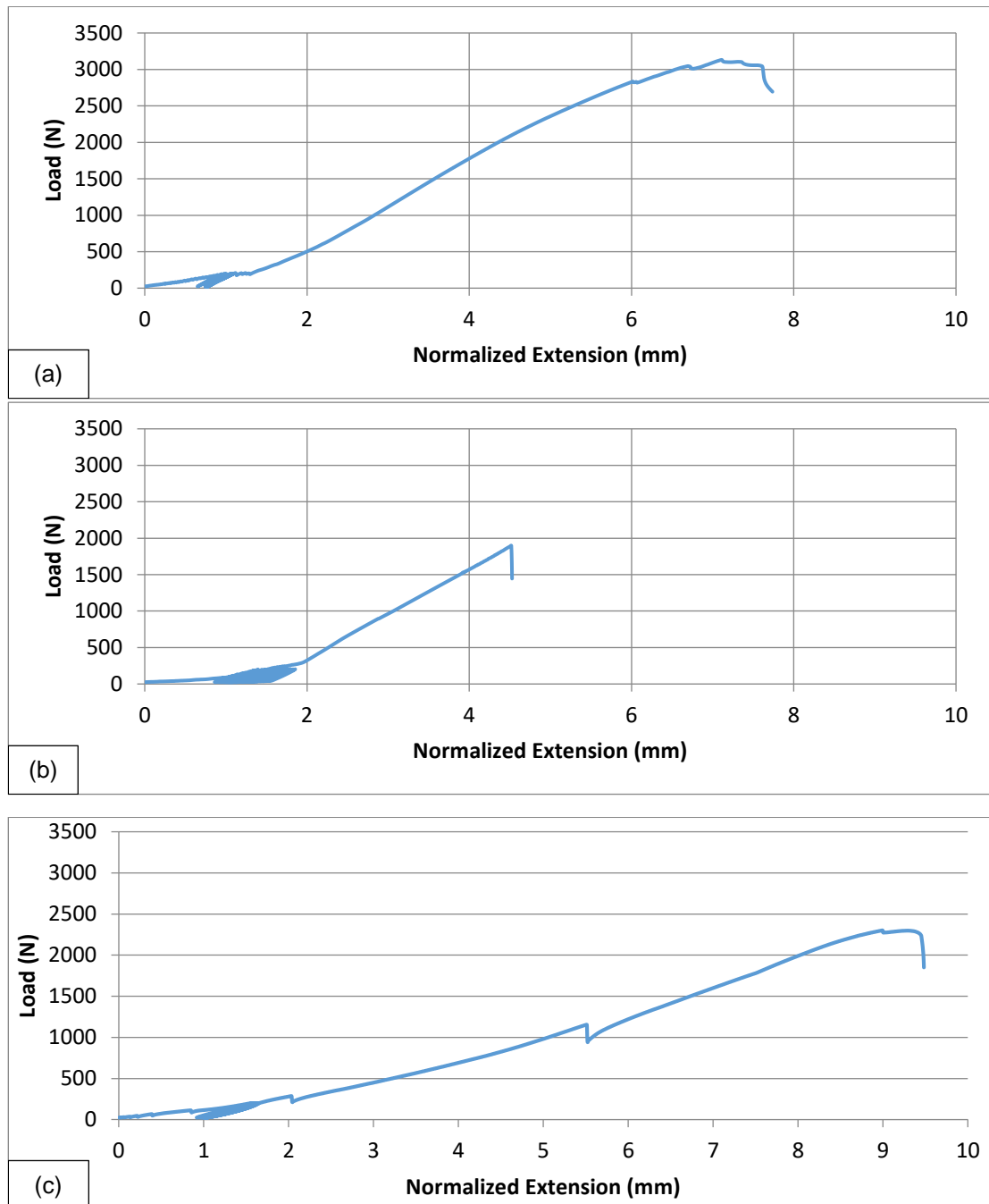


Figure D.5: Cyclic Failure Sample Test Data

Representative test data from the 3403-24 (a), 3503-11 (b), and 161569 (c).

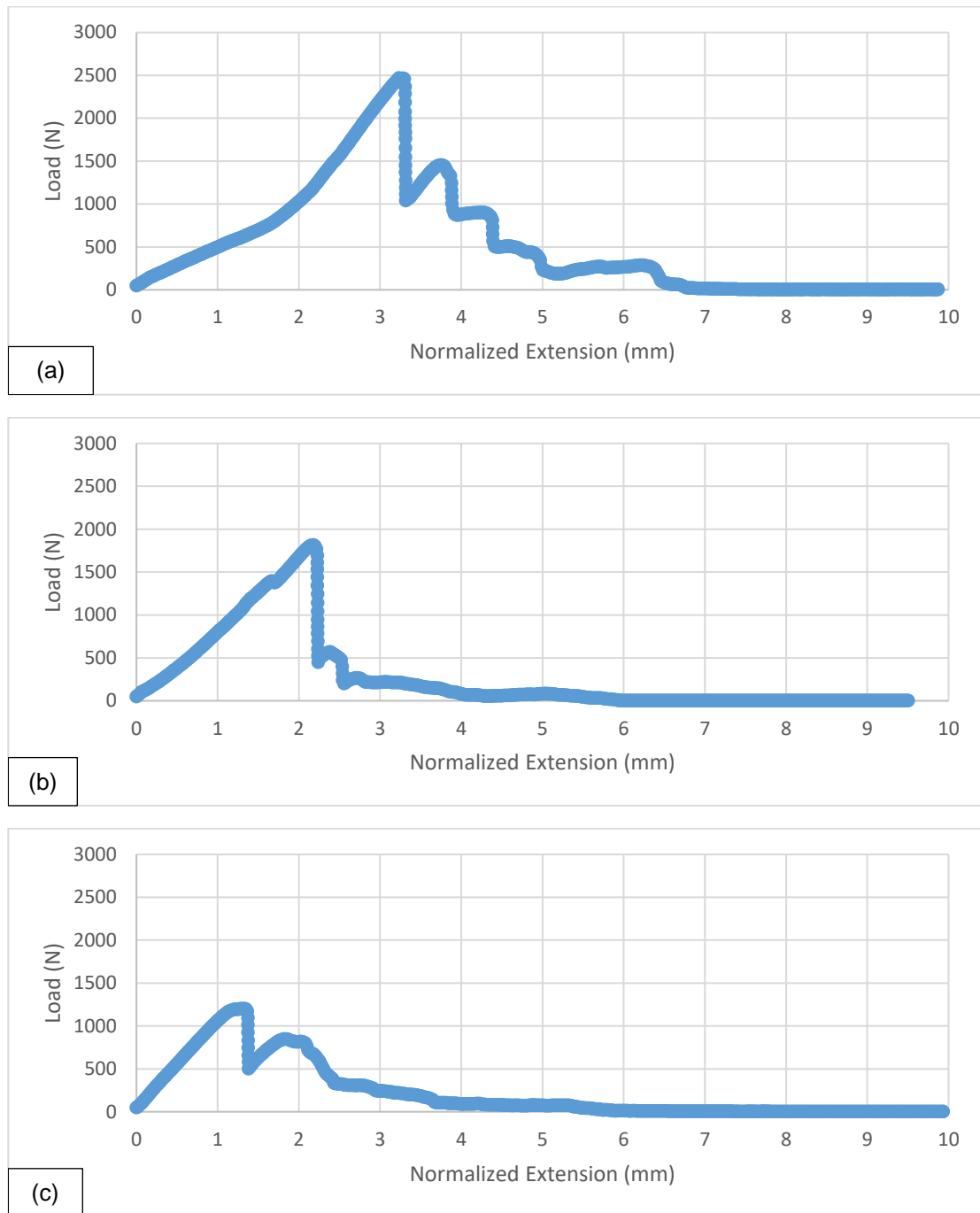
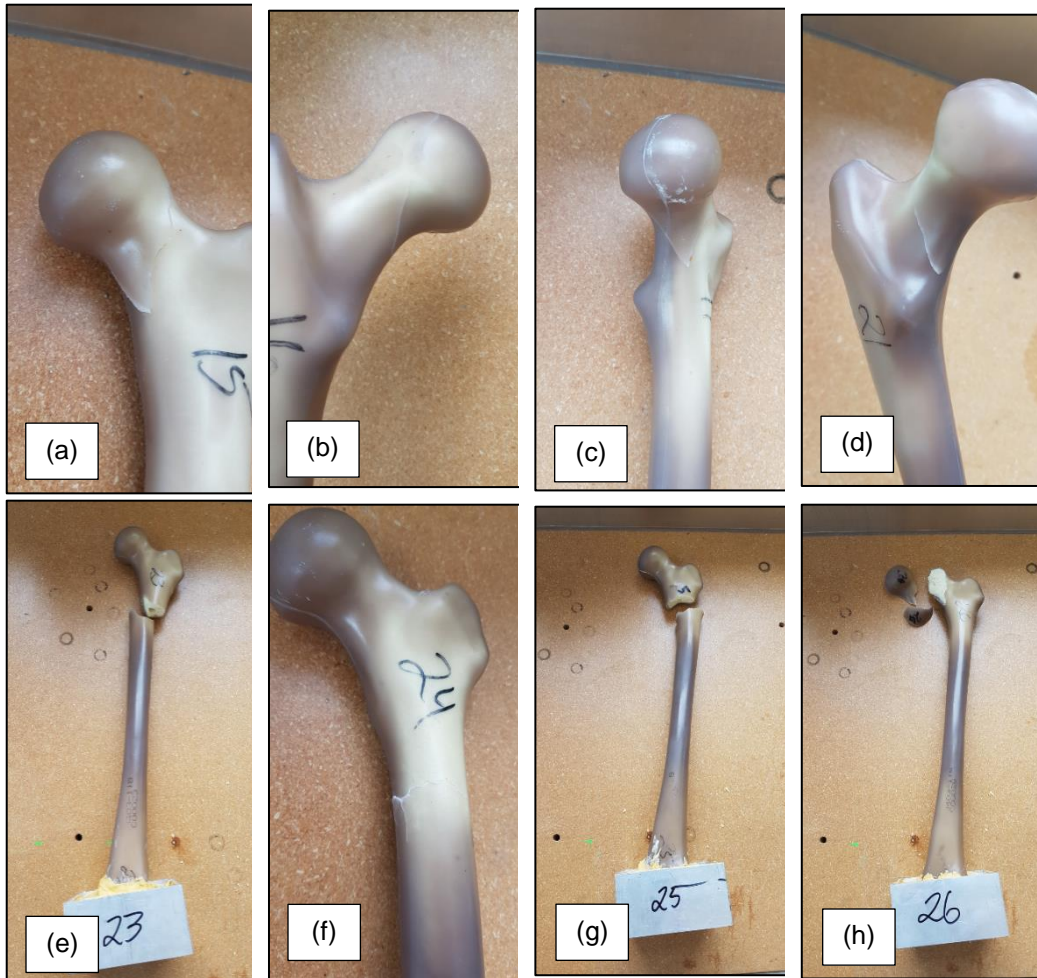


Figure D.6: Screw Pullout Sample Test Data
Representative test data from the 3403-23 (a), 3503-10 (b), and 161607 (c).

APPENDIX E: Fracture Images

(a) 3403-15

(b) 3403-16

(c) 3403-17

(d) 3403-21

(e) 3403-23

(f) 3403-24

(g) 3403-25

(h) 3403-26

Figure E.1: 3403 Series Fracture Images

Fracture modes in the 3403 set, predominately incomplete fracture in the femoral head through the femoral neck.



(a) 3503-05

(b) 3503-06

(c) 3503-07

(d) 3503-08

(e) 34503-09

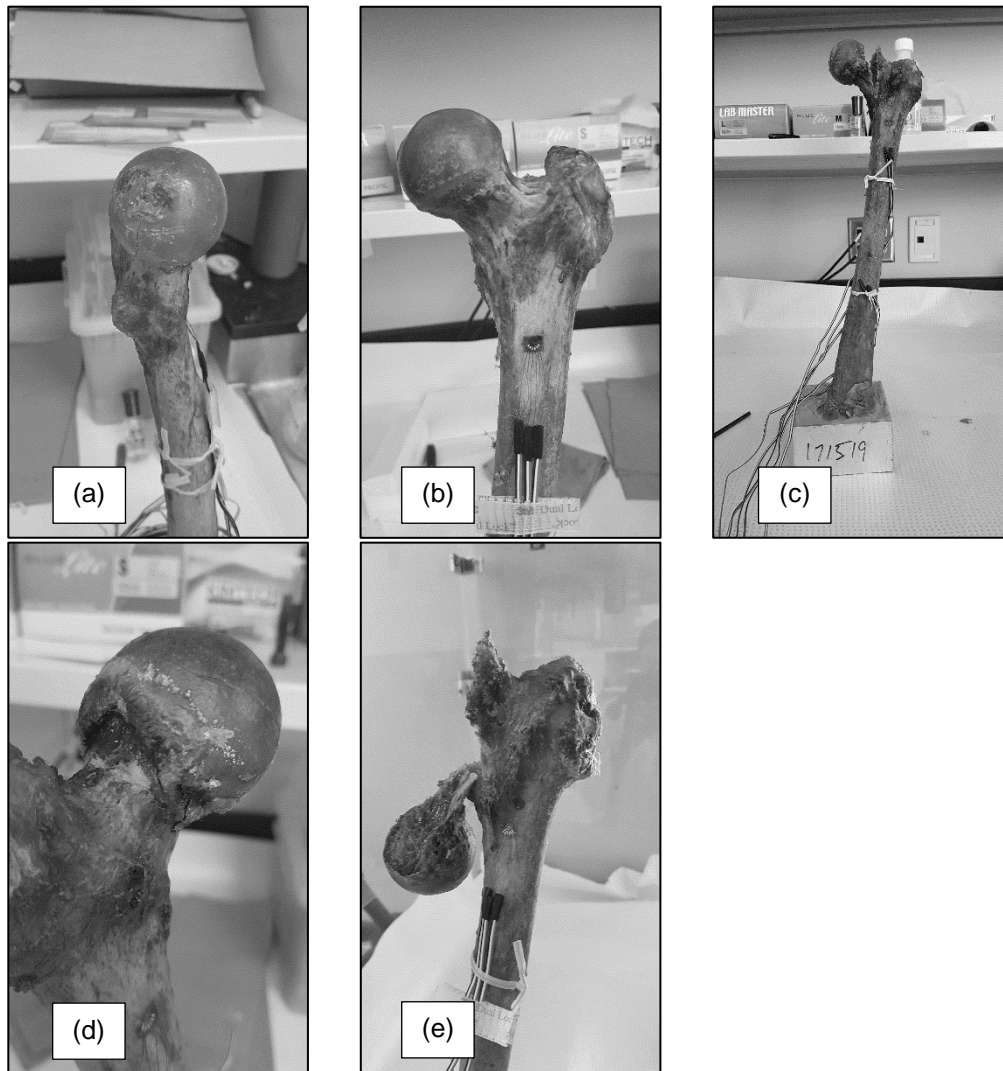
(f) 3503-10

(g) 3503-11

(h) 3503-15

Figure E.2: 3503 Series Fracture Images

Fracture modes in the 3503 set, predominately complete fracture through the pilot hole at the greater trochanter.



(a) 161569
(d) 171987

(b) 161607
(e) 172202

(c) 171519


Figure E.3: Natural Femur Fracture Images

Fracture modes in the natural set, either incomplete femoral head fracture or complete fracture in through the femoral neck in the sagittal plane.

APPENDIX F: Orphan Mesh to Part Conversion

Significant effort was made to convert the orphan mesh produced by Mimics/3-Matic to an editable part, with the intention that a part file would be simpler to mesh and manipulate. Three methods were attempted:

1. Geometry Edit in Abaqus

The 'Geometry Edit' feature is available in the Part module . The driving logic was to create and then join the faces to create a shell which could be turned to a solid feature. Selecting 'Face' > 'from element faces' allows the user to select a predefined surface or create one via criteria, such as 'individually', 'by angle', 'by layer', and 'by analytic'. Unfortunately, this process seems apt to failure, requiring many incremental steps to create new faces, often leaving large gaps exposed.

2. AutoCAD Mesh Enabler

Extensions are available online from AutoCAD to extend the abilities of AutoCAD Inventor. One such extension is Mesh Enabler, which will convert an orphan mesh to a solid part. By exporting the Mimics/3-Matic format to STL, the file can be imported into AutoCAD and the extension executed. Unfortunately, this feature seems to be designed with the intention of large, well-defined faces – not typically seen in human anatomy. The newly created part will be converted to discrete flat surfaces and nodes. To the author's knowledge, neither AutoCAD nor Abaqus are suited to deal with reducing the surfaces and smoothing the part. It is unclear how this affects the accuracy of the bone geometry.

3. Python Script

A python script is available online titled "abq3Dmesh2geom" available from Technische Universitat Graz, which can be called from within Abaqus to convert an imported orphan mesh into a part. This program does work, but is very, very time consuming. The part produced is similar to that of the AutoCAD Mesh Enable –surfaces are discretized to 2D and the overall geometry of the part is altered.

Link : <https://www.tugraz.at/en/institute/iwb/lehre/software/abaqus-cae/>

APPENDIX G: Second Moment of Area Calculation on 3403 Mid-diaphysis Samples

$$E = (-FL^3)/(48lymax)$$

D: Diameter A: Area
 I: Second moment of area d: distance from common centroid to y
 Subscript o: outer Subscript i: inner E: modulus t: thickness
 L: distance between supports y: part centroid to datum distance

L (m)	0.07
-------	------

	15A		16A		17A		25A		26A	
D	0.02650	m	0.02656	m	0.02669	m	0.02617	m	0.02651	m
t	0.00414	m	0.00571	m	0.00408	m	0.00508	m	0.00414	m
ro	0.01325	m	0.01328	m	0.013345	m	0.013085	m	0.013255	m
ri	0.00911	m	0.00757	m	0.009265	m	0.008005	m	0.009115	m
	ro	ri	ro	ri	ro	ri	ro	ri	ro	ri
radius (m)	1.33E-02	9.11E-03	1.33E-02	7.57E-03	1.33E-02	9.27E-03	1.31E-02	8.01E-03	1.33E-02	9.12E-03
Ai (m^2)	2.76E-04	1.30E-04	2.77E-04	9.00E-05	2.80E-04	1.35E-04	2.69E-04	1.01E-04	2.76E-04	1.31E-04
yi (m)	5.62E-03	3.87E-03	5.64E-03	3.21E-03	5.66E-03	3.93E-03	5.55E-03	3.40E-03	5.63E-03	3.87E-03
Ybar (m)	0.005059482		0.005041879		0.005100607		0.004966284		0.005061472	
I (m^4)	3.38E-09	7.56E-10	3.41E-09	3.60E-10	3.48E-09	8.09E-10	3.22E-09	4.51E-10	3.39E-09	7.58E-10
di (m)	5.64E-04	-1.19E-03	5.94E-04	-1.83E-03	5.63E-04	-1.17E-03	5.87E-04	-1.57E-03	5.64E-04	-1.19E-03
Ai*dyi^2 (m^4)	8.77E-11	1.86E-10	9.79E-11	3.01E-10	8.87E-11	1.84E-10	9.27E-11	2.48E-10	8.78E-11	1.86E-10

	15B		16B		17B		25B		26B	
D	0.02543 m		0.02519 m		0.02689 m		0.02528 m		0.02537 m	
t	0.00446 m		0.00346 m		0.00374 m		0.0034 m		0.0041 m	
ro	0.012715 m		0.012595 m		0.013445 m		0.01264 m		0.012685 m	
ri	0.008255 m		0.009135 m		0.009705 m		0.00924 m		0.008585 m	
radius (m) Ai (m ²) yi (m) Ybar (m) Ix (m ⁴) di (m) Ai*dyi ² (m ⁴)	15A	15b	16A	16B	17A	17B	25A	25B	26A	26B
	ro	ri	ro	ri	ro	ri	ro	ri	ro	ri
	1.27E-02	8.26E-03	1.26E-02	9.14E-03	1.34E-02	9.71E-03	1.26E-02	9.24E-03	1.27E-02	8.59E-03
	2.54E-04	1.07E-04	2.49E-04	1.31E-04	2.84E-04	1.48E-04	2.51E-04	1.34E-04	2.53E-04	1.16E-04
	5.40E-03	3.50E-03	5.35E-03	3.88E-03	5.71E-03	4.12E-03	5.36E-03	3.92E-03	5.38E-03	3.64E-03
	0.004835137		0.004839288		0.005162497		0.004862026		0.004837038	
	2.87E-09	5.10E-10	2.76E-09	7.64E-10	3.59E-09	9.74E-10	2.80E-09	8.00E-10	2.84E-09	5.96E-10
	5.61E-04	-1.33E-03	5.06E-04	-9.62E-04	5.44E-04	-1.04E-03	5.03E-04	-9.40E-04	5.47E-04	-1.19E-03
8.00E-11	1.90E-10	6.38E-11	1.21E-10	8.40E-11	1.61E-10	6.34E-11	1.19E-10	7.55E-11	1.65E-10	
I (m ⁴)	15A	15B	16A	16B	17A	17B	25A	25B	26A	26B
	2.53E-09	2.25E-09	2.85E-09	1.94E-09	2.58E-09	2.54E-09	2.61E-09	1.95E-09	2.53E-09	2.16E-09
F (N)	-	-	-	-	-	-	-	-	-	-
	2.95E+02	268.6223723	2.82E+02	237.703476	2.87E+02	278.025158	2.99E+02	257.96883	2.66E+02	249.866661
y _{max} (m)	-1.96E-04	-0.000281	-2.33E-04	-0.000468	-2.14E-04	-0.000262	-1.91E-04	-0.000329	-2.29E-04	-0.000338
E (Pa) E _{average} (GPa)	4.25E+09	3.04E+09	3.04E+09	1.87E+09	3.72E+09	2.99E+09	4.29E+09	2.88E+09	3.29E+09	2.45E+09
	3.64		2.45		3.36		3.58		2.87	